5-2015

Trilayer Tissue Engineered Heart Valves for Aortic Valve Replacement

Michael Paul Jaeggli
Clemson University

TRILAYER TISSUE ENGINEERED HEART VALVES FOR AORTIC VALVE REPLACEMENT

A Dissertation
Presented to
the Graduate School of
Clemson University

In Partial Fulfillment
of the Requirements for the Degree
Doctor of Philosophy
Bioenginering

---

by
Michael Paul Jaeggli
May 2015

Accepted by:
Dr. Dan Simionescu, Committee Chair
Dr. Martine LaBerge
Dr. Ken Webb
Dr. Timothy Williams

ABSTRACT

Heart valve disease often progresses asymptomatically until valve damage has advanced to the point where replacement is unavoidable. Unfortunately, current valve replacements - including mechanical, bioprosthetic and autografts - have serious drawbacks, which often require replacement surgeries or lifelong anticoagulant therapy. The field of tissue engineering aims to overcome these drawbacks by combining scaffolds, stem cells, and chemical and physical stimuli to produce living tissues. The aortic heart valve has a unique structure composed of three discrete layers – fibrosa, spongiosa, and ventricularis - that work together in concert with the resident valvular interstitial cells to maintain a functioning valve. As a result, current tissue-engineered heart valves miss the mark for successful aortic valve replacement in one of two ways: either by being too weak to endure the stresses of the aortic environment or by being insufficiently recellularized and incapable of self-repair.

The primary focus of this research was to create a functional heart valve replicating the unique trilayer structure developed by nature. We showed that valves can be modeled from medical imaging data, 3D printed, and used as molds to create patient-specific heart valves. The valve scaffolds supported cell attachment, growth, and proliferation.

Porous, dry scaffolds were effectively glued together to form one cohesive trilayer scaffold. These scaffolds resemble the human valve's unique histoarchitecture. A meta-analysis of literature defined maximum normal stresses and strains experienced by the native valve; providing a target set of mechanical properties to be replicated by the tissue-engineered valve. Increasing porosity and microneedle rolling treatments produced scaffolds with excellent mechanical strength that were more than strong enough to function in physiological conditions.

A novel cell seeding technique was developed to rapidly seed porous and microneedle treated fibrous scaffolds; resulting in full-thickness cell seeding. Functional heart valves were made using a crush-mounting system. This system allowed for rapid and reproducible production of valves for *in vitro* testing. A comparison between mechanical, bioprosthetic, and trilayer valves revealed outstanding hemodynamic performance of trilayer valves. These valves functioned well for three weeks in a heart valve bioreactor. This research produced functional, tissue-engineered heart valves with excellent mechanical and hemodynamic properties.

DEDICATION

This dissertation is dedicated to my wife, Katy. You have given me the encouragement, love, and support that sustained me throughout my studies. This documents is also for James and Emery; my beautiful children.

TABLE OF CONTENTS

Page

Title Page.....i

Abstract.....ii

Dedication.....iv

Table of Contents.....v

List of Figures.....xiii

Chapter 1: Review of Literature.....1

1.1 Aortic Valve Structure and Function.....1

1.1.1 The Importance of Trilayer Structure for Aortic Valve Function.....1

1.1.2 Aortic Heart Valve Cells.....3

1.2 Aortic Valve Disease and Prevalence.....5

1.3 Valve Replacement Options.....6

1.3.1 Limitations of Current Valve Replacement Options.....8

1.3.2 Patient Populations with Unmet Needs.....9

1.4 The Ideal Tissue Engineered Valve.....9

1.5 Approaches to Tissue Engineering the Heart Valve.....10

1.5.1 Approach 1: Scaffold Creation with In-Vitro Cell Seeding.....11

Table of Contents (Continued)

Page

1.5.2 Approach 2: Scaffold Creation with In-Vitro Cell Seeding, Remodeling, Decellularization, and Re-Cellularization 13

1.5.3 Approach 3: Scaffold Creation, Implantation and In-Vivo Cell Infiltration .. 14

1.5.4 Approach 4: De Novo Scaffold Creation 16

1.6 Conclusions 17

1.7 Chapter 1 References 18

Chapter 2: Patient-Specific Trilayer Heart Valves 27

2.1 Introduction 27

2.1.1 Research Motivation and Aim 27

2.1.2 Valve Geometry and Prosthesis-Patient Mismatch 29

2.2 Materials and Methods 31

2.2.1 Materials 31

2.2.2 Modeling of Aortic Heart Valve Cusps 32

2.2.3 Fibrous Scaffold Preparation 33

2.2.4 PGG Treatment of Fibrous Scaffolds 34

2.2.5 Cell Culture 34

Table of Contents (Continued)

Page

2.2.6 Static Cell Seeding on PGG-Fixed Fibrous Scaffold Surfaces 35

2.2.7 Creation of Cell-Seeded Hydrogel Spongiosa Scaffold 35

2.2.8 Assembly of Patient-Specific Trilayer Heart Valves 36

2.2.9 Bioreactor Testing of Trilayer Valves 36

2.2.10 Creation and Testing of Trilayer Valves with Simplified Geometry for Hydrogel Durability Analysis 37

2.2.11 Histology and Fluorescent Imaging..... 37

2.3 Results..... 38

2.3.1 Cell Seeded Scaffolds 38

2.3.2 Aortic Heart Valve Modeling..... 40

2.3.3 Patient-Specific Valve Production and Testing 44

2.3.4 Trilayer Valves with Simplified Geometry for Hydrogel Durability Analysis 46

2.4 Discussion 47

2.5 Conclusions 49

2.6 Chapter 2 References 50

Table of Contents (Continued)

Page

Chapter 3: Development and Characterization of Trilayer Scaffolds for Heart Valve Tissue Engineering 53

3.1 Introduction 53

3.1.1 Research Motivation and Aim 53

3.2 Materials and Methods 54

3.2.1 Materials 54

3.2.2 Fibrous Scaffold Preparation 54

3.2.3 Spongy Scaffold Preparation 55

3.2.4 Preparation of Human Heart Valve Tissue 56

3.2.5 Bovine Serum Albumin Glue Preparation 56

3.2.6 Increasing Porosity of Fibrous and Spongy Scaffolds 57

3.2.7 Assembly of Trilayer Scaffolds 57

3.2.8 Micro Needle Roller Treatment. 58

3.2.9 Histology 59

3.2.10 Scanning Electron Microscope Imaging 59

3.2.11 Mechanical Testing 59

Table of Contents (Continued)

Page

3.2.12 Statistical analysis 60

3.3 Results 61

3.3.1 Fibrous and Spongy Scaffold Characterization 61

3.3.2 Trilayer Cusp Creation 62

3.3.3 Physiologically Relevant Mechanical Loading Conditions 66

3.3.4 Mechanical Analysis of Fresh Aortic Valves 67

3.3.5 Mechanical Analysis of Fibrous Scaffolds 70

3.4 Discussion 76

3.4.1 Increasing Porosity and Dry Assembly of Scaffolds 77

3.4.2 Mechanical Properties of Porcine Aortic Valves 79

3.4.3 Impact of Increasing Porosity and Microneedle Rolling on Scaffold Mechanical Properties 80

3.5 Conclusion 81

3.6 Chapter 4 References 81

Chapter 4: Construction, Stem Cell Seeding, and Evaluation of Trilayer Heart Valves 85

4.1 Introduction 85

Table of Contents (Continued)

Page

4.1.1 Research Motivation and Aim 85

4.2 Materials and Methods 85

4.2.1 Materials 85

4.2.2 Fibrous and Spongy Scaffold Preparation 86

4.2.3 Poration of Fibrous and Spongy Scaffolds 86

4.2.4 Assembly of Trilayer Scaffolds 87

4.2.5 Micro Needle Roller Treatment 87

4.2.6 Cell Culture 88

4.2.7 Cell Seeding of Fibrous and Spongy Scaffolds 88

4.2.8 Analysis of Cell Distribution in Fibrous Scaffolds 88

4.2.9 Cell Seeding of Trilayer Cusps 89

4.2.10 Designing the Crush Mounting System 89

4.2.11 Producing the Crush Mount 90

4.2.12 Constructing the Crush Mounted Valve for Bioreactor Testing 91

4.2.13 Bioreactor Testing and Maturation of Trilayer Heart Valves 91

4.2.14 Constructing the Nitinol Stent Mounted Valve 92

Table of Contents (Continued)

Page

4.2.15 Geometric Orifice Area Measurement 93

4.2.16 Scanning Electron Microscope Imaging 94

4.2.17 Histology 94

4.2.18 Statistical Analysis 95

4.3 Results 95

4.3.1 Spongy Scaffold Seeding 95

4.3.2 Microneedle Rolling and Seeding of Fibrous Scaffolds 97

4.3.3 Assembly and Function of Trilayer Valves 103

4.3.4 Bioreactor Maturation of Trilayer Heart Valves 110

4.3.5 A Nitinol Stent-Mounted Trilayer Valve 113

4.4 Discussion 115

4.5 Conclusion 118

4.6 Chapter 4 References 118

Chapter 5: Conclusions and Recommendations for Future Work 122

5.1 Conclusions 122

5.2 Recommendations for Future Work 124

Table of Contents (Continued)

Page

5.2.1 Assessment of Stem Cell Phenotype in Bioreactor Conditioned Valves at Pulmonic and Aortic Conditons..... 124

5.3 Further Mechanical Analysis of Trilayer Scaffolds..... 125

5.3.1 Flexural Testing of Trilayer scaffolds 125

5.3.2 Viscoelastic Analysis through Incremental Loading 125

5.3.3 Testing Trilayer Valves in a Large Animal Model..... 126

5.4 Chapter 5 References 127

LIST OF FIGURES

Figure		Page
1.1	Cross sectional diagram of aortic heart valve……..	3
1.2	The five AVIC phenotypes……..	4
1.3	Artificial heart valves……	7
1.4	Leaflet contraction over time……..	16
2.1	Current tissue engineering paradigm……	28
2.2	Three-dimensional arrangement of the aortic root……	29
2.4	Assembly of scaffold-based heart valves……	31
2.5	Cell proliferation on PGG-treated fibrous scaffolds……..	39
2.6	Stem cells encapsulated in hydrogel……..	40
2.7	Selection and masking of blood volumes from CTA image data……..	42
2.8	Aorta and heart masks modeled in 3D……..	43
2.9	Individual cusps are separated in 3-matic CAD software……..	44
2.10	Patient-specific valve assembly……..	45
2.11	Simplified cusp geometry……..	47
3.1	Fibrous and spongy scaffolds……..	61
3.2	Histlogical analysis of fibrous and spongy scaffolds……..	62
3.3	Trilayer scaffold construction……..	64
3.4	Histological examination of BSA glue……..	65
3.5	Cross section SEM images of trilayer scaffolds……	65

List of Figures (Continued) Page

3.6 Comparison between trilayer scaffold and human aortic valve……. 66

3.7 Meta-analysis of maximum forces on the human aortic valve…… 67

3.8 Porcine aortic valve representative stress-strain curves……. 69

3.9 Porcine aortic valve mechanical testing results……. 70

3.11 Representative stress-strain curves for fibrous scaffolds…… 72

3.12 Ultimate tensile strength of fibrous scaffolds…… 73

3.13 Strain at break of fibrous scaffolds……. 74

3.14 Peak modulus of fibrous scaffolds…… 75

3.15 Secant modulus at strain=10% of fibrous scaffolds…….. 76

4.1 Cell seeding on porous spongy scaffolds……. 97

4.2 Microneedle rolling of fibrous scaffolds…….. 99

4.3 SEM imaging of fibrous scaffolds; results of microneedle rolling……. 100

4.4 Numerical analysis of cell distribution throughout scaffolds including representative DAPI images…… 102

4.5 H&E images of cell seeding on poroius and microneedle treated scaffolds…… 103

4.8 Assembly of crush-mounted valve……. 105

4.9 Diagram of the heart valve bioreactor…… 106

List of Figures (Continued) Page

4.10 Comparison of mechanical, trilayer, and bioprothetic valve hemodynamics…….. 108

4.11 Comparison of GOA, opening, and closing of valves…… 109

4.12 Trilayer heart valve after 3 weeks of bioreactor conditioning…… 111

4.13 Mechanical testing of bioreactor conditioned heart valves…… 112

4.14 Proof of concept construction of trilayer valve in collapsible stent…… 114

CHAPTER 1: REVIEW OF LITERATURE

1.1 Aortic Valve Structure and Function

The aortic valve is located between the left ventricle and aorta. It is a passive tissue whose movement is controlled by blood flow. When the heart contracts during systole, blood flows from the left ventricle, through the aortic valve, and into the aorta. During diastole, backpressure closes the aortic valve, preventing oxygenated blood from flowing back into the left ventricle. The aortic valve is made of three cusps, Left and Right coronary cusps, behind which the coronary arteries originate, and the non-coronary cusp. The cusps are subjected to transvalvular pressures that change from 10 to 120 mmHg is less than one tenth of one second after systole[1]. An average adult heart will beat nearly 3 billion times, placing a significant mechanical load on the aortic heart valve with every beat. For this reason, the aortic heart valve is considered the most mechanically stressed tissue in the body[2].

1.1.1 The Importance of Trilayer Structure for Aortic Valve Function

The aortic valve thickens over time, averaging 0.67mm thick in those under 20 years of age and 1.42mm in those over 60[3]. This size is remarkably thin considering the stresses placed upon the tissue. The aortic valve has developed a highly-organized trilayer structure capable of coping with the myriad of forces placed upon it while remaining thin

and flexible enough to open and close properly **(Fig 1.1)**. It is composed of three distinct layers - fibrosa, spongiosa, and ventricularis - each with unique structures and functions[4]. The fibrosa is closest to the outflow tract and is largely comprised of circumferentially aligned collagen fibers. It provides the majority of the strength required to maintain coaptation despite the high forces developed in diastole. Below the fibrosa sits the spongiosa – a highly hydrated, gel-like layer comprised primarily of glycosamingoglycans (GAGs) - which functions as a stress dampening layer,[5] allowing the fibrosa and ventricularis layers to locally shear during normal valve movement thus reducing overall valve stresses[6]. The ventricularis layer, located on the valve's inflow side, is mainly comprised of radially-aligned elastin fibers[7]. The ventricularis allows for swift radial retraction of the cusps during valve opening[8] and aids in recoil during systole[9]. Working together, these three individual layers act as one unit to ensure proper blood flow through the heart[10].

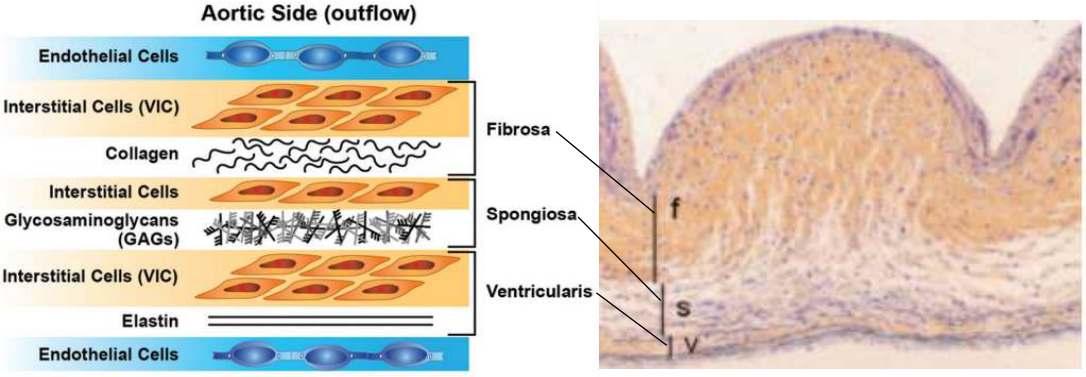

Figure 1.1. (A) Cross sectional diagram of aortic heart valve leaflet showing trilayered structure[85] (B) Radial cross section of the human aortic heart valve stained with Movat's Pentachrome showing the fibrosa (f), spongiosa (s), and ventricularis (v) depicting collagen in yellow, elastin fibers in black, and nuclei

1.1.2 Aortic Heart Valve Cells

The two main cell types in the aortic valve are aortic valve interstitial cells (AVICs) and aortic valve endothelial cells (AVECs). AVICs function to repair and remodel the valve matrix as small damages are accumulated through constant mechanical loading[11]. These cells can synthesize collagen, elastin, and proteoglycans at a rapid rate[12]. AVICS dynamically adopt a wide variety of phenotypes, and most commonly resemble fibroblasts, smooth muscle cells, or myofibroblasts[1314]. Because of the changing characteristics, markers, and behaviors of AVICs, an exact cell phenotype is not easily defined. Gotlieb et al have proposed a classification of these cells into five distinct phenotypes (**Fig 1.2**). The three phenotypes most pertinent to this discussion are qVICs (quiescent), aVICs (activated), and obViCs (osteoblastic). qVICs are fibroblast-like cells

that maintain valve structure in the normal valve. They are positive for vimentin while expressing very low levels of α smooth muscle actin (αSMA) and MMPs[15].

.

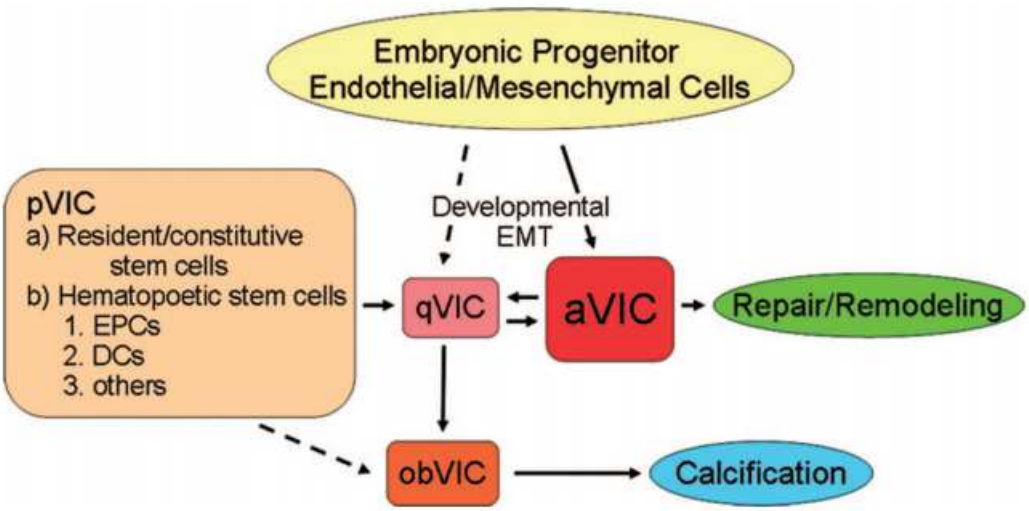

Figure 1.2 The five AVIC phenotypes proposed by Gotlieb et al.[14] Solid lines represent widely accepted transitions while hatched lines indicate transitions without sufficient evidence.

aVICs arise in response to injury, disease, or altered hemodynamic stress. These cells are contractile myofibroblasts, the hallmark of which is the expression of αSMA[16]. An upregulation of the aVIC phenotype produces increased ECM secretion, matrix metalloproteinase (MMP) expression, and tissue inhibitors of MMPs (TIMPs) which all work together to remodel the valvular tissue[17]. When the aVIC wound healing response is concluded, clearance of aVICs by apoptosis takes place. If this apoptotic removal does

not occur as intended, prolonged aVIC function may lead to valvular disease, mediated by the chronic inflammatory response, such as calcification, and fibrosis. Thus aVICs are important in repair and remodeling, but have the potential to cause severe pathological compilations if their activation is uncontrolled.

The final phenotype of note is the obVIC. Osteoblastic differentiation of qVICs can be induced *in-vitro* through the addition of organic phosphate, bone morphogenic proteins (BMPs), and tissue growth factor (TGF-β)[18]. The hallmark of this change is the expression of alkaline phosphatase, the activity of which is greatly enhanced during mineralization. obVIC activation can lead to calcification and valve stiffening.

The aortic valve has a distinct populations of endothelial cells; whereas vascular endothelial cells align parallel with blood flow, AVECs align perpendicular[19]. These cells perform the typical vascular endothelial functions; acting as a semi-selective barrier, providing cell signals to interstitial cells, and preventing thrombosis. Endothelial cells on the inflow surface are exposed to higher shear stresses than those on the outflow surface. Damage to the endothelial lining is a precursor to common valve disease processes including inflammation and calcification[20]. An intact endothelium is therefore an important component of a properly functioning valve.

1.2 Aortic Valve Disease and Prevalence

Aortic valve disease (AVD) is the cause of 370,000 yearly valve replacements worldwide[21]. Due to both increasing and aging populations, this is projected to increase

to 850,000 annual replacements by 2050[22]. Aortic stenosis, the main pathology behind valve replacement, occurs slowly as calcium deposits thicken the valve leaflets. Left ventricular hypertrophy often accompanies valve stenosis. This disease may progress asymptomatically for many years; when symptoms do occur, valve replacement is required within 3 to 5 years[21].

1.3 Valve Replacement Options

The first prosthetic heart valve to see widespread use was the ball and cage valve. This valve, first implanted in 1960, consists of a silicone ball that moves inside a metal cage. The tilting disc valve was introduced in 1970 and consisted of a circular disc supported by metal struts that pivoted to open and close[23]. This valve was eventually removed from the market due to repeated mechanical failures at the supporting strut[24]. The next major advance in mechanical heart valve technology was the bileaflet mechanical valve. This valve was introduced in 1979 and consisted of two semicircular pyrolytic carbon leaflets that rotate about struts mounted in the main valve body[25]. This basic design has not been drastically changed, and is currently the most common valve replacement in the world, with over 600,000 implanted[26].

Mechanical valves require a life-long regiment of anticoagulant therapy. To circumvent the negative side effects of anticoagulants, the biological prostheses was developed. The first bioprosthetic valve was introduced in 1965 and consisted of a porcine

aortic xenograft fixed in formaldehyde[27]. Due to poor valve durability, the fixative was changed to glutaraldehyde in 1968[28]. In 1971, the Ionescu-Shiley pericardial xenograft was introduced, using pericardial tissue mounted to a rigid stent to form a valve[29]. With the exception of minor stent modifications, suturing patterns, and anti-calcification treatments, currently available prosthetic valves do not differ from those developed in the 60s and 70s[30] (**Fig**. **1.3**).

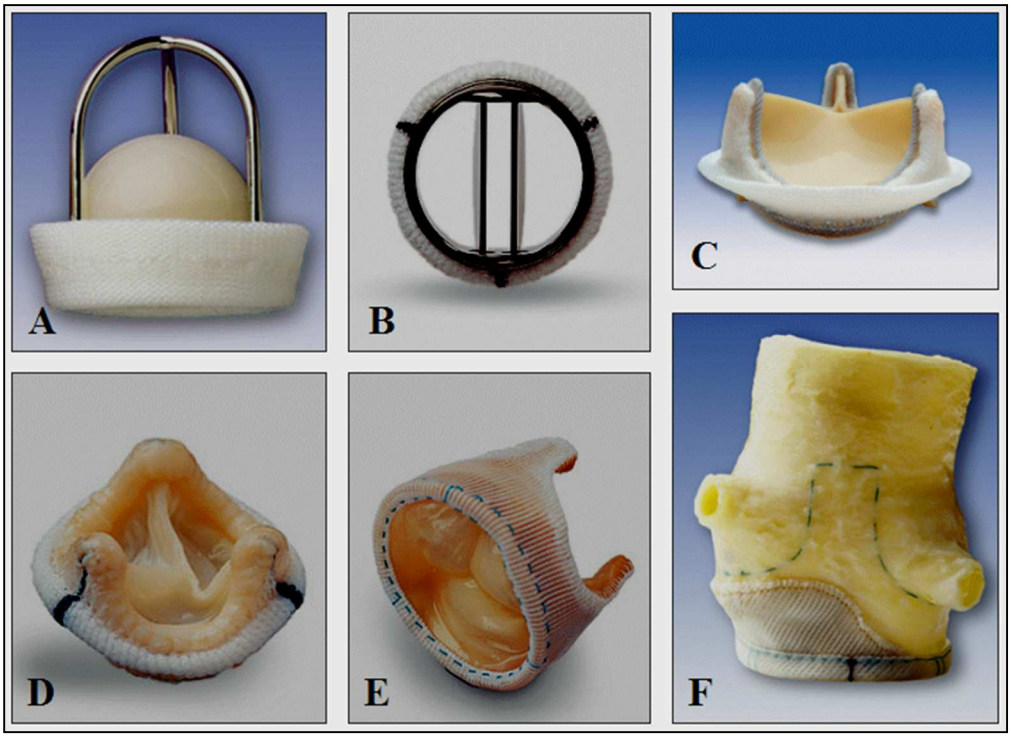

Figure 1.3. Artificial heart valves. Caged Ball (A), Hinged Leaflets (B), Stented Bovine Pericardium (C), Stented Porcine Valve (D), Stentless Porcine Valve (E), and Stentless Porcine Valve (F). From: Simionescu D, "Artificial Heart Valves", Wiley Encyclopedia of Biomedical Engineering, 2006. (A, C, F) Copyright Edwards Lifesciences, Inc. 2005 and (B, D, E) St. Jude Medical, Inc. 2005 All rights reserved[31]

1.3.1 Limitations of Current Valve Replacement Options

Current prosthetic heart valves fall into two categories: mechanical and biological valves; while both valve types are effective in treating AVD, they have significant limitations. Mechanical valves are very durable, but require life-long warfarin therapy[32] and are prone to pannus tissue overgrowth and thrombosis[33]. When a bileaflet mechanical valve is open, the two leaflets present a free edge normal to the flow of blood. This causes a layer of high shear stress across the leaflet surface, leading to blood trauma and cell rupture. Ruptured red blood cells release tissue factor[34], initiating the extrinsic blood coagulation pathway that leads to the formation of a thromboembolism[32].

Biological valves are constructed of non-viable, glutaraldehyde-fixed animal tissues. These valves do not develop the high shear stresses seen in mechanical valves and thus do not require warfarin therapy[35]. However, biological valves have a limited lifespan of 15-20 years in adult patients due to calcification and structural valve degeneration (SVD)[36–38]. Adult patients face a difficult choice between accepting the risk of a major bleeding event inherent with mechanical valves (which increases from 30% to 55% from age 50 to 75) and the risk of reoperation due to SVD inherent in bioprosthetic valves (which decreases from 45% to 10% as age increases from 50 to 75). This choice is especially difficult for a 55 year old patient, who faces nearly identical risks of major bleeding or reoperation depending on which valve is implanted[39].

1.3.2 Patient Populations with Unmet Needs

There are two main patient populations that have no ideal heart valve replacement. The first population is pregnant women, or women who wish to become pregnant in the future. The majority of births are had by women between the ages of 20 and 34[40]. Due to the limited lifespan of bioprosthetic valves, this age range almost exclusively receives mechanical valves[41]. However, mechanical valves require warfarin therapy, which is linked to a 70% failure rate in pregnancies[42], making mechanical valves a poor solution for potential mothers. Bioprosthetic valves have a 50% freedom from SVD 12 years post-implantation for 25 year old patients[43]. Therefore, a woman who opted for a bioprosthetic valve at a young age to avoid increased risk of a failed pregnancy would be facing multiple reoperations throughout her lifetime[39].

Pediatric populations are also underserved by current heart valve replacements. Bioprosthetic valves have a short lifespan in pediatric and young adult patients due to increased immunological activity[37] and high levels of circulating calcium[44]. Additionally, both mechanical and bioprosthetic valves valves lack the ability to grow with a developing patient, making them unsuitable long-term options for children[454647].

1.4 The Ideal Tissue Engineered Valve

The ideal valve replacement is nonthrombogenic, does not degenerate over time, possesses excellent hemodynamics, and is capable of somatic growth and remodeling[48].

A tissue engineered aortic valve replacement has the potential to meet these criteria. Living tissue will be able to resist degeneration, repair accumulated damage from applied mechanical stresses and has the potential for somatic growth in younger patients. Additionally, due to suitable hemodynamics, no anticoagulant therapy is required for tissue-engineered valves. Finally, tissue-engineered valves may resist calcification due to the absence of devitalized cells, a known nidus for calcification[4950].

1.5 Approaches to Tissue Engineering the Heart Valve

There are currently multiple strategies for producing tissue-engineered heart valves. All methods involve the creation of a scaffold and population of that scaffold with cells. The methods vary in the way the scaffolds are produced and how cells are incorporated. At this time, a wide variety of scaffolds are being investigated including synthetic polymers,[51525354] decellularized whole xenografts,[555657]and gel based biological scaffolds such as fibrin[5859] and collagen gels[6061]. Synthetic scaffolds have several advantages; they are quickly repopulated with cells[62], have a lack of immunogenic epitopes[63], and can be readily shaped into different geometries[64]. However, mechanical properties change as the polymer degrades. If implanted, the timescale of synthetic scaffold degradation must be carefully balanced with the cell-produced matrix that is taking the scaffold's place. If degradation outpaces cellular re-modelling, valve failure may occur. Xenogenic tissue scaffolds are one of the most promising areas of research

due to their inherent mechanical robustness. However, it is difficult to repopulate these scaffolds with cells, leading most studies to rely only on surface endothelialization instead of on full cellular revitalization[656667686970]. When tested in animal models, these scaffolds are often repopulated with host cells[7172]. However, a recent human study has shown that decellularized xenografts are not repopulated with cells and long term outcomes are poor[73]. Therefore, we hypothesize that the success of tissue-engineered heart valves cannot be based on host revitalization with cells and must instead be repopulated with host cells *prior to implantation*. An in-depth look at the five major approaches to tissue engineering the aortic valve is herein presented.

1.5.1 Approach 1: Scaffold Creation with In-Vitro Cell Seeding

This approach starts with a biological, polymer, or gel scaffold. The scaffold is then seeded *in-vitro* with interstitial or stem cells and possibly conditioned in a bioreactor prior to implantation *in-vivo*. The goal of this approach is to create a functional, cell-seed scaffold prior to implantation. The most common biological scaffold used in this approach is a detergent decellularized pulmonary valve. Full thickness *in*-vitro cell repopulation of pulmonary valves is challenging, therefore these scaffolds are often surface seeded with endothelial cells. A study by Lichtenburg et al. seeded autologous jugular veins endothelial cells onto a pulmonary valve before orthotopic implantation in sheep. After 3

months they observed a functional monolayer of endothelial cells and interstitial repopulation of the full thickness of the valve with host cells[74].

Biodegradeable polymeric scaffolds represent an attractive scaffold due to their ability to be formed into complex shapes and lack of xenoantigens. Shinoka et al. created a nonwoven, Poly-glycolic acid (PGA) fiber scaffold seeded with fibroblasts and endothelial cells. This valve was implanted for 8 weeks in lambs. Control leaflets (without cells) completely degraded while autologous cell-seeded scaffolds generated a functional matrix after 8 weeks *in-vivo*[52]. Composite PGA/PLLA nonwoven scaffolds have similarly been seeded, implanted in sheep 4 months with good result[54]. However, several studies report that scaffolds become increasingly regurgitant after 8-12 weeks *in*-vivo. Mesenchymal stem cells were isolated from neonatal sheep bone marrow and seeded onto a bioresorbable scaffold. After 4 weeks of culture, valved conduits were implanted. After 12 weeks of *in vivo* testing, valved conduit cusps were increasingly attenuated and regurgitant[75]. The polymeric valve that has been most studied is made by Hoerstrup's group. It consists of a biodegradeable synthetic scaffold composed of nonwoven PGA dip-coated with poly-4-hydroxybutyrate. Heating allows the scaffold to be molded and integrated into a self-expanding nitinol stent. The scaffold is next seeded with autologous myofibroblasts and endothelial cells, cultured for two weeks in a pulse-duplicating bioreactor, and implanted transapically through a catheter. Initially, valves showed escellent function, but long term testing resulted in thickened tissue containing cells positive for αSMA[76].

The third major type of scaffold used in this approach is fibrin gel. These valves are constructed by encapsulating dermal fibroblasts in fibrin gel. The gel is injected into a valve-shaped mold and polymerizes into a solid. During *in-vitro* culture, dermal fibroblasts replaced the fibrin matrix with endogenous tissue. When implanted *in-vivo* a compromise of function was seen at 4 weeks with complete loss of functionality observed by 8 weeks[77]. Valves thickened, lost flexibility, and demonstrated insufficiency. This was attributed to the use of fibroblasts which continued to produce collagen and contract *in-vivo*, eventually leading to valve failure[58][78].

1.5.2 Approach 2: Scaffold Creation with In-Vitro Cell Seeding, Remodeling, Decellularization, and Re-Cellularization

This approach is sometimes referred to as the "de-cell re-cell" technique. It was designed to prevent tissue contraction seen in polymer and fibrin valves by removing contractile cells after the endogenously produced matrix has been layed down[59]. This technique has been applied to both fibrin and polymeric valves, successfully removing contractile cells and replacing them with mesenchymal stem cells. Long term *in-vivo* performance of these valves has yet to be shown.

1.5.3 Approach 3: Scaffold Creation, Implantation and In-Vivo Cell Infiltration

This approach produces an acellular scaffold and relies on circulating host cells to repopulate the implanted valve. This is the only approach to be implanted in human subjects, and is therefore the closest to becoming a widespread clinical reality. The first human use of this approach was based on a proprietary cell removal technique developed by Crylife called synergraft. This technique was first used to decellularize pulmonary homograft valves. One patient who received this valve died 5 weeks post-op. Histological examination of the homograft showed superficial neutrophil and macrophage infiltration[79]. Another valve was analyzed after two years, also showing no full-thickness repopulation by host cells[80]. Despite the lack of host cell infiltration, synergraft homograft valves performed well. Synergraft technology was later used to decellularize xenogenic pulmonary valves with disastrous results. Implanting these valves in children and young adults lead to massive immune response, failure of valves, and deaths. Further investigation showed that some porcine cells had not been removed by synergraft treatment, leading to valve failure[81].

This approach was recently replicated by a German company called Autotissue using their matrix P Decellularized xenogenic porcine valves. While these valves have not shown the spectacular failure of the synergraft valves, they are not performing well. Early results have shown leaflet thickening, fibrosis, and severe inflammation[73]. The hypothesis

that the human body will repopulate an acellular biological matrix has been disproven multiple times. Long term studies on human allograft valves have shown that host cells do not repopulate the valve, which actually become acellular after implantation[82]. Despite this, the allograft valves perform remarkably well, often lasting 15-20 years without complications[83].

Biological scaffolds have not shown significant repopulation by hosts. However, studies with synthetic scaffolds have shown repopulation of implanted scaffolds in as little as five hours and full repopulation including a functional, intact endothelium were observed after eight weeks[62]. This remarkably quick repopulation has only been observed in the sheep model. The sheep model is known to have severe fibrotic responses and to readily repopulate valve matrices with cells. However, prolonged *in-vivo* testing has shown that these valves are still susceptible to leaflet contraction and insufficiency (**Figure 1.4)**.

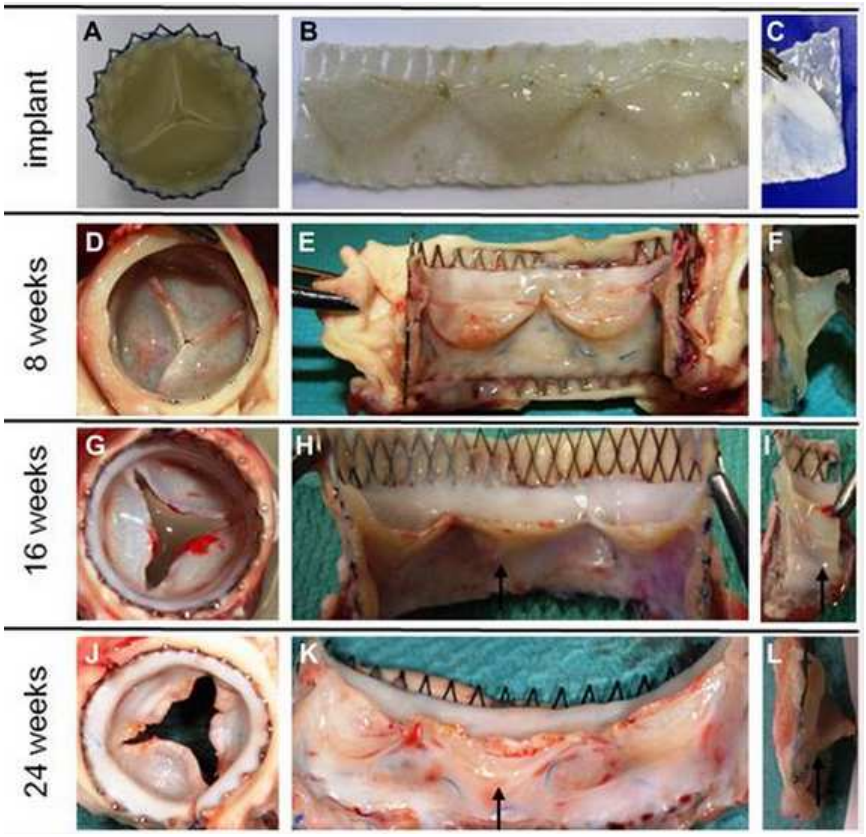

Figure 1.4. Leaflet contraction over time of acellular synthetic scaffolds implanted in the pulmonary position of sheep.

1.5.4 Approach 4: De Novo Scaffold Creation

Cell sheet engineering utilizes specially coated culture plates to allow for removal of cells without degrading the ECM holding them together. Cell sheets are thin, delicate structures, but they can be stacked and fused to form thicker, more robust tissues. Work by Tremblay et al. used dermal fibroblasts to create single cell sheets after 26 days of culture. Four of these sheets were stacked and cultured for an additional three weeks. Next, two of these stacks were fused for an additional five months, producing a single flat collagen scaffold used for creating a heart valve. The valve showed good function in a

pulse-duplicating bioreactor[84]. This approach is very time consuming, taking seven months of culture to produce a single valve.

1.6 Conclusions

Heart valve tissue engineering is a pressing problem that has the potential to revolutionize therapy for children, young women, and even adults. There are many approaches to heart valve tissue engineering, all of which are in different stages of progress. The most advanced valves, and the only approach to reach human use, is the implantation of acellular biological matrices. Results of this technique are mixed, with decellularized homografts showing the most success. However, no implanted biological scaffold has fulfilled the promise of becoming fully repopulated with host cells. Therefore, we hypothesize that the success of tissue-engineered heart valves cannot be based on host revitalization with cells and must instead be repopulated with host cells *prior to implantation*. The approach of using robust, proven biological scaffolds that are re-populated with autologous stem cells prior to implantation builds upon the most successful techniques, and is therefore the most promising avenue for the development of a tissue engineered valve for human use.

We hypothesize that the unique, trilayer structure developed by nature is essential to proper aortic valve function. Our aim is to create a tissue-engineered heart valve that uses explicitly-designed collagen scaffolds joined together to reproduce all three native valve layers. This valve will be fully populated with stem cells and conditioned

in a bioreactor, producing a valve capable of maintaining homeostasis and responding to accumulated injuries obtained during normal valve function.

1.7 Chapter 1 References

1. Guyton and Hall Textbook of Medical Physiology, 12e: 9781416045748

2. Bilodeau K, Mantovani D. Bioreactors for tissue engineering: focus on mechanical constraints. A comparative review. *Tissue Eng*. 2006;12(8):2367-2383. doi:10.1089/ten.2006.12.2367.

3. Sahasakul Y, Edwards WD, Naessens JM, Tajik AJ. Age-related changes in aortic and mitral valve thickness: Implications for two-dimensional echocardiography based on an autopsy study of 200 normal human hearts. *Am J Cardiol*. 1988;62(7):424-430. doi:10.1016/0002-9149(88)90971-X.

4. The Aortic Valve: Mano J. Thubrikar: 9780849347719

5. Buchanan RM, Sacks MS. Interlayer micromechanics of the aortic heart valve leaflet. *Biomech Model Mechanobiol*. 2014;13(4):813-826. doi:10.1007/s10237-013-0536-6.

6. Talman EA, Boughner DR. Internal shear properties of fresh porcine aortic valve cusps: implications for normal valve function. *J Heart Valve Dis*. 1996;5(2):152-159.

7. Sacks MS, Smith DB, Hiester ED. The aortic valve microstructure: effects of transvalvular pressure. *J Biomed Mater Res*. 1998;41(1):131-141.

8. Schoen FJ. Aortic valve structure-function correlations: role of elastic fibers no longer a stretch of the imagination. *J Heart Valve Dis*. 1997;6(1):1-6.

9. Vesely I. The role of elastin in aortic valve mechanics. *J Biomech*. 1998;31(2):115-123.

10. Vesely I, Noseworthy R. Micromechanics of the fibrosa and the ventricularis in aortic valve leaflets. *J Biomech*. 1992;25(1):101-113. doi:10.1016/0021-9290(92)90249-Z.

11. Schneider PJ, Deck JD. Tissue and cell renewal in the natural aortic valve of rats: an autoradiographic study. *Cardiovasc Res*. 1981;15(4):181-189.

12. Komuro T. Re-evaluation of fibroblasts and fibroblast-like cells. *Anat Embryol (Berl)*. 1990;182(2). doi:10.1007/BF00174011.

13. Messier RH, Bass BL, Aly HM, et al. Dual Structural and Functional Phenotypes of the Porcine Aortic Valve Interstitial Population: Characteristics of the Leaflet Myofibroblast. *J Surg Res*. 1994;57(1):1-21. doi:10.1006/jsre.1994.1102.

14. Liu AC, Joag VR, Gotlieb AI. The emerging role of valve interstitial cell phenotypes in regulating heart valve pathobiology. *Am J Pathol*. 2007;171(5):1407-1418. doi:10.2353/ajpath.2007.070251.

15. Rabkin-Aikawa E, Farber M, Aikawa M, Schoen FJ. Dynamic and reversible changes of interstitial cell phenotype during remodeling of cardiac valves. *J Heart Valve Dis*. 2004;13(5):841-847.

16. Della Rocca F, Sartore S, Guidolin D, et al. Cell composition of the human pulmonary valve: a comparative study with the aortic valve--the VESALIO Project. Vitalitate Exornatum Succedaneum Aorticum labore Ingegnoso Obtinebitur. *Ann Thorac Surg*. 2000;70(5):1594-1600.

17. Mulholland DL, Gotlieb AI. Cell biology of valvular interstitial cells. *Can J Cardiol*. 1996;12(3):231-236.

18. Osman L, Yacoub MH, Latif N, Amrani M, Chester AH. Role of human valve interstitial cells in valve calcification and their response to atorvastatin. *Circulation*. 2006;114(1 Suppl):I547-I552. doi:10.1161/CIRCULATIONAHA.105.001115.

19. Deck JD. Endothelial cell orientation on aortic valve leaflets. *Cardiovasc Res*. 1986;20(10):760-767.

20. Tao G, Kotick JD, Lincoln J. Heart valve development, maintenance, and disease: the role of endothelial cells. *Curr Top Dev Biol*. 2012;100:203-232. doi:10.1016/B978-0-12-387786-4.00006-3.

21. Butany J, Collins MJ. Analysis of prosthetic cardiac devices: a guide for the practising pathologist. *J Clin Pathol*. 2005;58(2):113-124. doi:10.1136/jcp.2004.020271.

22. Yacoub MH, Takkenberg JJM. Will heart valve tissue engineering change the world? *Nat Clin Pract Cardiovasc Med*. 2005;2(2):60-61. doi:10.1038/ncpcardio0112.

23. Björk VO. The central flow tilting disc valve prosthesis (Björk-Shiley) for mitral valve replacement. *Scand J Thorac Cardiovasc Surg*. 1970;4(1):15-23.

24. Blackstone EH. Could it happen again? the Björk-Shiley convexo-concave heart valve story. *Circulation*. 2005;111(21):2717-2719. doi:10.1161/CIRCULATIONAHA.105.540518.

25. Emery RW, Mettler E, Nicoloff DM. A new cardiac prosthesis: the St. Jude Medical cardiac valve: in vivo results. *Circulation*. 1979;60(2 Pt 2):48-54.

26. Bloomfield P. Choice of heart valve prosthesis. *Heart*. 2002;87(6):583-589.

27. Carpentier A. From valvular xenograft to valvular bioprosthesis (1965-1977). *Med Instrum*. 11(2):98-101.

28. Carpentier A, Lemaigre G, Robert L, Carpentier S, Dubost C. Biological factors affecting long-term results of valvular heterografts. *J Thorac Cardiovasc Surg*. 1969;58(4):467-483.

29. Ionescu MI, Tandon AP, Mary DA, Abid A. Heart valve replacement with the Ionescu-Shiley pericardial xenograft. *J Thorac Cardiovasc Surg*. 1977;73(1):31-42.

30. Zilla P, Brink J, Human P, Bezuidenhout D. Prosthetic heart valves: catering for the few. *Biomaterials*. 2008;29(4):385-406. doi:10.1016/j.biomaterials.2007.09.033.

31. Wiley: Wiley Encyclopedia of Biomedical Engineering, 6-Volume Set - Metin Akay. http://www.wiley.com/WileyCDA/WileyTitle/productCd-047124967X.html. Accessed April 7, 2015.

32. Shahriari S, Maleki H, Hassan I, Kadem L. Evaluation of shear stress accumulation on blood components in normal and dysfunctional bileaflet mechanical heart valves using smoothed particle hydrodynamics. *J Biomech*. 2012;45(15):2637-2644. doi:10.1016/j.jbiomech.2012.08.009.

33. Schoen FJ, Hobson CE. Anatomic analysis of removed prosthetic heart valves: causes of failure of 33 mechanical valves and 58 bioprostheses, 1980 to 1983. *Hum Pathol*. 1985;16(6):549-559.

34. Rodriguez RA, Ruel M, Labrosse M, Mesana T. Transcranial Doppler and acoustic pressure fluctuations for the assessment of cavitation and thromboembolism in patients with mechanical heart valves. *Interact Cardiovasc Thorac Surg*. 2007;7(2):179-183. doi:10.1510/icvts.2007.167569.

35. Ott DA, Coelho AT, Cooley DA, Reul GJ. Ionescu-Shiley pericardial xenograft valve: Hemodynamic evaluation and early clinical follow-up of 326 patients. *Cardiovasc Dis*. 1980;7(2):137-148.

36. Manji RA, Menkis AH, Ekser B, Cooper DKC. Porcine bioprosthetic heart valves: The next generation. *Am Heart J*. 2012;164(2):177-185. doi:10.1016/j.ahj.2012.05.011.

37. Dahm M, Lyman WD, Schwell AB, Factor SM, Frater RW. Immunogenicity of glutaraldehyde-tanned bovine pericardium. *J Thorac Cardiovasc Surg*. 1990;99(6):1082-1090.

38. Stock UA, Schenke-Layland K. Performance of decellularized xenogeneic tissue in heart valve replacement. *Biomaterials*. 2006;27(1):1-2. doi:10.1016/j.biomaterials.2005.05.100.

39. Rahimtoola SH. Choice of prosthetic heart valve in adults an update. *J Am Coll Cardiol*. 2010;55(22):2413-2426. doi:10.1016/j.jacc.2009.10.085.

40. Hamilton BE, Martin JA, Ventura SJ. Births: preliminary data for 2009. *Natl Vital Stat Rep*. 2010;59(3):1-19.

41. Hoffmann G, Lutter G, Cremer J. Durability of bioprosthetic cardiac valves. *Dtsch Arztebl Int*. 2008;105(8):143-148. doi:10.3238/arztebl.2008.0143.

42. Sadler L, McCowan L, White H, Stewart A, Bracken M, North R. Pregnancy outcomes and cardiac complications in women with mechanical, bioprosthetic and homograft valves. *BJOG*. 2000;107(2):245-253.

43. Takkenberg JJM, van Herwerden LA, Eijkemans MJC, Bekkers JA, Bogers AJJC. Evolution of allograft aortic valve replacement over 13 years: results of 275 procedures. *Eur J Cardiothorac Surg*. 2002;21(4):683-691; discussion 691.

44. Neuenschwander S, Hoerstrup SP. Heart valve tissue engineering. *Transpl Immunol*. 2004;12(3-4):359-365. doi:10.1016/j.trim.2003.12.010.

45. Henaine R, Roubertie F, Vergnat M, Ninet J. Valve replacement in children: a challenge for a whole life. *Arch Cardiovasc Dis*. 2012;105(10):517-528. doi:10.1016/j.acvd.2012.02.013.

46. Turrentine MW, Ruzmetov M, Vijay P, Bills RG, Brown JW. Biological versus mechanical aortic valve replacement in children. *Ann Thorac Surg*. 2001;71(5 Suppl):S356-S360.

47. Talwar S, Malankar D, Garg S, et al. Aortic valve replacement with biological substitutes in children. *Asian Cardiovasc Thorac Ann*. 2012;20(5):518-524. doi:10.1177/0218492312439400.

48. Roberts WC. Choosing a substitute cardiac valve: type, size, surgeon. *Am J Cardiol*. 1976;38(5):633-644.

49. Levy RJ, Schoen FJ, Levy JT, Nelson AC, Howard SL, Oshry LJ. Biologic determinants of dystrophic calcification and osteocalcin deposition in glutaraldehyde-preserved porcine aortic valve leaflets implanted subcutaneously in rats. *Am J Pathol*. 1983;113(2):143-155.

50. Schoen FJ. The future of bioprosthetic valves. A pathologist's perspective. *ASAIO Trans*. 34(4):1040-1042.

51. Dvorin EL, Wylie-Sears J, Kaushal S, Martin DP, Bischoff J. Quantitative evaluation of endothelial progenitors and cardiac valve endothelial cells: proliferation and differentiation on poly-glycolic acid/poly-4-hydroxybutyrate scaffold in response to vascular endothelial growth factor and transforming growth facto. *Tissue Eng*. 2003;9(3):487-493. doi:10.1089/107632703322066660.

52. Shinoka T, Ma PX, Shum-Tim D, et al. Tissue-engineered heart valves. Autologous valve leaflet replacement study in a lamb model. *Circulation*. 1996;94(9 Suppl):II164-II168.

53. Hoerstrup SP, Kadner A, Melnitchouk S, et al. Tissue engineering of functional trileaflet heart valves from human marrow stromal cells. *Circulation*. 2002;106(12 Suppl 1):I143-I150.

54. Sutherland FWH, Perry TE, Yu Y, et al. From stem cells to viable autologous semilunar heart valve. *Circulation*. 2005;111(21):2783-2791. doi:10.1161/CIRCULATIONAHA.104.498378.

55. Zeltinger J, Landeen LK, Alexander HG, Kidd ID, Sibanda B. Development and characterization of tissue-engineered aortic valves. *Tissue Eng*. 2001;7(1):9-22. doi:10.1089/107632701300003250.

56. Dohmen PM, Ozaki S, Nitsch R, Yperman J, Flameng W, Konertz W. A tissue engineered heart valve implanted in a juvenile sheep model. *Med Sci Monit*. 2003;9(4):BR97-BR104.

57. Bertipaglia B, Ortolani F, Petrelli L, et al. Cell characterization of porcine aortic valve and decellularized leaflets repopulated with aortic valve interstitial cells: the VESALIO Project (Vitalitate Exornatum Succedaneum Aorticum Labore Ingenioso Obtenibitur). *Ann Thorac Surg*. 2003;75(4):1274-1282.

58. Robinson PS, Johnson SL, Evans MC, Barocas VH, Tranquillo RT. Functional tissue-engineered valves from cell-remodeled fibrin with commissural alignment of cell-produced collagen. *Tissue Eng Part A*. 2008;14(1):83-95. doi:10.1089/ten.a.2007.0148.

59. Syedain ZH, Bradee AR, Kren S, Taylor DA, Tranquillo RT. Decellularized tissue-engineered heart valve leaflets with recellularization potential. *Tissue Eng Part A*. 2013;19(5-6):759-769. doi:10.1089/ten.TEA.2012.0365.

60. Rothenburger M, Vischer P, Völker W, et al. In vitro modelling of tissue using isolated vascular cells on a synthetic collagen matrix as a substitute for heart valves. *Thorac Cardiovasc Surg*. 2001;49(4):204-209. doi:10.1055/s-2001-16108.

61. Butcher JT, Nerem RM. Porcine aortic valve interstitial cells in three-dimensional culture: comparison of phenotype with aortic smooth muscle cells. *J Heart Valve Dis*. 2004;13(3):478-485; discussion 485-486.

62. Driessen-Mol A, Emmert MY, Dijkman PE, et al. Transcatheter implantation of homologous “off-the-shelf” tissue-engineered heart valves with self-repair capacity: long-term functionality and rapid in vivo remodeling in sheep. *J Am Coll Cardiol*. 2014;63(13):1320-1329. doi:10.1016/j.jacc.2013.09.082.

63. Brody S, Pandit A. Approaches to heart valve tissue engineering scaffold design. *J Biomed Mater Res B Appl Biomater*. 2007;83(1):16-43. doi:10.1002/jbm.b.30763.

64. Sodian R, Hoerstrup SP, Sperling JS, et al. Evaluation of biodegradable, three-dimensional matrices for tissue engineering of heart valves. *ASAIO J*. 46(1):107-110.

65. Schenke-Layland K, Riemann I, Opitz F, König K, Halbhuber KJ, Stock UA. Comparative study of cellular and extracellular matrix composition of native and tissue engineered heart valves. *Matrix Biol*. 2004;23(2):113-125. doi:10.1016/j.matbio.2004.03.005.

66. Grauss RW, Hazekamp MG, Oppenhuizen F, van Munsteren CJ, Gittenberger-de Groot AC, DeRuiter MC. Histological evaluation of decellularised porcine aortic valves: matrix changes due to different decellularisation methods. *Eur J Cardiothorac Surg*. 2005;27(4):566-571. doi:10.1016/j.ejcts.2004.12.052.

67. Kasimir M-T, Weigel G, Sharma J, et al. The decellularized porcine heart valve matrix in tissue engineering: platelet adhesion and activation. *Thromb Haemost*. 2005;94(3):562-567. doi:10.1160/TH05-01-0025.

68. Lichtenberg A, Cebotari S, Tudorache I, et al. Flow-dependent re-endothelialization of tissue-engineered heart valves. *J Heart Valve Dis*. 2006;15(2):287-293; discussion 293-294.

69. Lichtenberg A, Tudorache I, Cebotari S, et al. In vitro re-endothelialization of detergent decellularized heart valves under simulated physiological dynamic conditions. *Biomaterials*. 2006;27(23):4221-4229. doi:10.1016/j.biomaterials.2006.03.047.

70. Tudorache I, Calistru A, Baraki H, et al. Orthotopic replacement of aortic heart valves with tissue-engineered grafts. *Tissue Eng Part A*. 2013;19(15-16):1686-1694. doi:10.1089/ten.TEA.2012.0074.

71. Steinhoff G, Stock U, Karim N, et al. Tissue engineering of pulmonary heart valves on allogenic acellular matrix conduits: in vivo restoration of valve tissue. *Circulation*. 2000;102(19 Suppl 3):III50-III55.

72. Boldt J, Lutter G, Pohanke J, et al. Percutaneous tissue-engineered pulmonary valved stent implantation: comparison of bone marrow-derived CD133+-cells and cells obtained from carotid artery. *Tissue Eng Part C Methods*. 2013;19(5):363-374. doi:10.1089/ten.TEC.2012.0078.

73. Voges I, Brasen JH, Entenmann A, et al. Adverse results of a decellularized tissue-engineered pulmonary valve in humans assessed with magnetic resonance imaging. *Eur J Cardio-Thoracic Surg*. 2013;44(4):e272-e279. doi:10.1093/ejcts/ezt328.

74. Lichtenberg A, Tudorache I, Cebotari S, et al. Preclinical testing of tissue-engineered heart valves re-endothelialized under simulated physiological conditions. *Circulation*. 2006;114(1 Suppl):I559-I565. doi:10.1161/CIRCULATIONAHA.105.001206.

75. Gottlieb D, Kunal T, Emani S, et al. In vivo monitoring of function of autologous engineered pulmonary valve. *J Thorac Cardiovasc Surg*. 2010;139(3):723-731. doi:10.1016/j.jtcvs.2009.11.006.

76. Schmidt D, Dijkman PE, Driessen-Mol A, et al. Minimally-invasive implantation of living tissue engineered heart valves: a comprehensive approach from autologous vascular cells to stem cells. *J Am Coll Cardiol*. 2010;56(6):510-520. doi:10.1016/j.jacc.2010.04.024.

77. Syedain ZH, Lahti MT, Johnson SL, et al. Implantation of a Tissue-engineered Heart Valve from Human Fibroblasts Exhibiting Short Term Function in the Sheep Pulmonary Artery. *Cardiovasc Eng Technol*. 2011;2(2):101-112. doi:10.1007/s13239-011-0039-5.

78. Flanagan TC, Sachweh JS, Frese J, et al. In vivo remodeling and structural characterization of fibrin-based tissue-engineered heart valves in the adult sheep model. *Tissue Eng Part A*. 2009;15(10):2965-2976. doi:10.1089/ten.TEA.2009.0018.

79. Sayk F, Bos I, Schubert U, Wedel T, Sievers H-H. Histopathologic findings in a novel decellularized pulmonary homograft: an autopsy study. *Ann Thorac Surg*. 2005;79(5):1755-1758. doi:10.1016/j.athoracsur.2003.11.049.

80. Miller D V, Edwards WD, Zehr KJ. Endothelial and smooth muscle cell populations in a decellularized cryopreserved aortic homograft (SynerGraft) 2 years after implantation. *J Thorac Cardiovasc Surg*. 2006;132(1):175-176. doi:10.1016/j.jtcvs.2006.02.038.

81. Simon P, Kasimir MT, Seebacher G, et al. Early failure of the tissue engineered porcine heart valve SYNERGRAFT in pediatric patients. *Eur J Cardiothorac Surg*. 2003;23(6):1002-1006; discussion 1006.

82. Schoen FJ, Mitchell RN, Jonas RA. Pathological considerations in cryopreserved allograft heart valves. *J Heart Valve Dis*. 1995;4 Suppl 1:S72-S75; discussion S75-S76.

83. Da Costa ML, Ghofaili F Al, Oakley RM El. Allograft tissue for use in valve replacement. *Cell Tissue Bank*. 2006;7(4):337-348. doi:10.1007/s10561-006-9009-9.

84. Tremblay C, Ruel J, Bourget J-M, et al. A new construction technique for tissue-engineered heart valves using the self-assembly method. *Tissue Eng Part C Methods*. 2014;20(11):905-915. doi:10.1089/ten.TEC.2013.0698.

85. Rajamannan NM, Evans FJ, Aikawa E, et al. Calcific aortic valve disease: not simply a degenerative process: A review and agenda for research from the National Heart and Lung and Blood Institute Aortic Stenosis Working Group. Executive summary: Calcific aortic valve disease-2011 update. *Circulation*. 2011;124(16):1783-1791. doi:10.1161/CIRCULATIONAHA.110.006767.

86. Schoen FJ. Evolving concepts of cardiac valve dynamics: the continuum of development, functional structure, pathobiology, and tissue engineering. *Circulation*. 2008;118(18):1864-1880. doi:10.1161/CIRCULATIONAHA.108.805911.

CHAPTER 2: PATIENT-SPECIFIC TRILAYER HEART VALVES

2.1 Introduction

2.1.1 Research Motivation and Aim

Heart valve disease often progresses asymptomatically until valve damage has advanced to the point where replacement is unavoidable. Unfortunately, current valve replacements - including mechanical, bioprosthetic and autografts - have serious drawbacks, which often require replacement surgeries or lifelong anticoagulant therapy. The field of Tissue Engineering aims to overcome these drawbacks by combining scaffolds, stem cells, and chemical and physical stimuli to produce living tissues. The aortic heart valve has a unique structure composed of three discrete layers – fibrosa, spongiosa, and ventricularis - that work in concert with the resident valvular interstitial cells to maintain a functioning valve. As a result, current tissue-engineered heart valves miss the mark for successful aortic valve replacement in one of two ways: either by being too weak to endure the stresses of the aortic environment or by being insufficiently recellularized and incapable of self-repair. Our long-term goal is to create a living, non-thrombogenic, tissue-engineered aortic heart valve capable of ongoing remodeling and injury repair.

The current tissue engineering paradigm (**Fig 2.1 - green**) starts and ends with the patient. First, a patient's cells are harvested and used with minimal processing or expanded *in*-vitro. A scaffolds is then seeded with patient stem cells and matured in a bioreactor before being implanted back into the patient. This valve can be considered patient-specific because it contains autologous cells. However, the tissue-engineered construct's shape is not specific to the individual's unique anatomy. The aim of this research was to add onto this paradigm by creating a valve with patient-specific shape (**Fig 2.1 - blue**). Medical imaging data is acquired via CT scan, modeled, and 3D-printed to produce patient-specific molds. These molds are used to shape the scaffold into a custom, patient-specific shape.

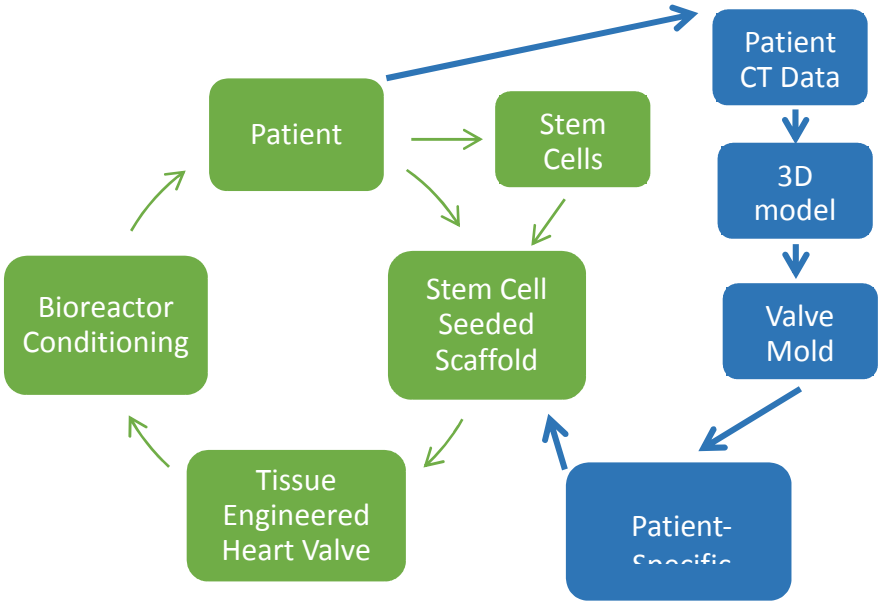

Figure 2.1. Current tissue engineering paradigm shown in green. Patient-specific shapeing steps shown in blue. Adapted from[1].

2.1.2 Valve Geometry and Prosthesis-Patient Mismatch

The aortic valve, while performing a seemingly simple function of opening and closing, contains a complex geometry that can vary widely from patient to patient. Current prosthetic heart valves come in sizes commonly ranging from 19 to 29mm in increments of 2mm.

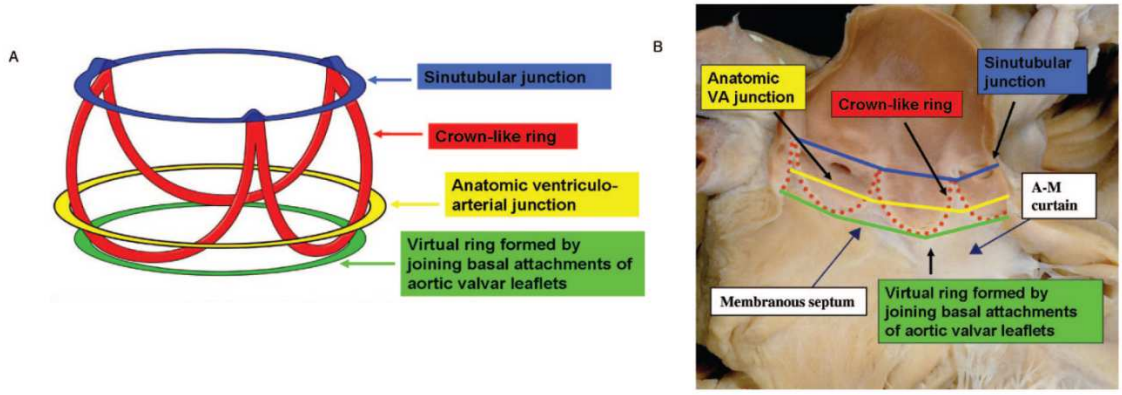

Fig 2.2. A, Three-dimensional arrangement of the aortic root, which contains 3 circular "rings," but with the leaflets suspended within the root in crown-like fashion. B, The leaflets have been removed from this specimen of the aortic root, showing the location of the 3 rings relative to the crown-like hinges of the leaflets. VA indicates ventriculoarterial; A-M, aortic-mitral.[2]

A one-shape fits all approach may lead to prosthesis-patient mismatch (PPM); if the implanted prosthesis is too small, higher than normal pressure gradients will arise[3]. Resistance to flow is described by the following equation, where R is resistance, η is blood viscosity, L is length, and r is valve radius:

$$R \propto \frac{\eta * L}{r^4}$$

From this equation, it is clear that implanting a smaller valve will cause an exponential increase in resistance to flow. Various studies have shown the incidence of moderate PPM to be 20 to 70% and severe PPM to occur in 2 to 11% of cases[3–7]. Native valve geometry is specially designed to produce proper blood flow and hemodynamics[8]. Abnormalities or deviations from original geometry produce improper mechanical loading and may lead to pathological conditions in the valve leaflets[9].

Several efforts have been made to model and produce a patient-specific valve[10,11]. Previous work in our lab used silicone molds of a porcine aorta to shape scaffolds (**Fig 2.4**). Other groups have used micro CT data or several anatomical landmarks to shape valves. While successful in creating a functional valve, these methods do not translate well to the clinic. Micro CT scans and silicone molding require the removal of the valve root as the first step of modeling. A true model of the patient aortic valve - based on readily available medical imaging data - has not been previously used to produce a tissue engineered valve. The method presented in this chapter is based on non-invasive techniques and could be used in the clinic. This work aims to produce a trilayer tissue-engineered heart valve made of a cell-seeded hydrogel spongiosa layer surrounded by a fibrous collagen scaffold representing fibrosa and ventricularis layers. This scaffold will be shaped to patient anatomy to eliminate the chance of patient-prosthesis mismatch.

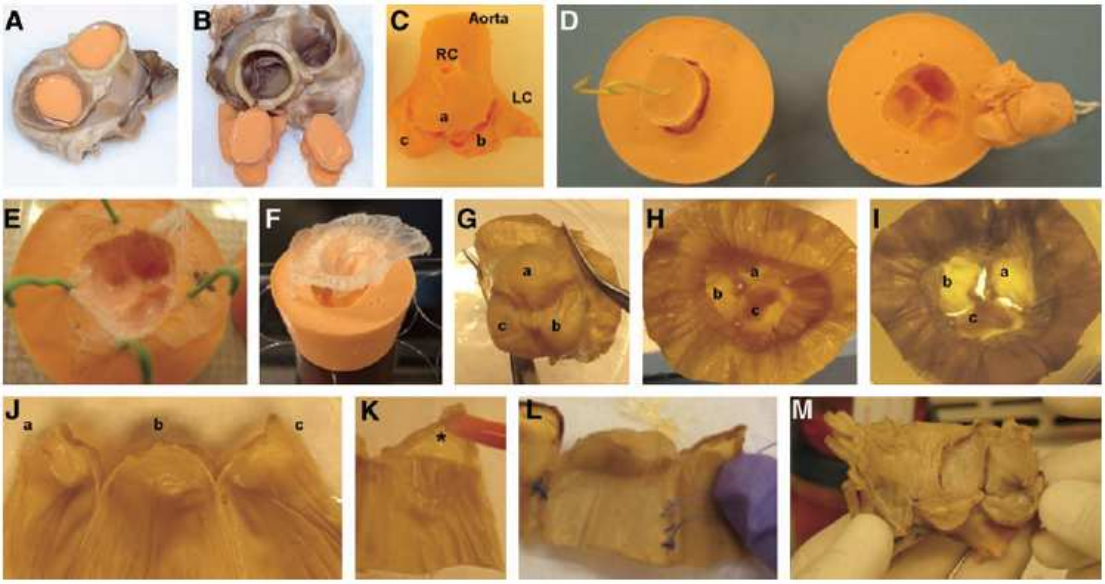

Fig 2.4 Assembly of scaffold-based heart valves. (A–D) Silicone molds were prepared from porcine heart valves. RC, right coronary; LC, left coronary; a, b, and c, the three leaflets. (E–I) Fibrous scaffolds were dried onto molds and PGG treated. (J–M) Valve-shape constructs were assembled by overlapping two identical fibrous scaffolds using BTglue and sutures placed at the level of valve wall, sinuses, and cusp insertion points. *Depicts the area between two fibrous scaffolds where the stem cell-seeded spongiosa was inserted[12].

2.2 Materials and Methods

2.2.1 Materials

Aortic valve molds were printed in a 3D Systems ProJet SD3000 printer using multijet technology to produce parts from an ABS-like plastic photopolymer - VisiJet SR200 and VisiJet s100 support material from 3D systems (Rock Hill, SC). Pericardial tissues were obtained from Animal Technologies, Inc. (Tyler, TX). Thiol-modified

hyaluronan, Thiol-reactive Polyethylene (glycol) Diacrylate (PEGDA), Thiol-modified collagen, and degassed, deionized water were obtained from Glycosan Biosystems (Alameda, CA). High-purity 1,2,3,4,6-Penta-O-galloyl-beta-D-glucose (PGG) was a generous gift from N.V. Ajinomoto OmniChem S.A. (Wetteren, Belgium). StemPro low-passage human adipose derived stem cells, MesenPro RS cell culture medium, Quant-iT PicoGreen dsDNA assay kit, and Alexafluor 647 Phalloidin were from Invitrogen (Carlsbad, CA). Pronectin - a Fibronectin-like Engineered Protein Polymer - and all other chemicals were of highest purity available and were obtained from Sigma-Aldrich Corporation (Lakewood, NJ).

2.2.2 Modeling of Aortic Heart Valve Cusps

Computed tomography angiography (CTA) heart imaging and ascending aorta in DICOM (Digital Imaging and Communications in Medicine) format was imported into medical 3D modeling software (Mimics Research v17.0, Materialise). DICOM images were 512x512 pixels, taken with a 180 mm field of view and a gantry tilt of 0°. Distances between planar slices was 0.75 mm. A profile line was then drawn across the abdominal aorta. Radiodensity was analyzed along this line and used to identify the range of Hounsfield units that represented the blood volume. Next, a thresholding operation was used to create a mask of the blood volume by selecting hounsfield units in the range specified by the profile line. The left ventricle and ascending aortic blood volumes were separated. Next, the soft tissue of the heart was thresholded into a separate mask. A Boolean subtraction of the aortic and left ventricle masks from the soft tissue mask

yielded an aortic valve mask, and used to generate a 3D model. The aortic valve model was then exported to computer aided design (CAD) software (3-Matic Research v9.0, Materialise).; a wrapping operation was done to close small holes in the model. Next, the sinus portion of the model was marked and removed. The three cusps were marked and separated into different parts and smoothed. The curve that defined the leaflet attachment to the left ventricular outflow tract was isolated and used to create an attachment point the leaflets. This attachment point was integrated into a circular mount that fit into the heart valve bioreactor and was used for functional testing. Files were then exported in stereolithography format to a ProJet SD3000 3D printer which built the parts by laying down a thin layer of photopolymer, curing that layer with UV light and repeating the process until the final shape is formed. Wax support material was melted away for four hours at 60ºC to yield finished parts.

2.2.3 Fibrous Scaffold Preparation

Fibrous collagen scaffolds were prepared following a previously-published protocol, with slight modifications[13]. Fresh tissues were received and cleaned, of peripheral attached fat and loose connective tissue, over wet ice. Tissue were placed in hypotonic conditions in pure, double-distilled water for 24 hours at 4ºC for cell lysis. Tissues were rinsed with double-distilled water and transferred to a sterile bottle. All further steps were done with sterile solutions with aseptic techniques. To remove cellular remnants, tissues were treated with 1 L of detergent solution consisting of 50mM Tris, 0.15% v/v Triton x-100, 0.25% Deoxycholic acid-sodium salt. 0.1% EDTA, and 0.02%

Sodium Azide for three days at room temperature on a shaker plate. The detergent solution was replaced and the tissues were treated for an additional three days. Tissues were then washed to remove the detergent solution. All washes were performed at room temperature on a shaker plate for 30 minutes. Two washes with double-distilled water were followed by two washes in 70% ethanol. Tissues were then washed twice more with double-distilled water. Removal of residual nucleic acids was achieved by treatment for 24 hours at 37ºC with 360 mUnits per mL of both deoxyribonuclease and ribonuclease dissolved in phosphate buffered saline containing 5 mM MgCl at a pH of 7.5. Tissues were washed as previously: twice with double-distilled water, 70% ethanol, and double-distilled water again. Tissues were stored at 4ºC in PBS with 0.02% sodium azide until use.

2.2.4 PGG Treatment of Fibrous Scaffolds

Acellular, fibrous scaffolds were treated with 0.075% PGG in a standard 9g/L saline solution containing 50mM Sodium Phosphate dibasic. Tissues were treated, while protected from light, at room temperature on a shaking plate overnight. Tissues were then washed three times for 30 minutes per wash in PBS. All solutions were sterile and aseptic technique was used throughout.

2.2.5 Cell Culture

Human, adipose-derived stem cells (StemPro, Life Technologies) were obtained and expanded in media (MesenPro, Life Technologies) specially formulated to preserve the stemness of hADSCs while increasing cell division rate. Media was supplemented with

1% L-glutamine and 1% antibiotic/antimycotic solution. hADSCs were grown T-175 tissue culture polystyrene flasks and subcultured with Trypsin-EDTA (Corning-Cellgro). Cells were used at passage 3 to 5.

2.2.6 Static Cell Seeding on PGG-Fixed Fibrous Scaffold Surfaces

Prior to use, PGG-fixed fibrous scaffolds were washed three times in double-distilled water, shaking, for 30 minutes. Scaffolds were then incubated overnight in a 1:1 ratio of DMEM:FBS. hADSCs were expanded in MesenPro medium and seeded in DMEM containing 10% FBS and 1% Ab/Am. Scaffolds were cut into circular sections, placed in 12-well plates, and seeded with hADSCs at a density of $8x10^5$ cells/cm^2. Scaffolds for histological analysis were fixed in 4% paraformaldehyde and paraffin embedded.

2.2.7 Creation of Cell-Seeded Hydrogel Spongiosa Scaffold

The HyStem-C hydrogel system was used according to the provided protocol. All procedures were performed aseptically. Thiol-modified hyaluronan, thiol-reactive PEGDA crosslinker, and thiol-modified collagen, and degassed, deionized (DG) water vials were heated to 37°C. 1 mL of DG water was added to the thiol-modified hyaluronan and thiol-modified collagen vials. Vials were placed on a shaking plate at 37°C for 30 minutes to allow the solids to dissolve. Next, 0.5 mL of DG water was added to the thiol-reactive PEGDA vial, which was dissolved by inverting several times. Pronectin was added to the vial containing the thiol-modified components at 50μg/mL followed by 200 μL of hADSCs

at a concentration of $1x10^7$ cells/mL to yield a final concentration of $2x10^6$ cells/mL gel. Thiol-reactive PEGDA crosslinker was added in a 1:4 ratio causing gelation in approximately 20 minutes.

2.2.8 Assembly of Patient-Specific Trilayer Heart Valves

Decellularized, PGG-treated scaffolds were Pericardium (white) wrapped around the plastic valve mold (yellow). The top of the pericardium was cut away and the mold was removed, leaving a void. The cusp was positioned inside the mounting ring (pink) and secured by threading sutures through the holes in the mounting ring. Cell-seeded hydrogel (blue) was injected into the void between pericardial layers - through the edge nearest the mounting ring - to form the spongiosa layer. The assembled valve sat inside the bioreactor mounting ring.

2.2.9 Bioreactor Testing of Trilayer Valves

Immediately after construction, cell-seeded trilayer heart valves were mounted in an early version of the heart valve bioreactor. The bioreactor was filled with 750mL of DMEM containing 10%FBS, 2%Ab/Am, and 0.1% Gentamycin, and placed in a standard cell-culture incubator at 37°C with 5% CO_2 and a humidified environment. Pressure was monitored in real time at points both above and below the valve. A custom LabView program displayed and recorded all information. A webcam with an LED light was attached to the top of the bioreactor and focused on the outflow side of the valve,

allowing for visualization of valve movement. Valves were conditioned for 14 days at a pressure of 15/2.5mmHg.

2.2.10 Creation and Testing of Trilayer Valves with Simplified Geometry for Hydrogel Durability Analysis

Decellularized, PGG-treated pericardium was wrapped around a mold with simplified geometry. The scaffold was trimmed to shape and the mold removed. The edge of the scaffold was closed with a running suture (4-0 prolene Ethicon, Somerville, NJ). Cell-seeded hydrogel was injected into the void where the mold was removed. The bioreactor was filled with 750mL of DMEM containing 10%FBS, 2%Ab/Am, and 0.1% Gentamycin and placed in a standard cell-culture incubator at 37°C with 5% CO_2 and a humidified environment. Pressure was monitored in real time at points both above and below the valve. A custom LabView program displayed and recorded all information. A webcam with an LED light was attached to the top of the bioreactor and focused on the outflow side of the valve, allowing for visualization of valve movement. Valves were conditioned for 14 days at a pressure of 15/2.5mmHg.

2.2.11 Histology and Fluorescent Imaging

Thin 5μm sections of paraffin-embedded samples were washed in xylene and rehydrated through a series of alcohol washes ending in deionized water. These sections were stained with hematoxylin and eosin (Richard-Allen Scientific, Thermo Scientific) to show general scaffold morphology and to identify cell location. Digital images of these

slides were obtained at various magnifications (25X to 100X) on a Zeiss Axiovert 40CFL microscope using AxioVision software (Carl Zeiss MicroImaging, Inc. Thornwood, NY). For en face surface imaging fibrous scaffolds were washed twice with 37°C PBS then fixed in 4% PFA for 1 hr at room temperature. Samples were then extracted with 0.1% Triton X-100 in PBS for 5 minutes, then washed two more times with PBS, incubated in 1% BSA for 20 minutes, and washed again. Alexafluor 647 Phalloidin was applied for 20 minutes to stain actin filaments. Samples were washed twice and imaged with a Nikon Eclipse Ti confocal microscope (Nikon Instruments, Melville, NY). Images are presented as flattened, maximum-intensity renderings of a stack of images.

Cell viability of hADSCs encapsulated in Hystem-C hydrogels was evaluated using the Live/Dead Viability Assay Kit (Life Technologies).

2.3 Results

2.3.1 Cell Seeded Scaffolds

Static seeding studies of hADSCs on PGG-fixed fibrous scaffolds showed attachment and proliferation over a four week time course. Actin staining showed increased cell coverage after 7 and 28 days. DNA content also increased at both 7 and 28 day time points, indicating proliferation of attached cells. (**Fig 2.5**).

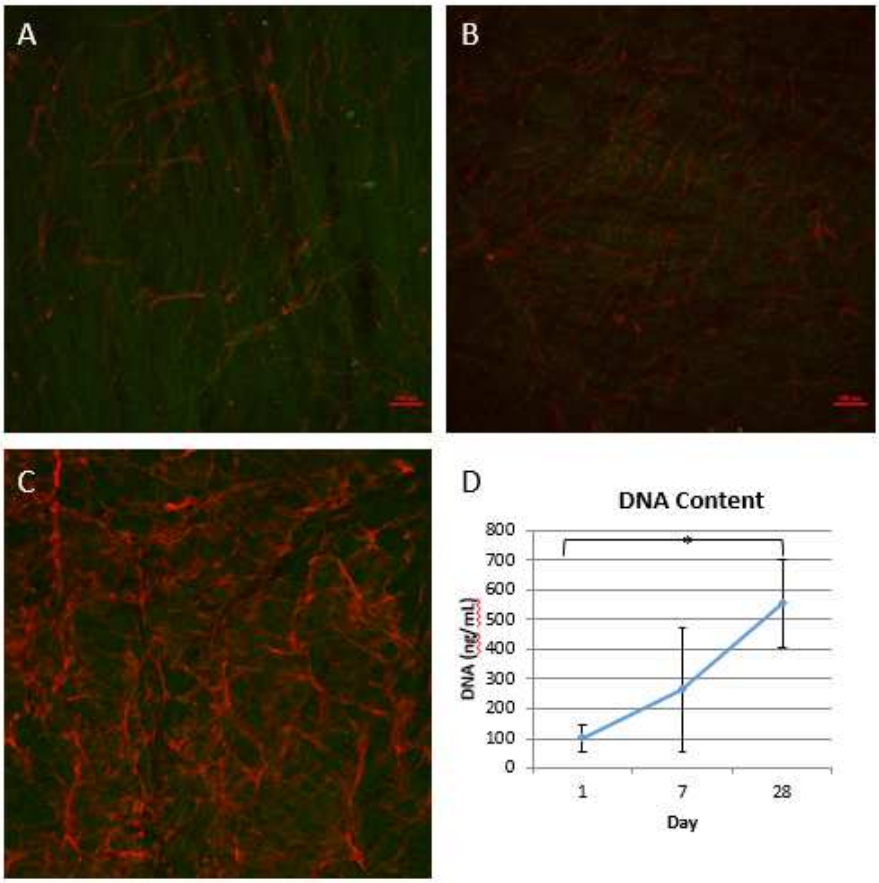

Figure 2.5. Cell proliferation on PGG-treated fibrous scaffolds. Immunofluorescence staining for actin (red) and fibrous scaffold (green autoflourescence) shows cell coverage at 1 (A), 7 (B), and 28 (C) days. DNA content of seeded scaffolds over the same time course (D).

Cells encapsulated in hydrogels showed good viability after 7 weeks of static seeding. Gels with the synthetic protein polymer pronectin added began to spread out through the gel with a longer and thinner morphology, while cells in pronectin-negative gels remained in a rounded, punctate morphology (**Fig 2.6**).

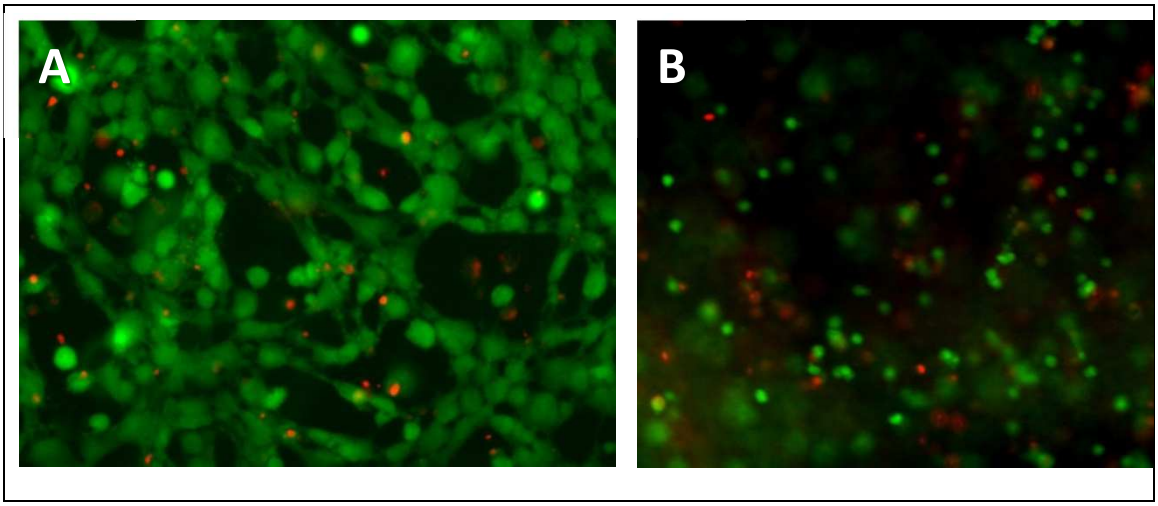

Figure 2.6. Live/Dead staining (green = live cells, red = dead cells) of hADSCs encapsulated in hydrogels with (A) and without (B) pronectin.

2.3.2 Aortic Heart Valve Modeling

Initial efforts in creating a tissue-engineered heart valve centered on re-creating patient-specific anatomy to produce a valve with optimal functionality. This was accomplished by modeling the aortic valve from medical imaging data. The Mimics Innovation Suite (Materialise, Belgium) was used to create masks of the aortic and left ventricular blood volumes (**Fig 2.7**). Subtracting these volumes from a mask of the soft tissue between them resulted in a mask containing the aortic valve anatomy. A 3D model of the valve surface and surrounding geometry was created (**Fig 2.8**).

The end goal of this modeling was to produce a unique mold for each valve cusp. To this end, the model was exported to 3-matic (Materialise, Belgium), where the three cusps were marked and separated into individual parts. The soft tissue modeling

operation included the sinus of valsalva and a portion of the ascending aorta. These portions were removed from the model, resulting in three cusp models consisting of surfaces defined by a network of triangles. Each vertex of each triangle was a defined coordinate in a three-dimensional space. The final mold quality depended on the number and quality of triangles – more triangles gave a smoother and more accurate surface. Triangle count and quality was optimized to produce three cusp models that were ready for export to the 3D printer (**Fig 2.9**).

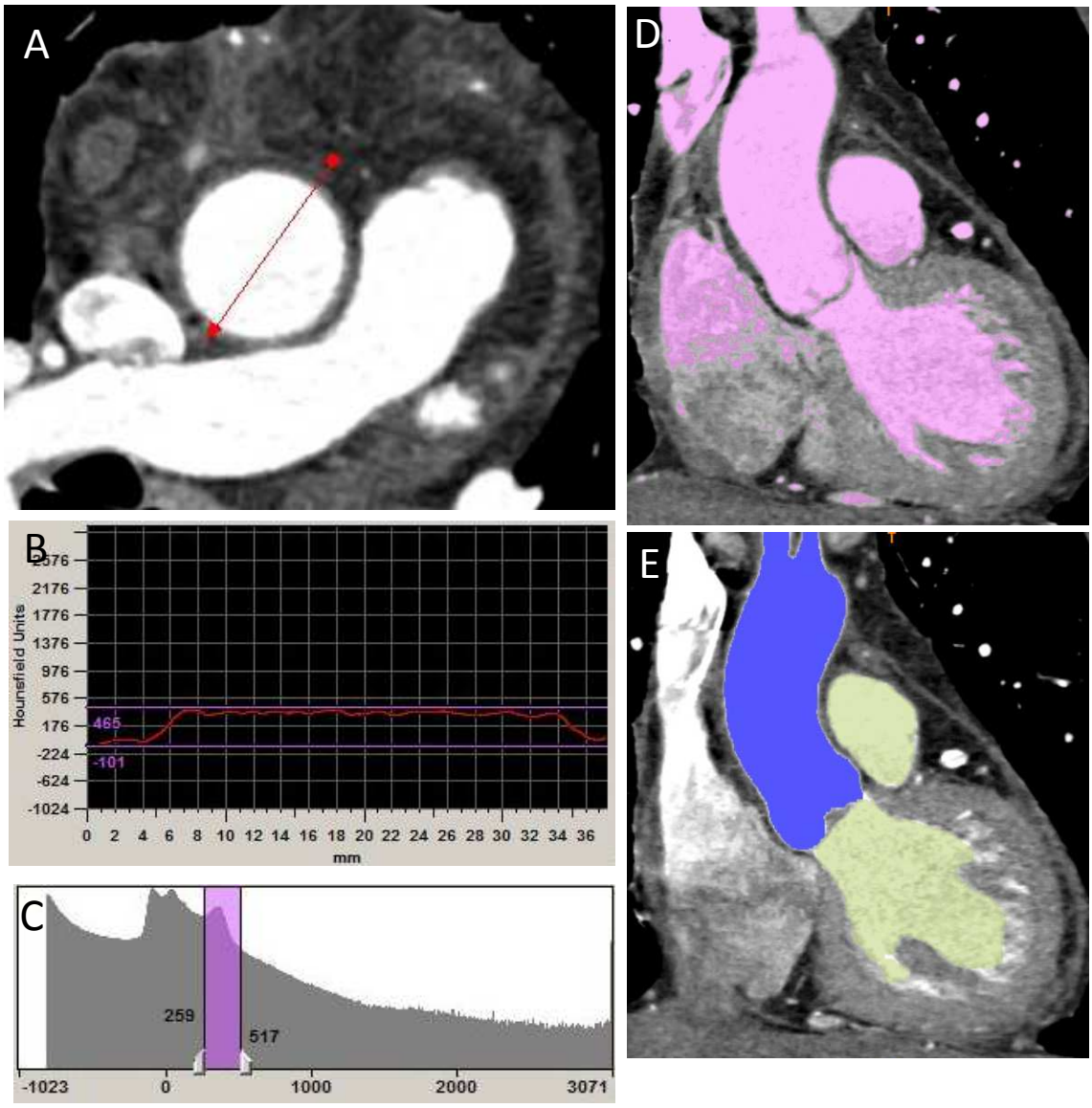

Fig 2.7. Selection and masking of blood volumes from CTA image data. A Profile line (A) is drawn across the blood volume in the transverse plane. Radiodensity is analyzed across the line and reported in Hounsfield units (B). The peak representing contrast-enhanced blood volume is selected and highlighted in pink on a histogram of the CT data set (C). The blood-volume is selected and masked off. Data from transverse planes is reconstructed in the sagittal plane showing the blood volume mask (D). The blood volume mask is separated into Aorta (blue) and heart (yellow) masks (E).

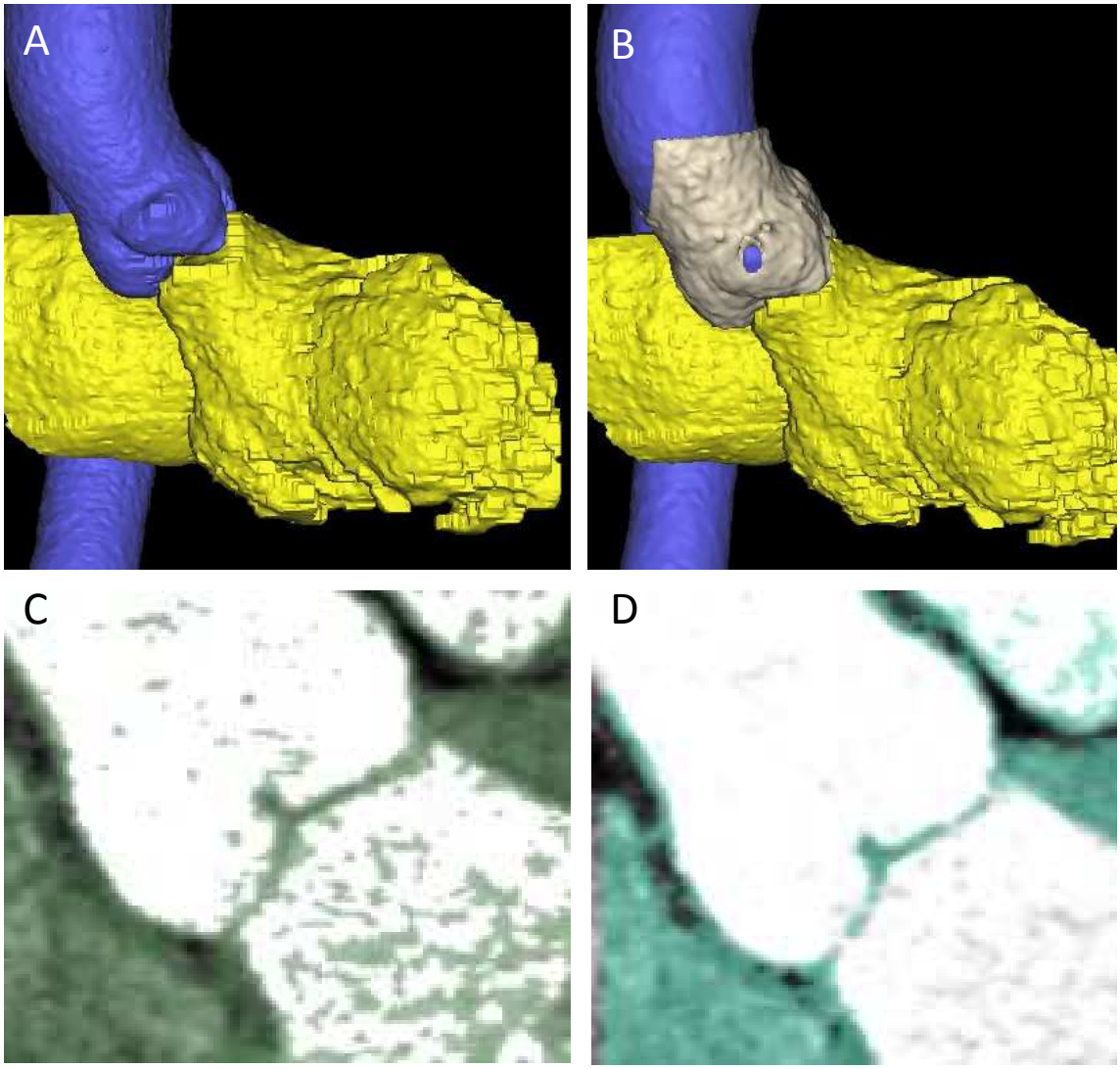

Figure 2.8. Aorta and heart masks are modeled in 3D (A). The aortic valve is located in the empty space between the two blood volumes, shown in tan (B). To generate the aortic valve model, the soft tissue of the heart was thresholded into a separate mask (C) which contained artifacts located in the blood volumes. A Boolean subtraction of the aorta and heart blood volume masks from the soft tissue mask yielded a mask of the aortic valve (D).

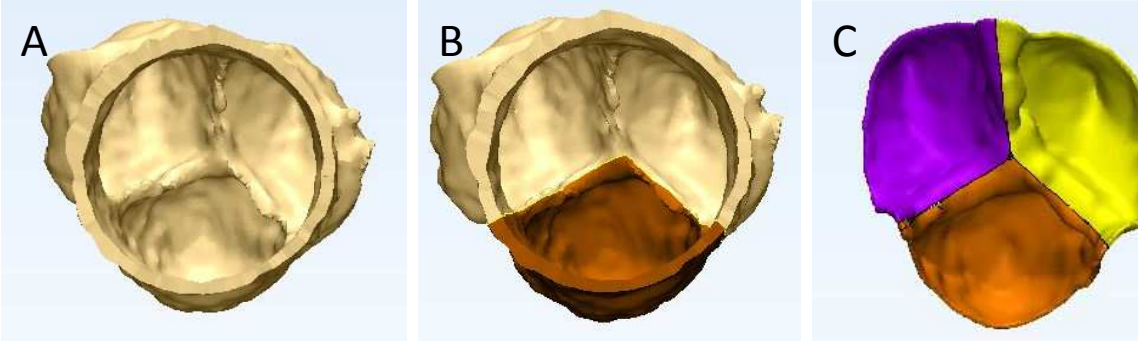

Figure 2.9. Individual cusps are separated in 3-matic CAD software. The aortic valve model is imported into 3-matic (A). A cusp is marked and separated into a new part (B). The process is repeated for the remaining cusps and excess aortic anatomy is removed to yield 3D models of each cusp.

2.3.3 Patient-Specific Valve Production and Testing

Patient-specific valves were produced by wrapping 3D printed molds with PGG-fixed fibrous scaffolds and allowing them to dry. The mold was removed and a cell-seeded hydrogel was injected into the void. Patient-specific valve shape was successfully replicated by securing the cusps to a custom mounting system designed for functional testing in the heart valve bioreactor (**Fig 2.10**). During bioreactor testing, a "ballooning" of the cusps was observed during systole (data not shown) where the space in the middle of the fibrous scaffold would fill with water, expanding like a balloon. We hypothesized that there was a failure at the interface between fibrous scaffold and hydrogel due to the mechanical forces placed upon the valve during multiple open/close cycles. To test this theory, a valve with simple geometry was created and tested.

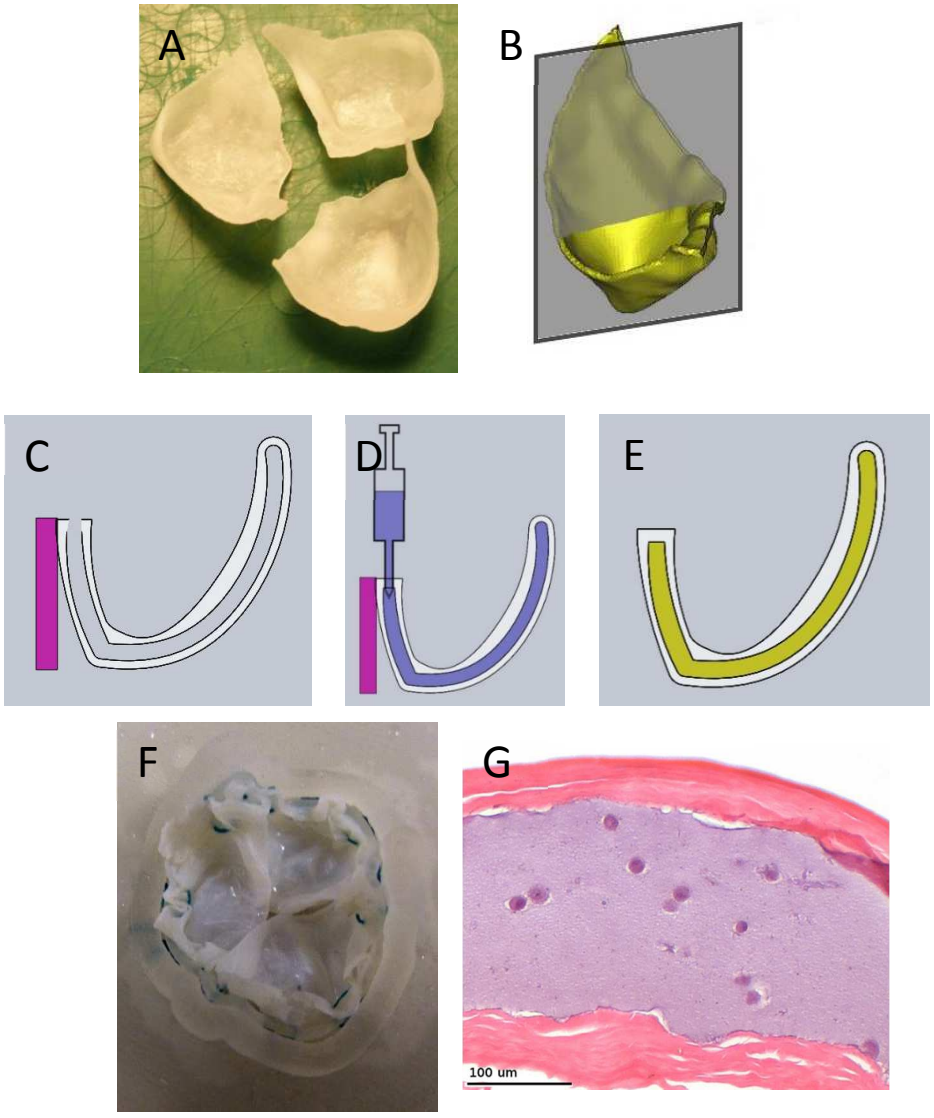

Figure 2.10. Cusps molds (A) are printed out of an ABS plastic-like material (3D systems Visijet SR200) on a rapid prototyper (3D Systems ProJet SD3000). Gray Plane (B) represents cross sectional view through cusp mold. Pericardium (white) is wrapped around the plastic valve mold (yellow) (C). The top of the pericardium is cut away and the mold is removed, leaving a void. The cusp is positioned inside the mounting ring (pink) (D). The cusp is secured by threading sutures through the holes in the mounting ring. Cell-seeded hydrogel (blue) is injected into the void between pericardial layers - through the edge nearest the mounting ring - to form the spongiosa layer (E). The assembled valve sits inside the bioreactor mounting ring (F). Cross-sectional view stained with H&E.

2.3.4 Trilayer Valves with Simplified Geometry for Hydrogel Durability Analysis

The valve with simplified geometry contained flat cusps, with a smooth interface between fibrous scaffolds and hydrogel. Valves were constructed from these cusps and tested in the heart valve bioreactor for 14 days. A similar "ballooning" of the cusps was observed in valves with simplified geometry. Histological analysis showed a break in the middle of the hydrogel, not at the hydrogel-tissue interface as hypothesized (**Fig 2.11 B**). Live/Dead staining of hydrogel removed from the valve showed viable cells after 14 days of bioreactor conditioning (**Fig 2.11 C**).

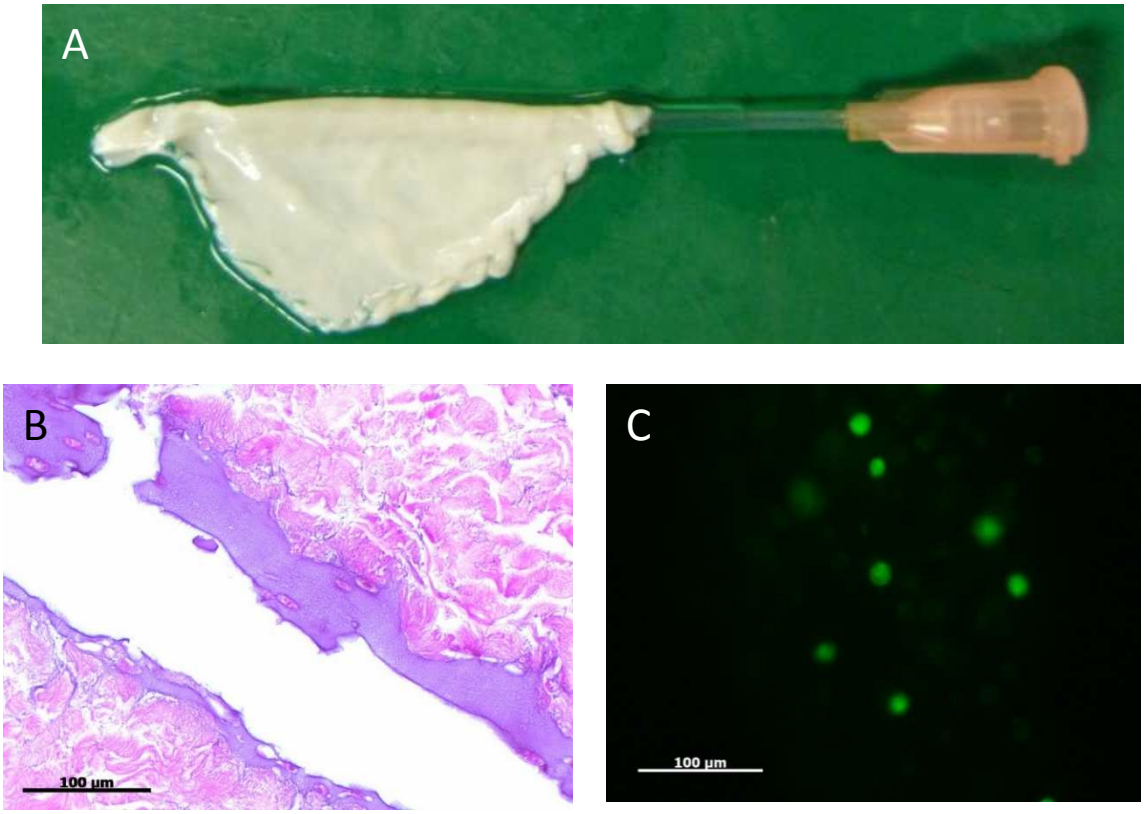

Figure 2.11. Simplified cusp geometry with blunt needle used to inject cusp with hydrogel (A). Hematoxylin and Eosin (H&E, dark purple = nuclei, pink = background substance) staining of trilayer scaffolds after 14 days in bioreactor (B). Live/Dead staining (green = live cells, red = dead cells) of gel extracted from the spongiosa layer after 14 days in bioreactor.

2.4 Discussion

The aortic valve has developed a specific geometry and a highly-organized internal trilayer structure that allows the thin tissue to maintain proper function in a mechanically-dynamic environment. Successfully replicating both valve geometry and internal structure would produce an ideal tissue-engineered heart valve. We developed an approach to reproduce both of these important features. Valve geometry was modeled from clinically-

relevant medical imaging data. Other valve geometry replication techniques rely on micro-CT scans[10] or a set of planar measurements[11] to produce custom valves, but obtaining a micro-CT scan of the valve is not an option clinical scenarios; our method of CTA scan-based geometry creation can be readily translated into clinical use.

Tissue-engineered scaffolds must allow for cell attachment and growth. In this study, fibrous scaffolds were treated with PGG, a naturally-derived collagen-binding polyphenol,[14] to assist in maintaining their molded geometry. Cells seeded on PGG treated scaffolds showed attachment, good viability, and replication over time. The fibrous scaffolds were robust enough to function in a heart valve bioreactor without complications. These finding are in agreement with the results of previous studies utilizing PGG treated scaffolds[12,13].

A hydrogel containing hyaluronic acid and gelatin was chosen to serve as the spongiosa layer. The native aortic valve spongiosa layer is largely composed of GAGs, such as hyaluronic acid, and collagen[15]. The Hystem gel was of similar composition to the native spongiosa, and therefore a logical representation. Hystem hydrogels have supported viable hADSCs at ten weeks in an *in-vivo* rabbit model, allowing cells to adopt an elongated fibroblast-like appearance[16]. hADSCs viability was confirmed by cell encapsulation and culture for seven days, confirmed by Live/Dead analysis. The cell seeding end goal was to have the resident stem cells interact with and remodel the gel in which they are seeded. Early studies showed a rounded cell morphology that was not

indicative of cell-gel interaction. The amino acid sequence RGD present in many ECM proteins binds to a wide variety of integrins[17], and is important to cell attachment and proliferation[18]. Pronectin - a synthetic polypeptide containing repeated RGD sequences[19] – was added to increase cell-gel interactions and promote cell integration into the scaffold.

Histological analysis of patient-specific valves showed a cohesive trilayer structure, with good connection between gel and fibrous scaffolds. However, when valves were tested in a pulse-duplicating bioreactor, a "ballooning" effect was observed. We hypothesize that shear forces placed on the valve during normal function disrupted hydrogel integrity. To further investigate the mode of failure, a new valve was constructed with simplified geometry; this valve had a flat, uniform interface between scaffolds, without the complicated patient-specific geometry. These valves did not withstand the bioreactor's forces. Further histological inspection revealed the presence of a thin hydrogel layer containing viable cells. These finding indicate that the spongiosa hydrogel's integrity was disrupted, and not the interface between gel and fibrous scaffold. A more mechanically-robust spongiosa was required for valve functionality.

2.5 Conclusions

This study demonstrated that CTA scans can be modeled, 3D printed, and used to create patient-specific heart valves. The valve scaffolds supported cell attachment, growth, and proliferation. The addition of pronectin to the spongiosa hydrogel had

significant effect on cell morphology. Functional testing revealed insufficiently-robust spongiosa scaffolds to be the cause of mechanical failure. Further studies into robust, moldable scaffolds shaped using the modeling process described could produce a mechanically-viable patient-specific heart valve.

2.6 Chapter 2 References

1. Dvir T, Timko BP, Kohane DS, Langer R. Nanotechnological strategies for engineering complex tissues. *Nat Nanotechnol*. 2011;6(1):13-22. doi:10.1038/nnano.2010.246.

2. Piazza N, de Jaegere P, Schultz C, Becker AE, Serruys PW, Anderson RH. Anatomy of the aortic valvar complex and its implications for transcatheter implantation of the aortic valve. *Circ Cardiovasc Interv*. 2008;1(1):74-81. doi:10.1161/CIRCINTERVENTIONS.108.780858.

3. Pibarot P, Dumesnil JG. Prosthesis-patient mismatch: definition, clinical impact, and prevention. *Heart*. 2006;92(8):1022-1029. doi:10.1136/hrt.2005.067363.

4. Blais C, Dumesnil JG, Baillot R, Simard S, Doyle D, Pibarot P. Impact of valve prosthesis-patient mismatch on short-term mortality after aortic valve replacement. *Circulation*. 2003;108(8):983-988. doi:10.1161/01.CIR.0000085167.67105.32.

5. Rao V, Jamieson WR, Ivanov J, Armstrong S, David TE. Prosthesis-patient mismatch affects survival after aortic valve replacement. *Circulation*. 2000;102(19 Suppl 3):III5-III9.

6. Pibarot P, Dumesnil JG, Lemieux M, Cartier P, Métras J, Durand LG. Impact of prosthesis-patient mismatch on hemodynamic and symptomatic status, morbidity and mortality after aortic valve replacement with a bioprosthetic heart valve. *J Heart Valve Dis*. 1998;7(2):211-218.

7. Pibarot P, Dumesnil JG. Hemodynamic and clinical impact of prosthesis-patient mismatch in the aortic valve position and its prevention. *J Am Coll Cardiol*. 2000;36(4):1131-1141.

8. Vesely I. Aortic root dilation prior to valve opening explained by passive hemodynamics. *J Heart Valve Dis*. 2000;9(1):16-20.

9. Dagum P, Green GR, Nistal FJ, et al. Deformational dynamics of the aortic root: modes and physiologic determinants. *Circulation*. 1999;100(19 Suppl):II54-II62.

10. Hockaday LA, Kang KH, Colangelo NW, et al. Rapid 3D printing of anatomically accurate and mechanically heterogeneous aortic valve hydrogel scaffolds. *Biofabrication*. 2012;4(3):035005. doi:10.1088/1758-5082/4/3/035005.

11. Labrosse MR, Beller CJ, Boodhwani M, Hudson C, Sohmer B. Subject-specific finite-element modeling of normal aortic valve biomechanics from 3D+t TEE images. *Med Image Anal*. 2015;20(1):162-172. doi:10.1016/j.media.2014.11.003.

12. Tedder ME, Simionescu A, Chen J, Liao J, Simionescu DT. Assembly and testing of stem cell-seeded layered collagen constructs for heart valve tissue engineering. *Tissue Eng Part A*. 2011;17(1-2):25-36. doi:10.1089/ten.TEA.2010.0138.

13. Tedder ME, Liao J, Weed B, et al. Stabilized collagen scaffolds for heart valve tissue engineering. *Tissue Eng Part A*. 2009;15(6):1257-1268. doi:10.1089/ten.tea.2008.0263.

14. Isenburg JC, Karamchandani N V, Simionescu DT, Vyavahare NR. Structural requirements for stabilization of vascular elastin by polyphenolic tannins. *Biomaterials*. 2006;27(19):3645-3651. doi:10.1016/j.biomaterials.2006.02.016.

15. Tseng H, Grande-Allen KJ. Elastic fibers in the aortic valve spongiosa: a fresh perspective on its structure and role in overall tissue function. *Acta Biomater*. 2011;7(5):2101-2108. doi:10.1016/j.actbio.2011.01.022.

16. Espandar L, Bunnell B, Wang GY, Gregory P, McBride C, Moshirfar M. Adipose-derived stem cells on hyaluronic acid-derived scaffold: a new horizon in bioengineered cornea. *Arch Ophthalmol*. 2012;130(2):202-208. doi:10.1001/archopthalmol.2011.1398.

17. Ruoslahti E. RGD and other recognition sequences for integrins. *Annu Rev Cell Dev Biol*. 1996;12:697-715. doi:10.1146/annurev.cellbio.12.1.697.

18. Hynes RO. Integrins: versatility, modulation, and signaling in cell adhesion. *Cell*. 1992;69(1):11-25.

19. Somamoto S, Tabata Y. Effect of ProNectin F derivatives on cell attachment and proliferation. *Acta Biomater*. 2013;9(2):5194-5200. doi:10.1016/j.actbio.2012.07.039.

CHAPTER 3: DEVELOPMENT AND CHARACTERIZATION OF TRILAYER SCAFFOLDS FOR HEART VALVE TISSUE ENGINEERING

3.1 Introduction

3.1.1 Research Motivation and Aim

Due to its mechanically-demanding environment, the aortic valve has a highly-organized structure capable of coping with the myriad of forces placed upon it. The aim of this research is to replicate the trilayer structure of native valves. Biological scaffolds were used to recreate the native structure of the valve - consisting of fibrosa, spongiosa, and ventricularis layers. Decellularized porcine pericardium (fibrous scaffold) was used for the fibrosa and ventricularis layers, while the spongiosa layer was created from decellularized, elastase-treated porcine pulmonary artery (spongy scaffold). The scaffolds were rendered porous (and thus more readily recellularized) through treatment with acetic acid followed by lyophilization. The trilayer structure of the valve was then recreated by gluing the fibrous and spongy scaffolds with bovine serum albumin-glutaradehyde (BSAG) glue will be used to join the three scaffold layers to form single cohesive valve scaffold.

A previous iteration of the trilayer scaffold failed during functional testing due to insufficient mechanical strength of the spongiosa layer. This research presents a new spongy scaffold and assembly technique that results in a robust, trilayer scaffold.

3.2 Materials and Methods

3.2.1 Materials

Cusp molds were printed using a 3D Systems ProJet SD3000 printer using multijet technology to produce parts from an ABS-like plastic photopolymer - VisiJet SR200 and VisiJet s100 support material from 3D systems (Rock Hill, SC). Thick pericardial tissues were obtained from Animal Technologies, Inc. (Tyler, TX). Thin pericardial tissues and porcine pulmonary arteries were obtained from Tissue Source LLC (Lafayette, IN). Porcine hearts were a generous gift from snow creek meat processing (Seneca, SC). High purity porcine elastase was supplied by elastin products company (Owensville MO). Micro needle rollers were manufactured by Melodysusie (Newark, CA). All other chemicals were of highest purity available and were obtained from Sigma-Aldrich Corporation (Lakewood, NJ).

3.2.2 Fibrous Scaffold Preparation

Fibrous scaffolds were prepared following a decellularization protocol consisting of detergent and nuclease treatments as previously described, with minor modifications[6] as described in section 3.2.3.

3.2.3 Spongy Scaffold Preparation.

Spongy collagen scaffolds to be used as the spongiosa layer of the cusp were prepared following a previously published protocol, with slight modifications[67]. Briefly, Fresh tissues (Tissue Source) were received as intact pulmonary arteries approximately 8 cm in length starting from the pulmonary valve and ending near the first branches of the artery. Tissues were cut lengthwise and laid flat to form a rectangular scaffold. Tissue were placed in hypotonic conditions in pure, double-distilled water for 24 hours at 4ºC for cell lysis. Tissues were rinsed with double-distilled water and transferred to a sterile bottle. All further steps were done with sterile solutions with aseptic techniques. To remove cellular remnants, tissues were treated with one liter of detergent solution consisting of 50mM Tris, 0.15% v/v Triton x-100, 0.25% Deoxycholic acid-sodium salt. 0.1% EDTA, and 0.02% Sodium Azide for 3 days at room temperature on a shaker plate. The detergent solution was replaced and the tissues were treated for an additional 3 days. Tissues were then washed to remove the detergent solution. All washes were performed at room temperature on a shaker plate for 30 minutes. Two washes with double-distilled water were followed by two washes in 70% ethanol. Tissues were then washed twice more with double-distilled water. Removal of residual nucleic acids was achieved by treatment for 24 hours at 37ºC with 360 mUnits per mL of both deoxyribonuclease and

ribonuclease dissolved in phosphate buffered saline containing 5 mM MgCl at a pH of 7.5. Tissues were washed as previously; twice with double-distilled water, 70% ethanol, and double-distilled water again. Next, an elastase solution was applied to degrade elastin fibers and create more hydrated scaffold. The elastase solution consisted of 10 units/mL elastase in a 50 mM Tris buffer containing 1 mM $CaCl_2$, and 0.02% NaN_3 at a pH of 8.0. Porcine pulmonary arteries were treated for six days at 37°C. Elastase solution was changed after 3 days. Finally, tissues were washed as previously; twice with double-distilled water, 70% ethanol, and double-distilled water again and stored at 4°C in PBS with 0.02% sodium azide.

3.2.4 Preparation of Human Heart Valve Tissue

A human heart was provided through the national disease research interchange (NDRI Philadelphia, PA). The heart was not diseased and was from a 68 year old Caucasian male who died of multisystem organ failure. The heart was delivered in DMEM + antibiotics. Upon receiving, the heart was washed in PBS and fixed in 10% neutral buffered formalin. Valves were dissected and processed for histology as described in section 3.2.9.

3.2.5 Bovine Serum Albumin Glue Preparation

Bovine serum albumin (BSA) was obtained at a concentration of 45%. BSA concentration was increased to 55% by slowly adding dry BSA powder while gently stirring to dissolve BSA without causing excess frothing of the solution. The 55% BSA solution was

sterile filtered using a Steriflip (EMD Millipore) and kept at 4°C until use. 50% biological grade glutaraldehyde was diluted to 10% with double-distilled water and sterile filtered prior to use.

3.2.6 Increasing Porosity of Fibrous and Spongy Scaffolds

Scaffold porosity was increased to allow for effective gluing and cell infiltration. Scaffolds were first washed to remove residual sodium azide indouble-distilled water three times, shaking, for ten minutes at room temperature. Poration was achieved following a protocol similar to that used by Chang et al[8,9]. Briefly, glacial acetic acid was diluted to 0.2M. Scaffolds were treated with 0.2M acetic acid for 1 hour at room temperature under gentle agitation. Scaffolds were removed and placed in petri dishes, these dishes were placed in a sterile bag and then immediately moved to a -80°C freezer and allowed to freeze overnight. A lyophilization flask was sterilized and fitted with a sterile filter between the flask and the tube leading to the vacuum chamber. Petri dishes containing frozen scaffolds were transferred to the flask under aseptic conditions. The scaffolds were lyophilized for 72 hours with a collector temperature of -48°C and a vacuum below 0.080 mBar.

3.2.7 Assembly of Trilayer Scaffolds

Trilayer scaffolds were assembled in two ways; with dry scaffolds and with wet scaffolds. Both methods were done according to the following protocol. However, wet assembled scaffolds were first rehydrated in PBS before being cut and glued together.

Fibrous porous scaffolds (both wet and dry) were folded around a cusp-shaped mold designed to mimic the cusp shape in the Edwards Perimount valve. The fibrous scaffold was trimmed along the edge of the mold, the mold was removed, and the scaffold was layed flat. Porous, spongy scaffolds were trimmed using the same mold, but were not folded over the mold. Instead the mold was placed on top of the spongy scaffold and a scalpel was used to trim the scaffold to shape. Next, 55% BSA was pipetted onto the dry fibrous scaffold at 10µL per cm^2. The edge of the pipette was used to spread the BSA evenly across the surface of the scaffold. Immediately after application of BSA, 10% glutaraldehyde solution was misted onto the fibrous scaffold. The spongy scaffold was quickly set into place and the fibrous scaffold was folded in half and pressed firmly in place for 30 seconds. Dry trilayer scaffolds were then rehydrated in PBS.

3.2.8 Micro Needle Roller Treatment.

Micro needle roller treatments were done to allow seeded cells access to the interior of the scaffolds. Trilayer scaffolds were treated with acetic acid as described in section 3.2.5. However, the acetic acid treatment was used to swell the tissues, not to cause further poration. Accordingly, trilayer scaffolds were immersed in 0.2M acetic acid for 20 minutes. Tissues were frozen and lyophilized as previously described. All techniques were done aseptically. Dry trilayer scaffolds were removed from the lyophilizer and placed on a self-healing cutting mat (Harris). Micro needle rollers consisting of 540 stainless steel needles uniformly arranged around a polystyrene drum were used to create many small punctures through the scaffold surface.

3.2.9 Histology

Thin 5µm sections of paraffin-embedded samples were washed in xylene and rehydrated through a series of alcohol washes ending in deionized water. These sections were stained with hematoxylin and eosin and Mason's Trichrome (Richard-Allen Scientific, Thermo Scientific) to show general scaffold morphology and to identify cell location. Digital images of these slides were obtained at various magnifications (25X to 200X) on a Zeiss Axiovert 40CFL microscope using AxioVision software (Carl Zeiss MicroImaging, Inc. Thornwood, NY).

3.2.10 Scanning Electron Microscope Imaging

To prepare for SEM imaging samples were fixed overnight in Karnovsky's; a solution of 2% paraformaldehyde and 2.5% glutaraldehyde buffered in 0.2M cacodylic acid. Samples were than dehydrated in a graded series of ethanol moving from 35%, 50%, 70%, 95%, and 100% each for 30 minutes. Samples were then placed in pure Hexamethyldisilazane (HMDS). HMDS was allowed to fully evaporate in a fume hood. Samples were then mounted on metal stubs with double sided tape and sputter coated with platinum. Scaffolds were imaged with a Hitachi TM3000 tabletop backscatter SEM using a 15kV beam.

3.2.11 Mechanical Testing

Fibrous scaffolds were assumed to be isotropic and were cut into 10x20 mm sections without regard to collagen fiber orientation. Fresh porcine hearts were obtained from snow creak meat processing. Fresh aortic valves were excised from the heart and tested immediately. Aortic valves were cut into 10x10 mm strips, with only one section harvested per cusp. Cusps were sectioned in both radial and circumferential directions. Samples were clamped into a MTS load frame (MTS system Corp. Eden Prarie, MN) and wetted with PBS throughout testing. Uniaxial tensile tests were performed by preloading the scaffolds to 0.01N and extending to failure at a rate of 5mm/min using a 100N load cell. Results were collected in Testworks 4 software (MTS system Corp.) and exported for analysis as comma delimited files.

3.2.12 Statistical analysis

Results are expressed as means ± standard deviations (SD). For normally distributed data with equal variances, unpaired t-tests were used to compare means. Welch's correction was applied to means with different variances. To compare multiple means, a one-way analysis of variance was performed (ANOVA) with Tukey's multiple comparison test using multiplicity adjusted P values. P values less than 0.05 were considered statistically significant. Statistical significance is indicated as follows, ns if $P > 0.05$, * if $P \leq 0.05$, ** if $P \leq 0.01$, *** if $P \leq 0.001$, and **** if $P \leq 0.0001$. Analysis was carried out in GraphPad Prism 6 (Graphpad Software, La Jolla, CA).

3.3 Results

3.3.1 Fibrous and Spongy Scaffold Characterization

Decellularization and poration steps produced robust, flat, fibrous sheets of collagen (**Fig. 3.1A**) to be used as fibroas and ventricularis layers. After treatment with elastase, spongy scaffolds were highly hydrated, gel-like structures that resulted in extremely porous collagen scaffolds when dried (**Fig 3.1B**). Histological analysis of fibrous scaffolds shows complete removal of cells from both scaffolds after decellularization steps. The fibrous scaffold consists of thick, rope-like collagen fibers with little spacing between them. Elastase treatment of spongy scaffolds results in a loose network of fine collagen strands without any of the elastic fibers (red) seen in the fresh tissue. Poration produces a fibrous scaffold that still contains rope-like collagen fibers, but has large pores distributed throughout the scaffold. Porous spongy scaffolds contain very fine collagen fibers and large, empty pores (**Fig 3.2**).

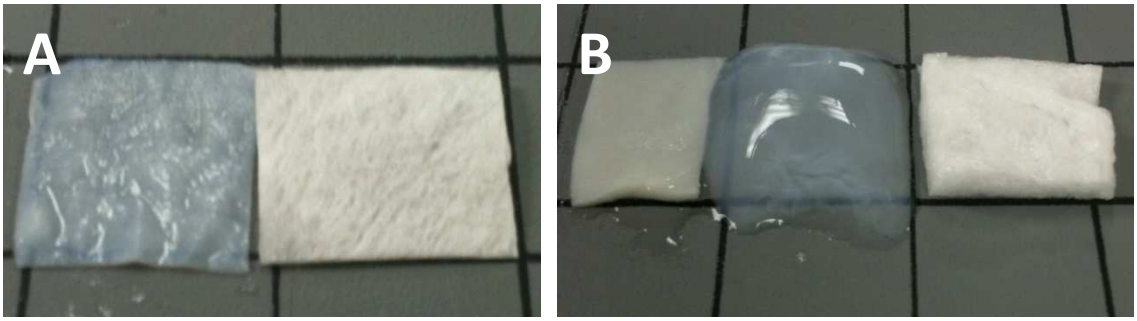

Figure 3.1. Fibrous Scaffolds (A) Nonporous on the left and porous on the right. Spongy scaffolds (B) from left to right fresh, Decellularized and elastase treated, and porous.

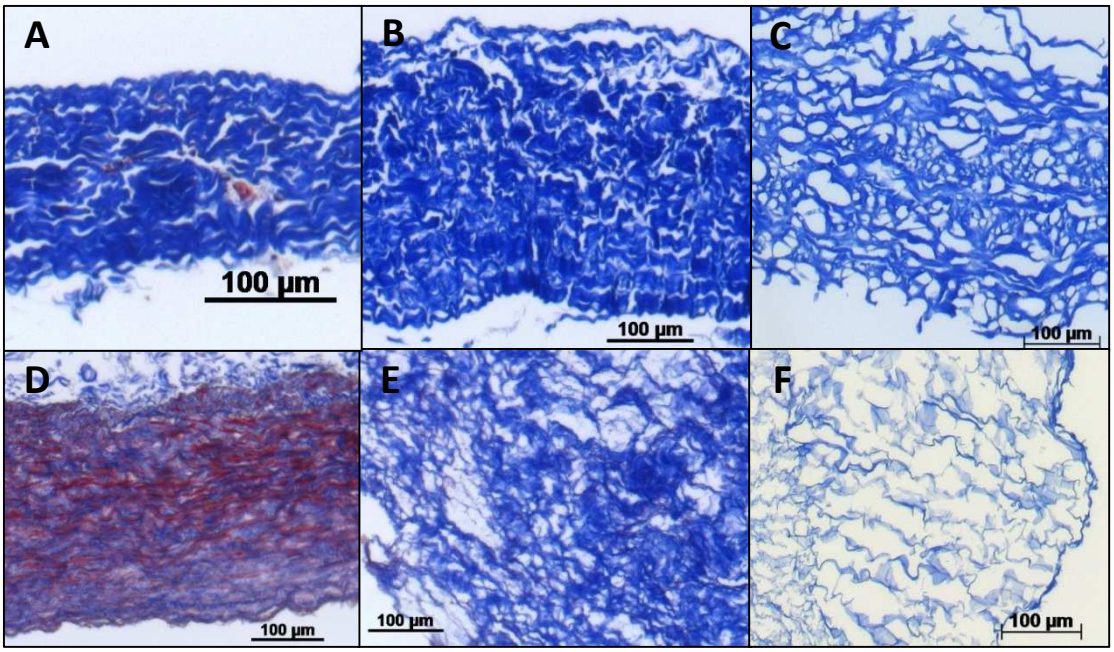

Figure 3.2. Mason's Trichrome (Nuclei =black, Cytoplasm and intercellular fibers = red, collagen = blue) images of fibrous (top row) and spongy (bottom row) scaffolds. Fresh (A,D) Decellularized (B,E) and porous (C,F) scaffolds are shown.

3.3.2 Trilayer Cusp Creation

Trilayer cusps were produced by gluing a spongy scaffold between a folded fibrous scaffold with 55% BSA adhesive. The resulting cusp has three layers. The fibrosa and ventricularis portions, made of fibrous scaffold, and the middle spongiosa layer made of spongy scaffold (**Fig 3.3**).

Applying BSA to a dry scaffolds allows the glue to partially infiltrate the scaffolds being joined, allowing for a strong bond that will not shear apart under physiological mechanical loads. Mason's trichrome shows regions of red and blue overlap where the

BSA glue (red) has bound tightly to collagen fibers (blue) in adjacent regions of both fibrous and spongy scaffolds (**Fig 3.4**).

Cross sectional SEM images show the importance of assembling the scaffolds while dry. BSA glue (**Fig 3.5A** – white arrow) is applied as a liquid to the dry porous scaffold and can infiltrate the pores immediately adjacent to the interface between scaffolds, allowing for a strong bond. Achieving the same effect with wet scaffolds would require the glue to displace the water in the adjacent pores, which does not occur. Instead, a flat plane of glue forms a weak bond with adjacent scaffolds, leading to separation between layers (**Fig 3.5B** – white arrow).

The goal of using two separate scaffolds to create three layers was to mimic the histoarchitecture of the native valve. When stained with Mason's Trichrome and viewed side by side (**Fig 3.6**) the structural similarities between trilayer scaffolds and the human valve are apparent. Both are of similar thickness, with a fibrosa composed of rope-like collagen fibers. Both scaffolds contain a hydrated, porous spongiosa layer in the middle. The human valve has a ventricularis composed of collagen and elastin, while the trilayer valve's ventricularis layer is purely collagen.

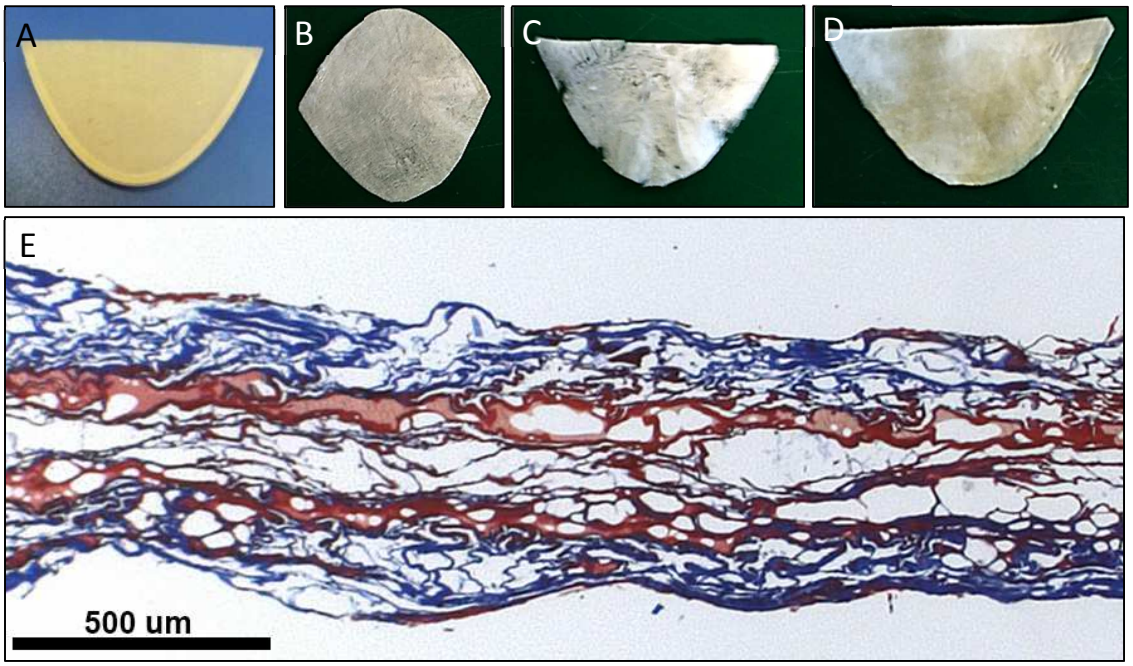

Figure 3.3. Plastic mold (A) used to shape fibrous (B) and spongy scaffolds (C). The scaffolds are glued together to for a trilayer cusp (D). Resulting trilayer construct (E) is shown stained with Mason's Trichrome (Collagen = blue, BSA glue = red).

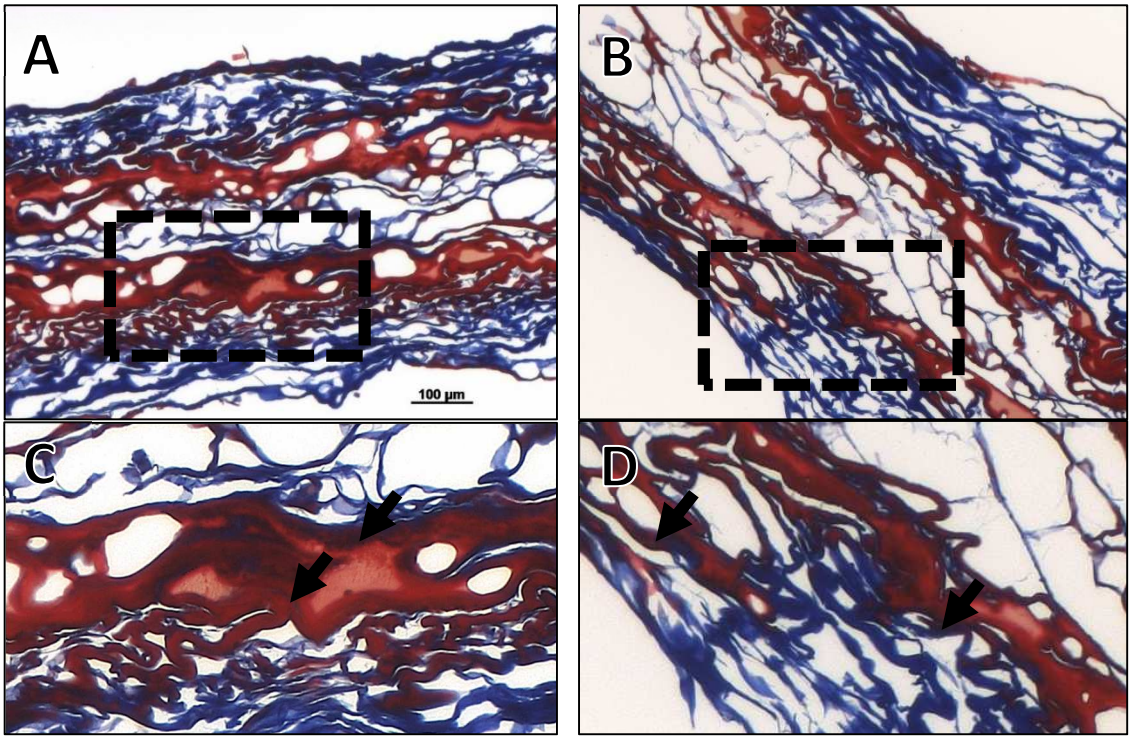

Figure 3.4. Trilayer constructs (A,B) are shown in Mason's Trichrome stain (Collagen = blue, BSA glue = red). Boxes indicate magnified regions. Regions of red and blue overlap (indicated by black arrows) show BSA glue infiltrating both adjacent scaffolds to produce one cohesive trilayer structure (C,D).

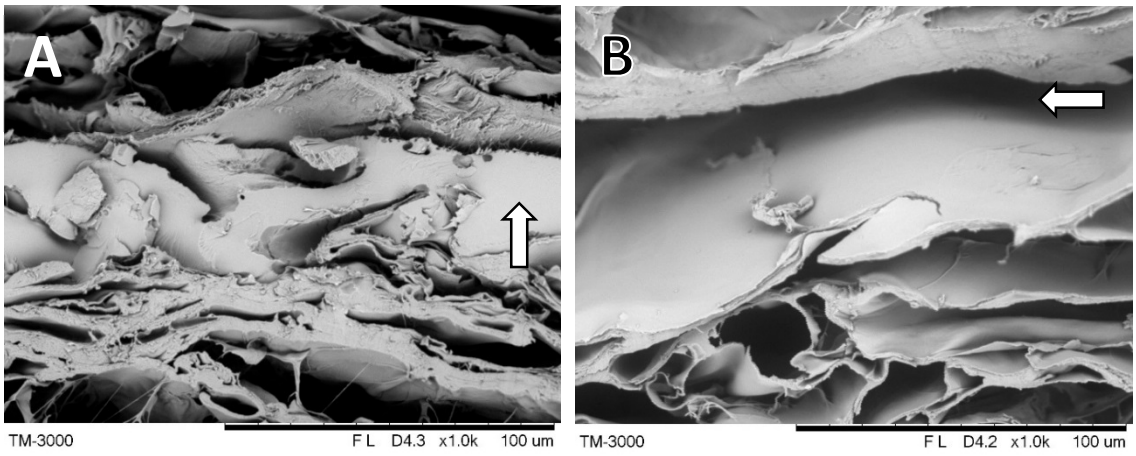

Figure 3.5. Cross sectional SEM images of trilayer scaffold glued while dry (A) and wet (B). White arrows indicate interfaces between fibrous and spongy scaffolds.

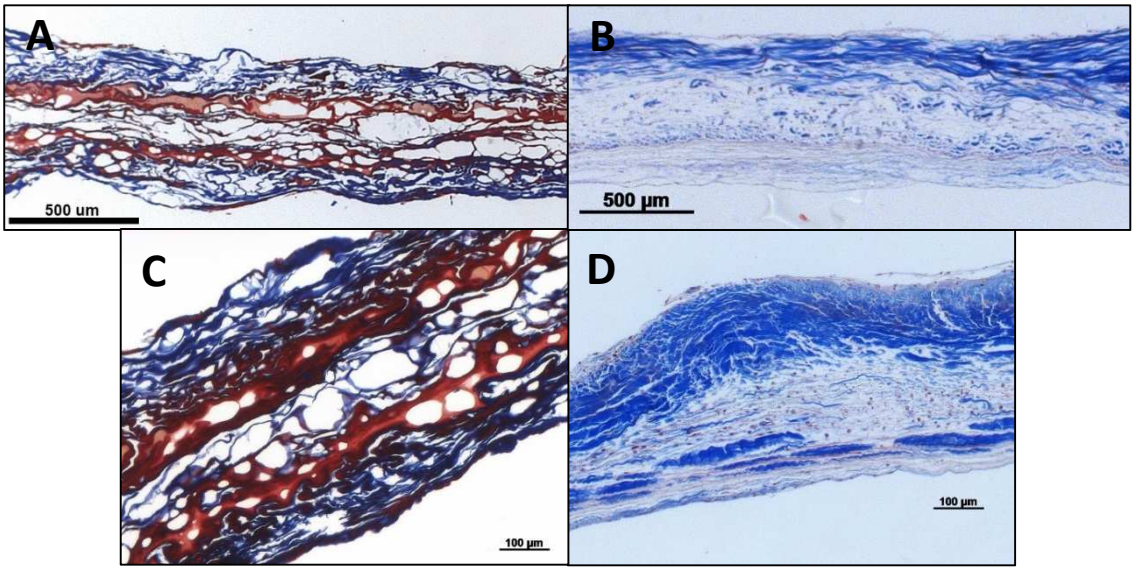

Figure 3.6. Structural similarities between trilayer scaffold (A,C) and adult human aortic heart valve (B,D) stained with Mason's Trichrome.

3.3.3 Physiologically Relevant Mechanical Loading Conditions

UTS, peak modulus, and strain at break values provide useful information about the mechanical behavior of biological tissues. However, these values all occur well outside of physiologically relevant conditions. Maximum in-vivo stresses and strains during a normal cardiac cycle have been calculated by several groups. A meta-analysis of these studies provided a range of maximum physiological stresses and strains in a normally functioning aortic valve. Circumferential stress values ranged from 118kPa to 930kPa[10,11]. However, most studies have reported values between 400kPa and 550kPa[12–16]. Normal maximum circumferential strains lie between 5% and 16%[14,16–19]. Radial strains have been reported in the range of 15%-27%[10,18,19]. Stradins et al. performed uniaxial tensile tests in

both circumferential and radial directions on aortic valves harvested from 11 healthy cadaveric hearts (**Figure 3.9**)[20]. The bounds of normal physiological stress and strain ranges from the meta-analysis have been reconciled with the Stradins curves to produce a theoretical normal physiological range of stresses and strains in both circumferential (**Fig 3.9 – red box**) and radial (**Fig 3.9 – green box**) directions. This data provides target mechanical propertied for tissue engineered valves to replicate.

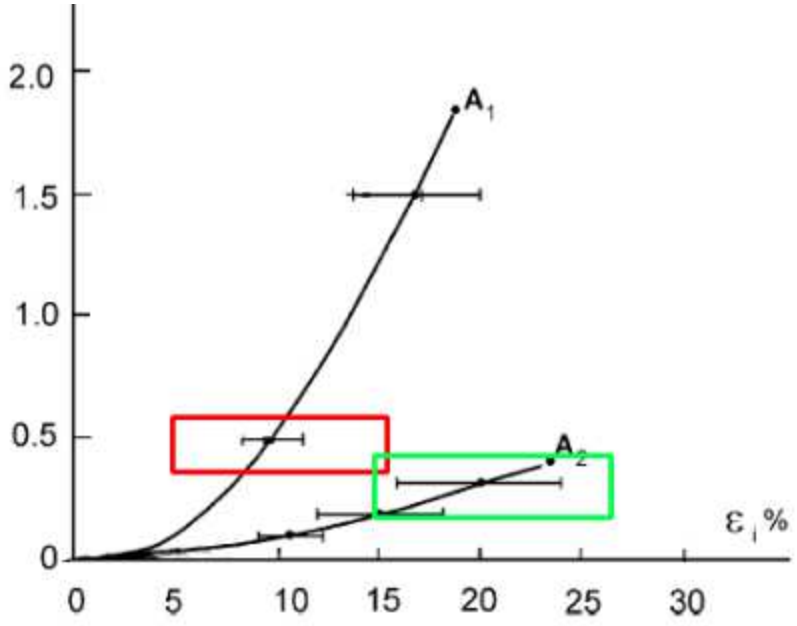

Figure 3.7. Stress-Strain behavior of human aortic valve cusps in circumferential (A_1) and Radial (A_2) directions. Boxes represent normal physiological maximum stress-strains in circumferential (red) and radial (green) directions. Adapted from[20].

3.3.4 Mechanical Analysis of Fresh Aortic Valves

Uniaxial tensile testing showed distinct anisotropic properties in fresh porcine aortic heart valves. Representative stress/ strain curves for samples cut in both radial and

circumferential directions are shown (**Fig 3.8**). Circumferential samples show relatively little stress in the initial stain range of 0-10%. There is a transition period between 10-15% strain after which the stress rises rapidly from 15% strain until break. Radially aligned samples experienced significantly less stress at the same strains. Circumferential samples had significantly higher ultimate tensile strength, peak modulus, and secant modulus at a strain of 10% and a lower strain at break than radial samples (**Fig 3.9**).

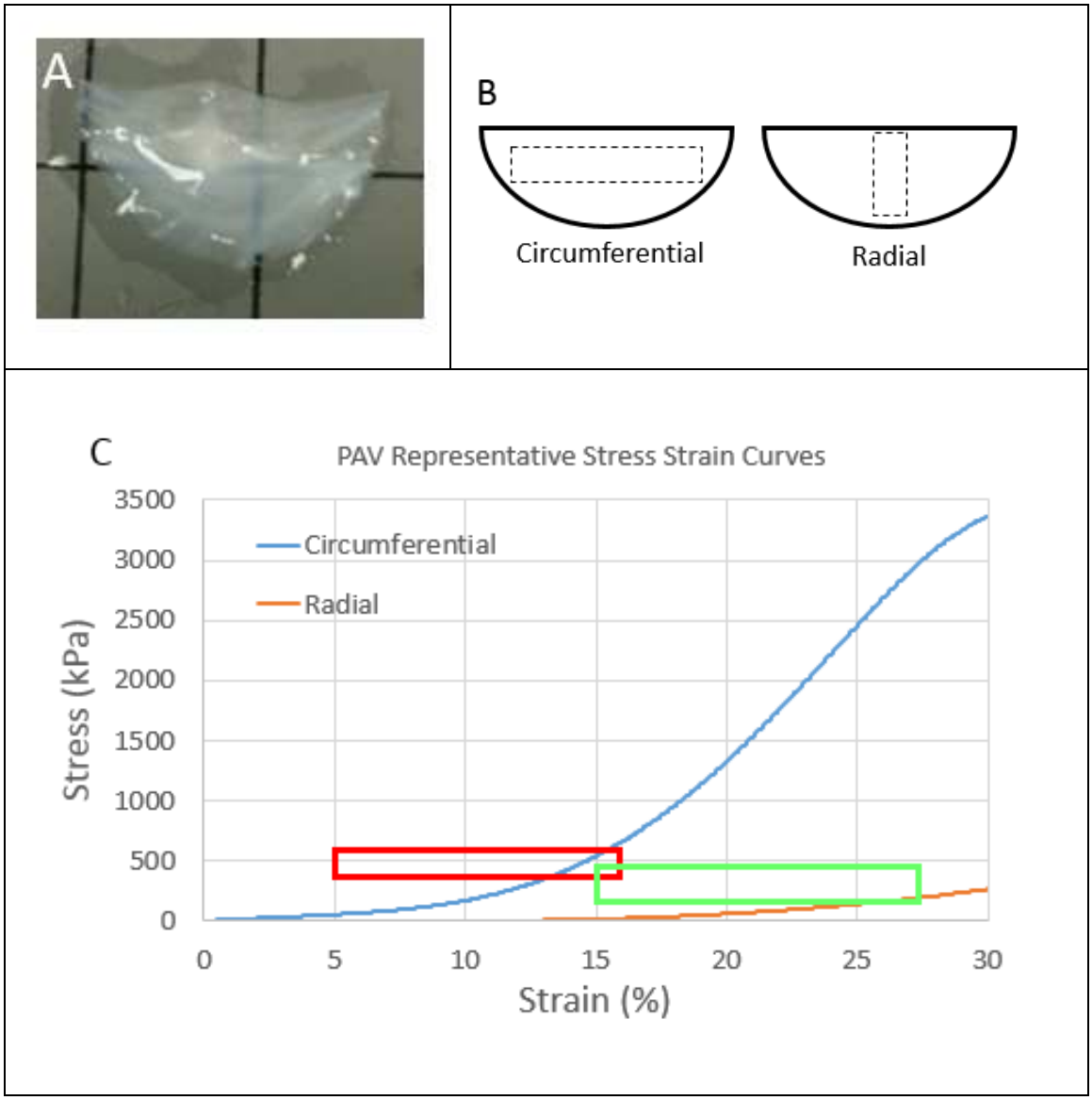

Figure 3.8. Fresh porcine aortic valve (A) used for mechanical testing. Strips were cut in circumferential and radial directions (B). Representative stress-strain curves for circumferential and radial samples are shown in (C) with maximum physiological boundaries for circumferential (red box) and radial (green box) shown.

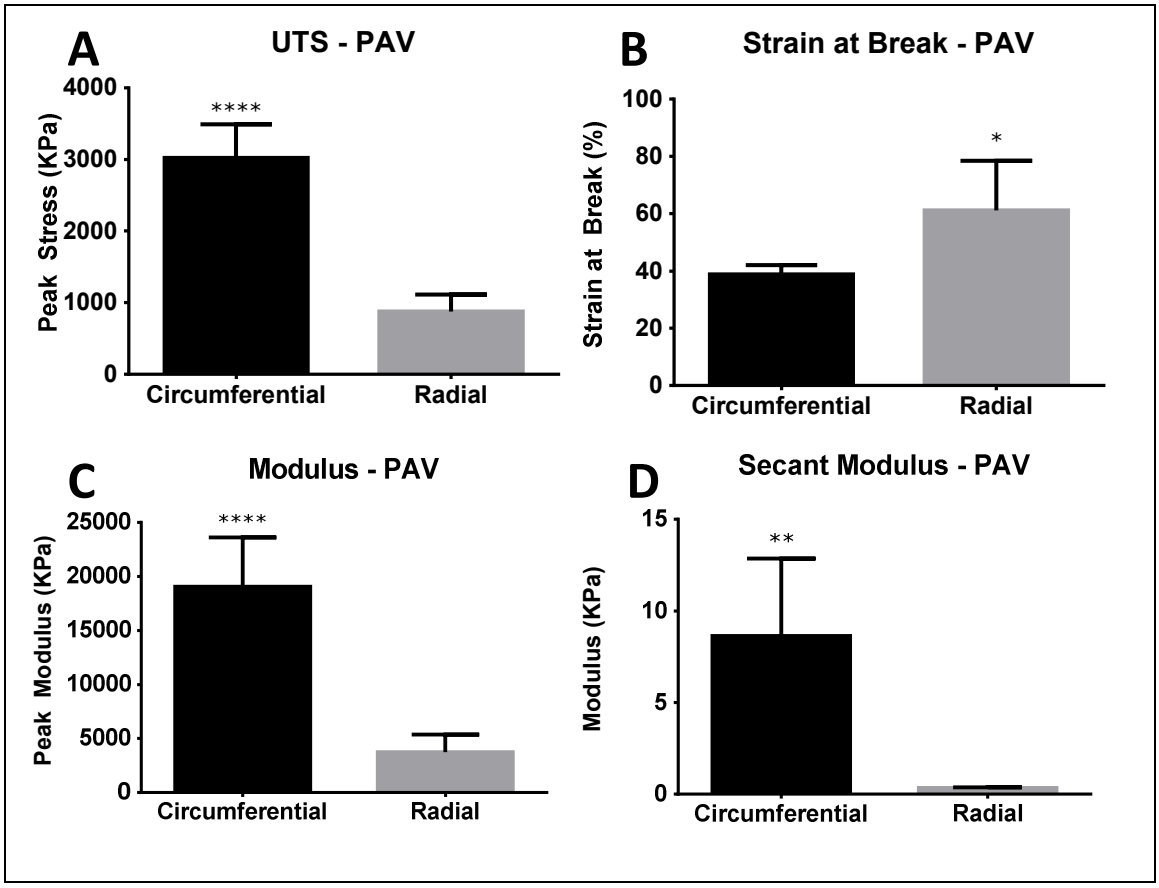

Figure 3.9. Tensile testing confirmed the anisotropic properties of native heart valves. Ultimate tensile strength (A), strain at break (B), peak modulus (C), and secant modulus at a strain of 10% (D) are shown for circumferential and radial samples.

3.3.5 Mechanical Analysis of Fibrous Scaffolds

Uniaxial tensile testing was performed on fibrous scaffolds to assess the impact of increasing porosity and microneedle rolling on fibrous scaffold mechanical properties. Representative stress/ strain curves for decellularized (NonPorous), porous, porous rolled 6 times (6 Roll), porous rolled 14 times (14 Roll), and trilayer scaffolds are shown (**Fig 3.11**). Results for ultimate tensile strength (UTS), elongation at break, peak modulus, and secant modulus at a strain of 10% are depicted in the following figures. Tukey's multiple

comparison test with multiplicity adjusted P values gives an exact P value for each comparison between means. These P values are shown in the tables below each graph (non-significant differences = red, significant differences = light green).

Increasing scaffold porosity did not significantly lower UTS. However, microneedle roller treatment did significantly lower the UTS of fibrous scaffolds. Trilayer scaffolds had a significantly lower UTS than all other scaffolds (**Fig 3.12**). Porous scaffolds had significantly higher strain at break values than nonporous scaffolds. Microneedle rolling of porous scaffolds did not significantly increase strain at break. There was no significant difference between trilayer and nonporous scaffold strain at break values (**Fig 3.13**). Poration and microneedle rolling treatments both caused significant reductions in peak modulus values. Trilayer scaffolds had a significantly lower peak modulus when compared to nonporous scaffolds and no difference when compared to porous and microneedle rolled scaffolds (**Fig 3.14**). Secant modulus at 10% strain is an indication of scaffold stiffness at a physiologically relevant strain. Nonporous and trilayer scaffolds were not significantly stiffer when directly compared, and were significantly stiffer than both porous and microneedle rolled scaffolds (**Fig 3.14**).

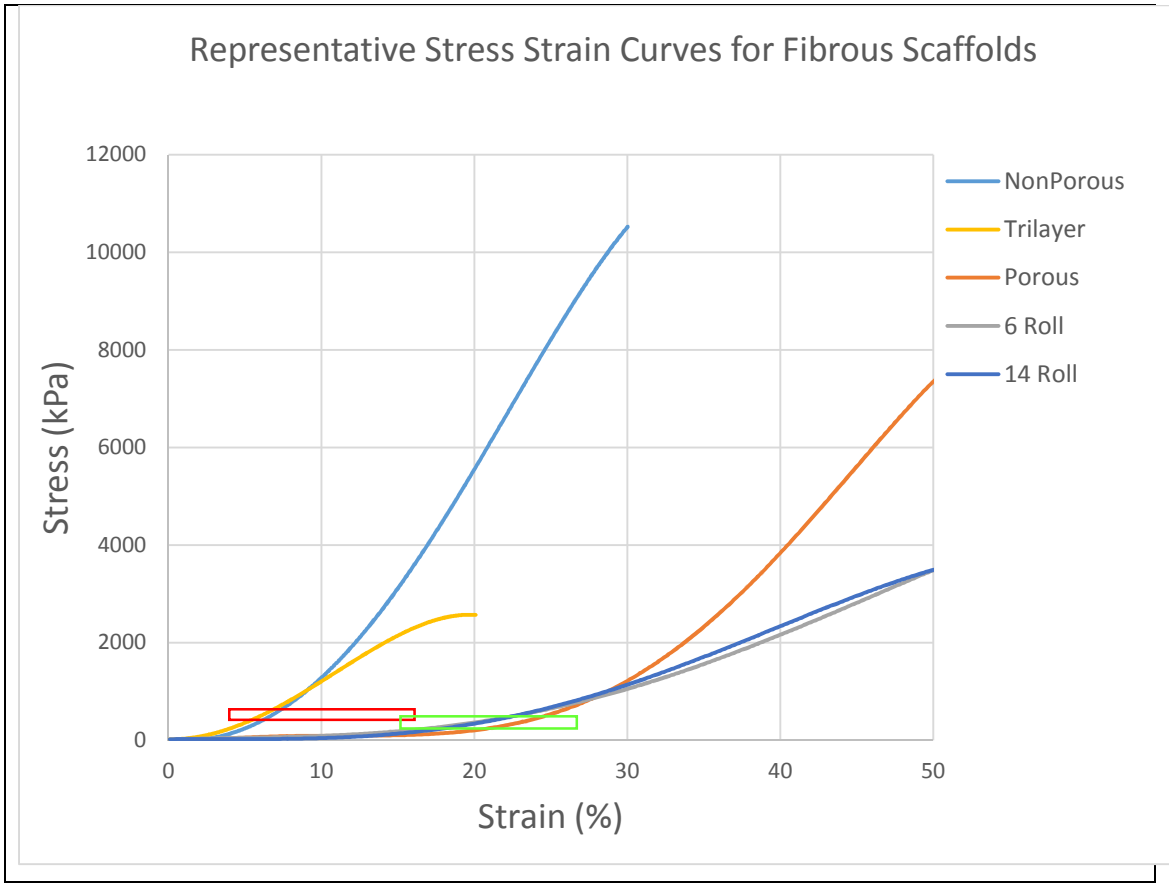

Figure 3.11. Representative stress-strain curves for fibrous scaffolds. Maximum physiological boundaries for circumferential (red box) and radial (green box) shown

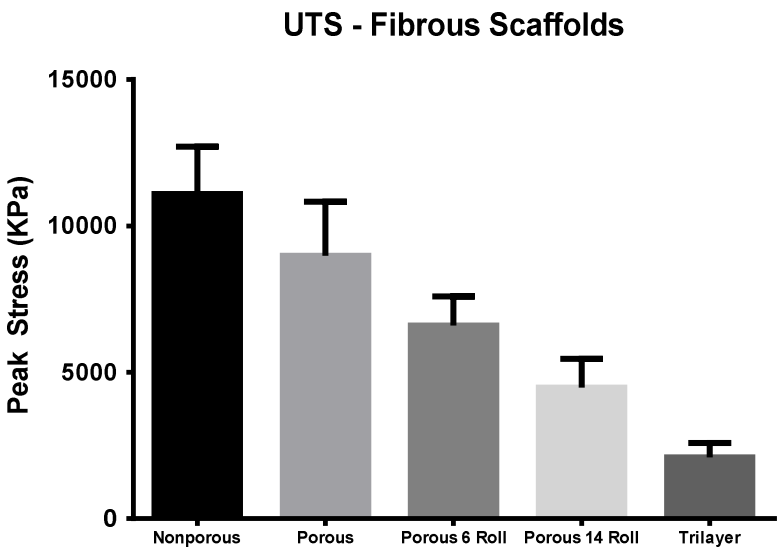

	Porous	Porous 6 Roll	Porous 14 Roll	Trilayer
NonPorous	ns	0.0003	< 0.0001	< 0.0001
Porous		0.0469	< 0.0001	< 0.0001
Porous 6 Roll			0.1091	0.0005
Porous 14 Roll				0.0846

Figure 3.12. Ultimate tensile strength of fibrous scaffolds (top). P values for comparison between means (bottom).

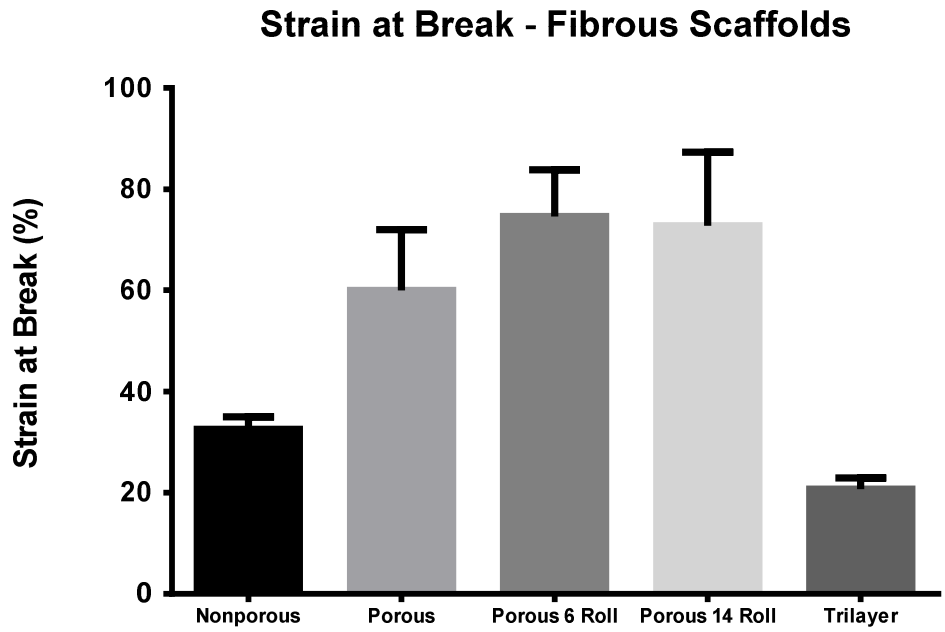

	Porous	Porous 6 Roll	Porous 14 Roll	Trilayer
NonPorous	0.0012	< 0.0001	< 0.0001	0.4416
Porous		0.14	0.1982	< 0.0001
Porous 6 Roll			0.9982	< 0.0001
Porous 14 Roll				< 0.0001

Figure 3.13. Strain at break of fibrous scaffolds (top). P values for comparison between means (bottom).

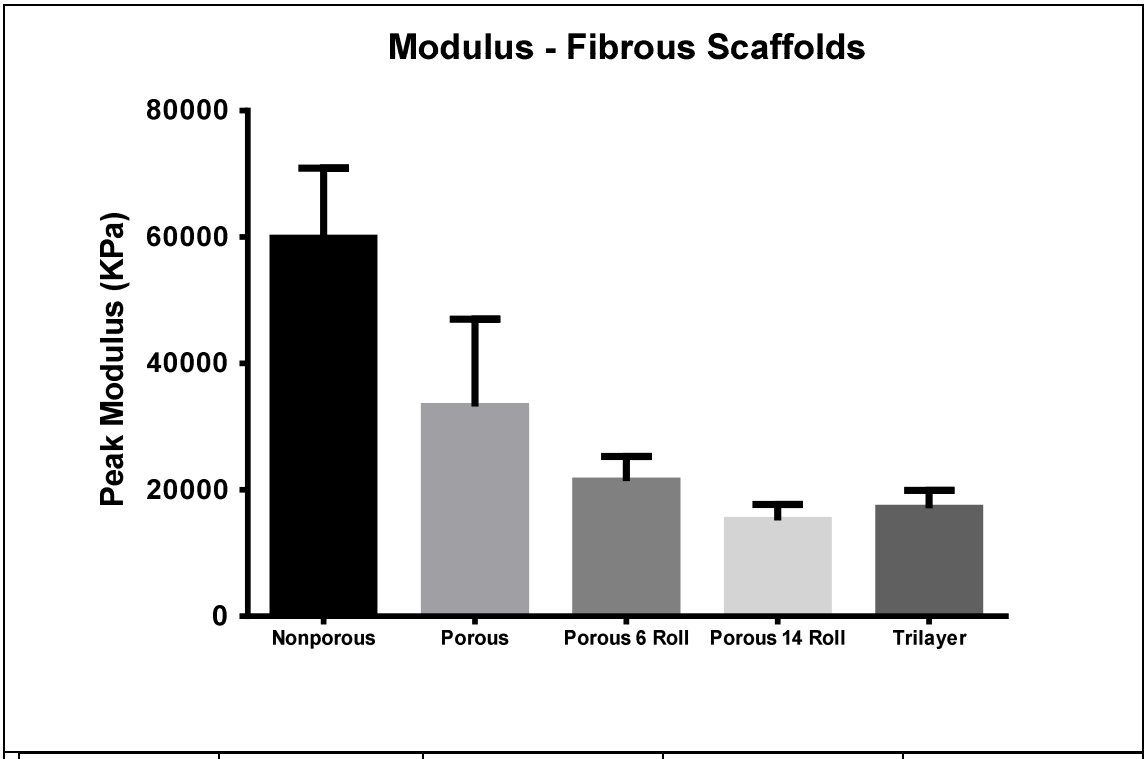

	Porous	Porous 6 Roll	Porous 14 Roll	Trilayer
NonPorous	0.0004	< 0.0001	< 0.0001	< 0.0001
Porous		0.1993	0.0118	0.0601
Porous 6 Roll			0.7762	0.948
Porous 14 Roll				0.9973

Figure 3.14. Peak modulus of fibrous scaffolds (top). P values for comparison between means (bottom).

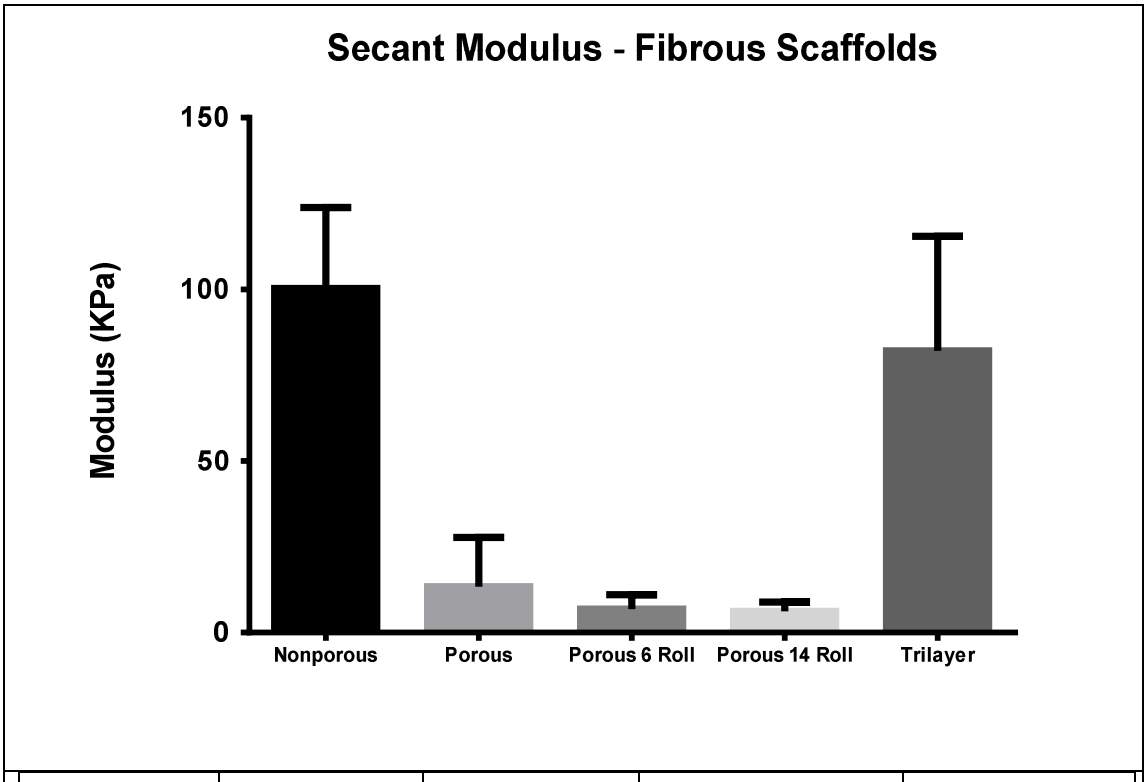

	Porous	Porous 6 Roll	Porous 14 Roll	Trilayer
NonPorous	< 0.0001	< 0.0001	< 0.0001	0.555
Porous		0.9682	0.9474	< 0.0001
Porous 6 Roll			> 0.9999	< 0.0001
Porous 14 Roll				< 0.0001

Figure 3.15. Secant modulus at strain=10% of fibrous scaffolds (top). P values for comparison between means (bottom)

3.4 Discussion

The results presented in this chapter demonstrate the successful development of a trilayer scaffold that replicates the native histoarchitecture of the aortic valve while maintaining robust mechanical properties. The scaffold presented in chapter two incorporated patient-specific design and a trilayer structure, but was unable to remain intact when subjected to functional testing. The new scaffold was developed with

mechanical strength and resistance to internal delamination of layers as primary considerations. The most notable differences in this new scaffold are the use of a biological spongiosa scaffold, BSA glue to bind layers, and the introduction of porosity and microneedle treatments. A full characterization of the scaffold with emphasis placed on the rationale behind implementing these differences is presented. The effect of microneedle rolling on cellular repopulation of the valve will be discussed in further detail in chapter four.

3.4.1 Increasing Porosity and Dry Assembly of Scaffolds

Porcine pericardium is a widely used and well researched scaffold for prosthetic heart valve creation[21]. This tissue is available in flat collagenous sheets of near uniform thickness and has excellent mechanical strength while remaining thin and flexible[22]. These properties make it an excellent choice for the outer layers of the trilayer scaffold.

The primary role the pericardium is to maintain a thin layer of lubricating pericardial fluid around the heart. The dense collagenous composition of the pericardium is responsible for its excellent mechanical strength and impermeability to fluids[23]. However, this same dense structure causes difficulties in binding scaffold layers together and prevents cells from rapidly repopulating the scaffold *in-vitro*. The same issues are present in the porcine pulmonary artery, the source for the spongiosa scaffold.

The scaffolds forming the trilayer leaflets are glued together with a thin layer of 55% BSA crosslinked with 10% glutaraldehyde. Decellularized porcine pericardium

presents a nearly un-broken, dense sheet of collagen on its surface, specifically designed to prevent liquids from penetrating. Applying BSA to this surface results in a weak bond due to poor integration into the scaffold. The process of swelling, freezing, and drying the scaffold creates a surface that BSA glue will infiltrate, leading to a strong bond between scaffolds.

Collagen swells in acetic acid[24], loses fibrillary appearance and may partially dissolve to yield a viscous solution[25]. Increasing H^+ ions allows water to access the collagen fibers. This water is held in by electrostatic forces between charged polar groups (electrostatic swelling) or by hydrogen bonding between uncharged polar groups and negative atoms (lyotropic hydration)[26]. The end result of the acetic acid treatment is a disruption of interchain collagen binding, causing the scaffold to swell. The swollen shape is then "locked" into place by freezing. Lyophilization removes the volatile acetic acid, leaving a porous, dry scaffold behind.

Mason's trichrome colors collagen fibers a dark blue and BSA glue a deep red. Scaffolds assembled and glued while dry show overlap of glue and collagen fibers. Scaffolds assembled and glued while wet result in almost no overlap of glue and scaffold, leading to delamination under functional testing conditions. SEM imaging of dry-assembled scaffolds shows BSA glue infiltrating adjacent layers, creating a single, cohesive trilayer scaffold. A void space is observed between layers when wet, porous scaffolds are glued together.

Comparing trilayer scaffolds to human valves highlights the similarities between the two. Both trilayer scaffolds and human valves are of similar thicknesses. Both tissues show three distinct layers, with a thick collagen fibrosa layer at the top, a porous spongiosa, and a denser ventricularis at the bottom.

3.4.2 Mechanical Properties of Porcine Aortic Valves

Obtaining healthy human aortic valve tissue is challenging. These tissues are in high demand for use as allografts in young adult patients[27]. However, porcine aortic tissue is readily available and similar in mechanical properties to human valves[28]. Analysis of ten studies provided normal physiological maximum stress-strains in circumferential and radial directions. Interestingly, the stress-strain curves generated by Stradins et al. fell almost exactly in the center of the ranges described by the meta-analysis. Mechanical testing of PAVs resulted in stress-strain curves that passed through the normal physiological ranges for human valves. Therefore, the mechanical properties of PAVs can be used as a valid comparison in place of human valves.

The anisotropic mechanical behavior of aortic valves has been well documented[29]. Tensile tests showed significant differences between circumferential and radial samples in all tests. PAVs show higher UTS, modulus, and secant modulus than radial samples while radial samples break at a larger strain value.

Secant modulus at a strain of 10% is reported as a metric of scaffold stiffness. While modulus also represents scaffold stiffness, the modulus values reported occur at

supra-physiological strains. Therefore, reporting the secant modulus of scaffolds is a way of comparing physiologically relevant stiffness.

3.4.3 Impact of Increasing Porosity and Microneedle Rolling on Scaffold Mechanical Properties

Increasing scaffold porosity, drying, and microneedle treatment were required to produce a robust scaffold capable of cellular in-growth. However, it is important to determine the effect of these procedures on scaffold mechanical properties. UTS was not significantly lowered by increasing scaffold porosity. Dermaroller treatment caused a significant drop in UTS of fibrous scaffolds. Trlayer scaffolds composed of porous, rolled scaffolds displayed the lowest UTS; but still failed at a stress much higher than would ever be experienced in physiological conditions. Increasing porosity significantly increased stain at break whereas microneedle rolling did not have a significant effect on strain at break. Trilayer scaffolds had significantly lower strain at break; most likely due to the BSA glue's stiffening of the interfaces between layers. Modulus decreased with both increased porosity and microneedle treatment. Secant modulus of nonporous and trilayer scaffolds were not different from one another; and were significantly higher than porous and microneedle treated scaffolds. Nonporous and trilayer scaffolds had mechanical properties that resembled those of the circumferentially tested aortic valve. Porous and micro needle treatments changed scaffold mechanical properties to more closely resemble radially tested aortic valves.

3.5 Conclusion

The results presented in this chapter show that porous, dry scaffolds can be effectively glued together to form one cohesive trilayer scaffold. These scaffolds resemble the human valve's unique histoarchitecture. A meta-analysis of literature defined maximum normal stresses and strains experienced by the native valve; providing a target set of mechanical properties to be replicated by the tissue-engineered valve. Increasing porosity and microneedle rolling treatments produced scaffolds with excellent mechanical strength. The application of these scaffolds to create a functional, tissue engineered heart valve is discussed in the following chapter.

3.6 Chapter 4 References

1. The Aortic Valve: Mano J. Thubrikar: 9780849347719: Amazon.com: Books. http://www.amazon.com/The-Aortic-Valve-Mano-Thubrikar/dp/0849347718. Accessed August 27, 2014.

2. Buchanan RM, Sacks MS. Interlayer micromechanics of the aortic heart valve leaflet. *Biomech Model Mechanobiol*. 2014;13(4):813-826. doi:10.1007/s10237-013-0536-6.

3. Schoen FJ. Aortic valve structure-function correlations: role of elastic fibers no longer a stretch of the imagination. *J Heart Valve Dis*. 1997;6(1):1-6.

4. Vesely I. The role of elastin in aortic valve mechanics. *J Biomech*. 1998;31(2):115-123.

5. Vesely I, Noseworthy R. Micromechanics of the fibrosa and the ventricularis in aortic valve leaflets. *J Biomech*. 1992;25(1):101-113. doi:10.1016/0021-9290(92)90249-Z.

6. Tedder ME, Liao J, Weed B, et al. Stabilized collagen scaffolds for heart valve tissue engineering. *Tissue Eng Part A*. 2009;15(6):1257-1268. doi:10.1089/ten.tea.2008.0263.

7. Tedder ME, Simionescu A, Chen J, Liao J, Simionescu DT. Assembly and testing of stem cell-seeded layered collagen constructs for heart valve tissue engineering. *Tissue Eng Part A*. 2011;17(1-2):25-36. doi:10.1089/ten.TEA.2010.0138.

8. Chang Y, Lai P-H, Wei H-J, et al. Tissue regeneration observed in a basic fibroblast growth factor–loaded porous acellular bovine pericardium populated with mesenchymal stem cells. *J Thorac Cardiovasc Surg*. 2007;134(1):65-73.e4. doi:10.1016/j.jtcvs.2007.02.019.

9. Chang Y, Chen S-C, Wei H-J, et al. Tissue regeneration observed in a porous acellular bovine pericardium used to repair a myocardial defect in the right ventricle of a rat model. *J Thorac Cardiovasc Surg*. 2005;130(3):705-711. doi:10.1016/j.jtcvs.2005.04.007.

10. Thubrikar MJ, Aouad J, Nolan SP. Comparison of the in vivo and in vitro mechanical properties of aortic valve leaflets. *J Thorac Cardiovasc Surg*. 1986;92(1):29-36.

11. Deck JD, Thubrikar MJ, Schneider PJ, Nolan SP. Structure, stress, and tissue repair in aortic valve leaflets. *Cardiovasc Res*. 1988;22(1):7-16.

12. Gnyaneshwar R, Kumar RK, Balakrishnan KR. Dynamic analysis of the aortic valve using a finite element model. *Ann Thorac Surg*. 2002;73(4):1122-1129.

13. Cataloglu A, Clark RE, Gould PL. Stress analysis of aortic valve leaflets with smoothed geometrical data. *J Biomech*. 1977;10(3):153-158.

14. Thubrikar M, Piepgrass WC, Deck JD, Nolan SP. Stresses of natural versus prosthetic aortic valve leaflets in vivo. *Ann Thorac Surg*. 1980;30(3):230-239.

15. Li J, Luo XY, Kuang ZB. A nonlinear anisotropic model for porcine aortic heart valves. *J Biomech*. 2001;34(10):1279-1289.

16. Grande KJ, Cochran RP, Reinhall PG, Kunzelman KS. Stress variations in the human aortic root and valve: the role of anatomic asymmetry. *Ann Biomed Eng*. 26(4):534-545.

17. Sacks MS, He Z, Baijens L, et al. Surface strains in the anterior leaflet of the functioning mitral valve. *Ann Biomed Eng*. 30(10):1281-1290.

18. Lo D, Vesely I. Biaxial strain analysis of the porcine aortic valve. *Ann Thorac Surg*. 1995;60(2 Suppl):S374-S378.

19. Adamczyk MM, Vesely I. Characteristics of compressive strains in porcine aortic valves cusps. *J Heart Valve Dis*. 2002;11(1):75-83.

20. Stradins P, Lacis R, Ozolanta I, et al. Comparison of biomechanical and structural properties between human aortic and pulmonary valve. *Eur J Cardiothorac Surg*. 2004;26(3):634-639. doi:10.1016/j.ejcts.2004.05.043.

21. Sharma V, Deo S V, Altarabsheh SE, Cho YH, Erwin PJ, Park SJ. Comparison of the early haemodynamics of stented pericardial and porcine aortic valves. *Eur J Cardiothorac Surg*. 2015;47(1):4-10. doi:10.1093/ejcts/ezu272.

22. Yoganathan AP, He Z, Casey Jones S. Fluid mechanics of heart valves. *Annu Rev Biomed Eng*. 2004;6:331-362. doi:10.1146/annurev.bioeng.6.040803.140111.

23. Vogiatzidis K, Zarogiannis SG, Aidonidis I, et al. Physiology of pericardial fluid production and drainage. *Front Physiol*. 2015;6. doi:10.3389/fphys.2015.00062.

24. Randall JT, Fraser RDB, North ACT. The Structure of Collagen. *Proc R Soc London Ser B, Biol Sci*. 1953;141(902):62-66 CR - Copyright © 1953 The Royal Societ. doi:10.2307/82782.

25. GILLETTE EP. Anatomie et, physiologie du tissu conjonctif ou lamineux. *Arch Gén Méd*. 1873;XXI:228-230.

26. Giménez B, Turnay J, Lizarbe MA, Montero P, Gómez-Guillén MC. Use of lactic acid for extraction of fish skin gelatin. *Food Hydrocoll*. 2005;19(6):941-950. doi:10.1016/j.foodhyd.2004.09.011.

27. Chambers JC, Somerville J, Stone S, Ross DN. Pulmonary autograft procedure for aortic valve disease: long-term results of the pioneer series. *Circulation*. 1997;96(7):2206-2214.

28. Kalejs M, Stradins P, Lacis R, Ozolanta I, Pavars J, Kasyanov V. St Jude Epic heart valve bioprostheses versus native human and porcine aortic valves - comparison of mechanical properties. *Interact Cardiovasc Thorac Surg*. 2009;8(5):553-556. doi:10.1510/icvts.2008.196220.

29. Gould RA, Chin K, Santisakultarm TP, et al. Cyclic strain anisotropy regulates valvular interstitial cell phenotype and tissue remodeling in three-dimensional culture. *Acta Biomater*. 2012;8(5):1710-1719. doi:10.1016/j.actbio.2012.01.006.

CHAPTER 4: CONSTRUCTION, STEM CELL SEEDING, AND EVALUATION OF TRILAYER HEART VALVES

4.1 Introduction

4.1.1 Research Motivation and Aim

We hypothesized that the unique, trilayer structure developed by nature is essential to proper aortic valve function. Data presented in chapter 3 has shown that fibrous and spongy biological scaffolds can be assembled to form trilayer structures that mimic the native valve's histoarchitecture. The aim of this project is to use these trilayer structures to create a tissue-engineered heart valve. This valve will be fully populated with stem cells and matured in a heart valve bioreactor.

Trilayered heart valve scaffolds were rendered porous during construction, treated with microneedle rollers, and seeded while dry to allow for capillary action to draw cells throughout the entire structure. Once seeded, valves were conditioned for three weeks in a heart valve bioreactor, capable of recreating physiological conditions.

4.2 Materials and Methods

4.2.1 Materials

StemPro low passage human adipose derived stem cells, MesenPro RS cell culture medium were from Invitrogen (Carlsbad, CA). Thin pericardial tissues and porcine pulmonary arteries were obtained from Tissue Source LLC (Lafayette, IN). Thick pericardial tissues were obtained from Animal Technologies, Inc. (Tyler, TX). Edwards Perimount valves were a generous gift from Dr. Williams and the Bon Secours St. Francis Health System. St. Jude Medical Regent heart valves were generously donated by St. Jude Medical (St. Paul, MN). 3D printed parts were made from Digital ABS II (Stratasys, Eden Prairie, MN) and produced on an ObJet Eden 350V 3D printer (Stratasys, Eden Prairie, MN). Thin pericardial tissues and porcine pulmonary arteries were obtained from Tissue Source LLC (Lafayette, IN). Micro needle rollers were manufactured by Melodysusie (Newark, CA). Nitinol stents were a gift from Dr. George Lutter at the University of Kiel, Germany. All other chemicals were of highest purity available and were obtained from Sigma-Aldrich Corporation (Lakewood, NJ).

4.2.2 Fibrous and Spongy Scaffold Preparation

Fibrous and spongy scaffolds were prepared following a decellularization protocol consisting of detergent and nuclease treatments as previously described, with minor modifications[1] as described in sections 3.2.3 and 4.2.3.

4.2.3 Poration of Fibrous and Spongy Scaffolds

Scaffolds were porated as described in section 4.2.6 with the exception of spongy scaffolds used in initial seeding experiments. Briefly, these scaffolds were treated with

0.2M acetic acid for 1 hour at room temperature under gentle agitation. Scaffolds were removed and placed in petri dishes. Liquid nitrogen was poured into the petri dishes to snap freeze the scaffolds. Frozen scaffolds were immediately transferred to a lyophilization flask and dried for 72 hours with a collector temperature of -48°C and a vacuum below 0.080 mBar.

4.2.4 Assembly of Trilayer Scaffolds

Trilayer scaffolds were assembled in the same manner as described in section 4.2.7. Trilayer cusps were assembled with dry tissue only.

4.2.5 Micro Needle Roller Treatment

Trilayer scaffolds were once again treated with acetic acid. However, the acetic acid treatment was used to swell the tissues, not to cause further poration. Accordingly, trilayer scaffolds were immersed in 0.2M acetic acid for 20 minutes. Tissues were frozen overnight at -80°C and lyophilized for 72 hours. Dry trilayer scaffolds were removed from the lyophilizer and placed on a self-healing cutting mat (Harris). Micro needle rollers consisting of 540 stainless steel needles uniformly arranged around a polystyrene drum were used to create many small punctures through the scaffold surface. Two needle length were used, 0.25mm to allow cells into the fibrous scaffolds, and 0.5mm to penetrate into the spongiosa layer. The Micro needles were rolled forward across the scaffold and back; this was considered one roll. Scaffolds were rolled in 4 directions, each time moving 45° clockwise.

4.2.6 Cell Culture

Human adipose derived stem cells (StemPro, Life Technologies) were obtained and expanded in media (MesenPro, Life Technologies) specially formulated to preserve the stemness of hADSCs while increasing cell division rate. Media was supplemented with 1% L-glutamine and 1% antibiotic/antimycotic solution. hADSCs were grown T-175 tissue culture polystyrene flasks and subcultured with Trypsin-EDTA (Corning-Cellgro). Cells were used at passage 3-5.

4.2.7 Cell Seeding of Fibrous and Spongy Scaffolds

Fibrous and Spongy scaffolds were removed from the lyophilizer and used dry, with the exception of the nonporous scaffolds which were rehydrated in PBS prior to use. hADSCs were expanded in MesenPro medium and seeded in DMEM containing 10% FBS and 1% Ab/Am. For cell seeding studies, scaffolds (n=4) were cut into square sections 1cm in length and placed in 12 well plates. A cell suspension of 1E6 hADSCs in 200µL DMEM was added to the top of the scaffold. Due to the hydrophobic nature of the collagen scaffolds and the surface tension of the media, a bead was formed on top of the scaffolds. Care was taken to prevent the bead of suspended cells from rolling off the scaffold onto the TCPS. Cells were left to soak into the dry scaffolds for 45 minutes. After 45 minutes, DMEM was added and the samples were cultured for 3 days.

4.2.8 Analysis of Cell Distribution in Fibrous Scaffolds

Histological sections stained with DAPI were imported into ImageJ (National Institutes of Health, Bethesda, MS) image analysis software. First, the scale bar was used to determine the number of pixels per µm. Next, color images were converted to 8 bit grayscale. Images were then rotated and cropped so the top of the scaffold was aligned horizontally at the topmost portion of the image (y=0). Images were thresholded using the "Li" method to select the stained nuclei. A watershed algorithm was used to separate nuclei that were very close or overlapping. The analyze particles feature was used with the settings: size 10-infinity, circularity 0.2-1, record starts. This feature counts all cell nuclei and reports the y-start value as the topmost portion of the counted region. The y-start value was used to determine cell infiltration depth.

4.2.9 Cell Seeding of Trilayer Cusps

Trilayer were removed from the lyophilizer and used dry. Dry trilayer cusps were placed in a petri dish and seeded with a cell suspension of 4E6 hADSCs in 400µL DMEM was added to the top of the cusp. Care was taken to prevent the cell suspension from rolling off the cusp onto the TCPS. Cells were left to soak into the dry cusps for 20 minutes. After 20 minutes, scaffolds were flipped over cell seeding was repeated on the other side of the cusp. DMEM was added and the cells were allowed to attach overnight.

4.2.10 Designing the Crush Mounting System

The Edwards perimount bioprosthetric valve was chosen as a model because it is considered to be the gold standard in longevity and hemodynamics. A sealed 29mm valve

was opened and removed from the glutaraldehyde storage solution. Due to the symmetry of the valve, only a 60° section starting at the middle of one flexible stent post and ending in the middle of the cusp needed to be modeled. Calipers were used to measure the x and y location of marked points along the rigid stent edge of the valve. Points were measured along planes in the z direction every 1 mm. Solidworks CAD software (asdasd) was used to create the valve model. Briefly, z planes were created every 1 mm and the measured points were placed in a sketch on each plane. Next, a 3D spline was made to pass through each point. The spline was mirrored once to create one 120° section of the stent. Next, a rounded rectangular sketch was swept around the 3D sketch to form the outer portion of one cusp. This sweep feature was then mirrored twice to create the perfect 120° symmetry observed in the bioprosthetic valve. The curve was extruded up and pockets representing the sinus of Valsalva were added. Next, evenly spaced holes were made to allow scaffolds to be sutured to the top of the crush mount. Finally, the edge of the stent was replicated to form the bottom part of the crush mount. A groove for an o-ring was placed in the top portion of the crush mount to hold the mount together when fully assembled.

4.2.11 Producing the Crush Mount

Solidworks files were exported in stereolithography format to an ObJet Eden 350V 3d printer which built the parts by laying down a thin layer of photopolymer (Digital ABS II), curing that layer with UV light and repeating the process until the final shape is formed.

The majority of support material was removed via water jet. Parts were then cleaned overnight in 1% sodium hydroxide and washed in distilled water.

4.2.12 Constructing the Crush Mounted Valve for Bioreactor Testing

The top of the crush mount was placed upside down on a sterile field. Trilayer cusps were placed on the edge of the crush mount and attached to the crush mount with a surgeon's knot using size 4-0 prolene sutures (Ethicon, Somerville, NJ). Cusps were kept in media until use and were periodically wetted with media throughout assembly. When all three cusps were attached and aligned properly, an o-ring was inserted into the groove and the two pieces of the crush mount were pressed firmly together, sealing the edges of the cusps between them.

4.2.13 Bioreactor Testing and Maturation of Trilayer Heart Valves

Immediately after construction, cell-seeded trilayer heart valves were mounted in the heart valve bioreactor. The bioreactor was filled with 750mL of DMEM containing 10%FBS, 1%Ab/Am, and 0.1% Gentamycin. The bioreactor was placed in a standard cell-culture incubator at 37°C with 5% CO_2 and a humidified environment. Supplemental antibiotics (1%Ab/Am, and 0.1% Gentamycin) were introduced after three days of culture. Media was changed every seven days, with supplemental antibiotics being added three days after each media change. Pressure was monitored in real time at points both above and below the valve. A flow meter recorded the volume of media pumped through the

system with each stroke. A custom LabView program displayed and recorded all information. A webcam with an LED light was attached to the top of the bioreactor and focused on the outflow side of the valve, allowing for visualization of valve movement. Initial pressure and flow was set to low levels (2/0 mmHg, stroke volume below measurement threshold) to allow further cell attachment. Pressures were slowly increased so as not to dislodge cells. Pulmonary conditions of 22/10 mmHg and 55mL/stroke were reached after 1 week and maintained for an additional two weeks.

4.2.14 Constructing the Nitinol Stent Mounted Valve

Nitinol stent mounted valves were made on the benchtop as a proof of concept, aseptic technique was not used. Fibrous and porous scaffolds were cut according to 3D printed molds designed to produce a 22mm heart valve. The fibrous scaffold was made with two regions to serve different functions. The first region was made to provide a skirt below the valves that would seal to the outer wall of the placement site. The second region was made to be folded around the spongiosa scaffold to create the trilayer cusps. Spongy scaffolds were cut into individual, cusp-shaped sections. 55% BSA glue was applied at 10µm/cm^2 and spread evenly across the fibrous scaffold. 10% glutaraldehyde was then sprayed over the glue, spongy scaffolds were quickly placed in position and folded into place. The resulting scaffold was rectangular in shape with a length equal to the circumference of the inside of the nitinol stent. The bottom of the valve consisting of the fibrous scaffold skirt was first sutured to the stent posts with 4-0 silk braided sutures (specific brand). Next, the trilayer potion of the valve was sutured to the stent following

the edge of the cusps. This allowed the individual trilayer cusps to coapt while keeping the lower portion of the valve sealed to the stent.

4.2.15 Geometric Orifice Area Measurement

Mechanical (Masters Series, St. Jude, St. Paul, MN), trilayer, and bioprosthetic (Perimount Aortic, Carpentier-Edwards, Irvine, CA) valves were mounted in the heart valve bioreactor. Valves were placed under pulmonary conditions consisting of a pressure of 25/10 mmHg with a stroke volume of 70mL and a stroke rate of 70.58 peats per minute. The trilayer valve was conditioned for 5 days prior to testing. Videos were taken of each valve at 240 frames per second and at a resolution of 320 by 240 pixels. Effort is made to remove bubbles from the system and videos are the length of several extra beats to ensure that three clean cycles can be used for analysis. Video editing software (Free Studio v. 6.4) is used to convert every frame of the video to its own numbered image file. The sequence of images are imported into ImageJ. The scale is set for the sequence by tracing a line of known distance (the outer diameter of the metal bracket or crush mount) and defining its length and the appropriate units. The threshold is adjusted so that the open orifice is clearly defined from the leaflet tissue, and the sequence is converted to binary, rendering the orifice black and the leaflets white. The orifice is then selected using the Wand (tracing) tool, and the area measured. The orifice area for each frame is manually selected and measured in this way for three cycles of open and close beginning at least 20 frames before the start of opening and ending at least 20 frames after the end of close. The area of one pixel is selected and used a place holder for frames where there

is no orifice visible. The shape of the orifice must be periodically checked visually against the corresponding unaltered frame as artifacts such as bubbles may affect the measured area. The cycles are aligned so that the start of the valve opening is on the same frame in the cycle. Both Bioprosthetic and Trilayer valves were 29mm. The mechanical valves was 27mm. Therefore the mechanical valve GOA was multiplied by (29/27) to control for valve size.

4.2.16 Scanning Electron Microscope Imaging

To prepare for SEM imaging samples were fixed overnight in Karnovsky's; a solution of 2% paraformaldehyde and 2.5% glutaraldehyde buffered in 0.2M cacodylic acid. Samples were than dehydrated in a graded series of ethanol moving from 35%, 50%, 70%, 95%, and 100% each for 30 minutes. Samples were then placed in pure Hexamethyldisilazane (HMDS). HMDS was allowed to fully evaporate in a fume hood. Samples were then mounted on metal stubs with double sided tape and sputter coated with platinum. Scaffolds were imaged with a Hitachi TM3000 tabletop backscatter SEM using a 15kV beam.

4.2.17 Histology

Thin 5µm sections of paraffin-embedded samples were washed in xylene and rehydrated through a series of alcohol washes ending in deionized water. These sections were stained with hematoxylin and eosin and Mason's Trichrome (Richard-Allen Scientific, Thermo Scientific) to show general scaffold morphology and to identify cell

location. Digital images of these slides were obtained at various magnifications (25X to 200X) on a Zeiss Axiovert 40CFL microscope using AxioVision software (Carl Zeiss MicroImaging, Inc. Thornwood, NY).

4.2.18 Statistical Analysis

Results are expressed as means ± standard deviations (SD). For normally distributed data with equal variances, unpaired t-tests were used to compare means. Welch's correction was applied to means with different variances. To compare multiple means, a one-way analysis of variance was performed (ANOVA) with Tukey's multiple comparison test using multiplicity adjusted P values. For non-parametrically distributed data, the Kruskal-wallis one-way analysis of variance with Dunn's multiple comparison test was used. P values less than or equal to 0.05 were considered statistically significant. Statistical significance is indicated as follows, ns if $P > 0.05$, * if $P \leq 0.05$, ** if $P \leq 0.01$, *** if $P \leq 0.001$, and **** if $P \leq 0.0001$. Analysis was carried out in GraphPad Prism 6 (Graphpad Software, La Jolla, CA).

4.3 Results

Cells drop seeded onto nonporous fibrous and spongy scaffolds formed a monolayer on the scaffold surface. Poration and microneedle rolling techniques were used to increase cell infiltration into scaffolds.

4.3.1 Spongy Scaffold Seeding

Initial cell seeding studies were done on snap-frozen and lyophilized spongy scaffolds. A monolayer of cells formed on the surface of nonporous spongy scaffolds while cells infiltrated dry, porous spongy scaffolds. Decellularized (nonporous) scaffolds showed an increased thickness after poration and drying, which was reversed upon rehydration with cells suspended in media (**Fig 4.1**).

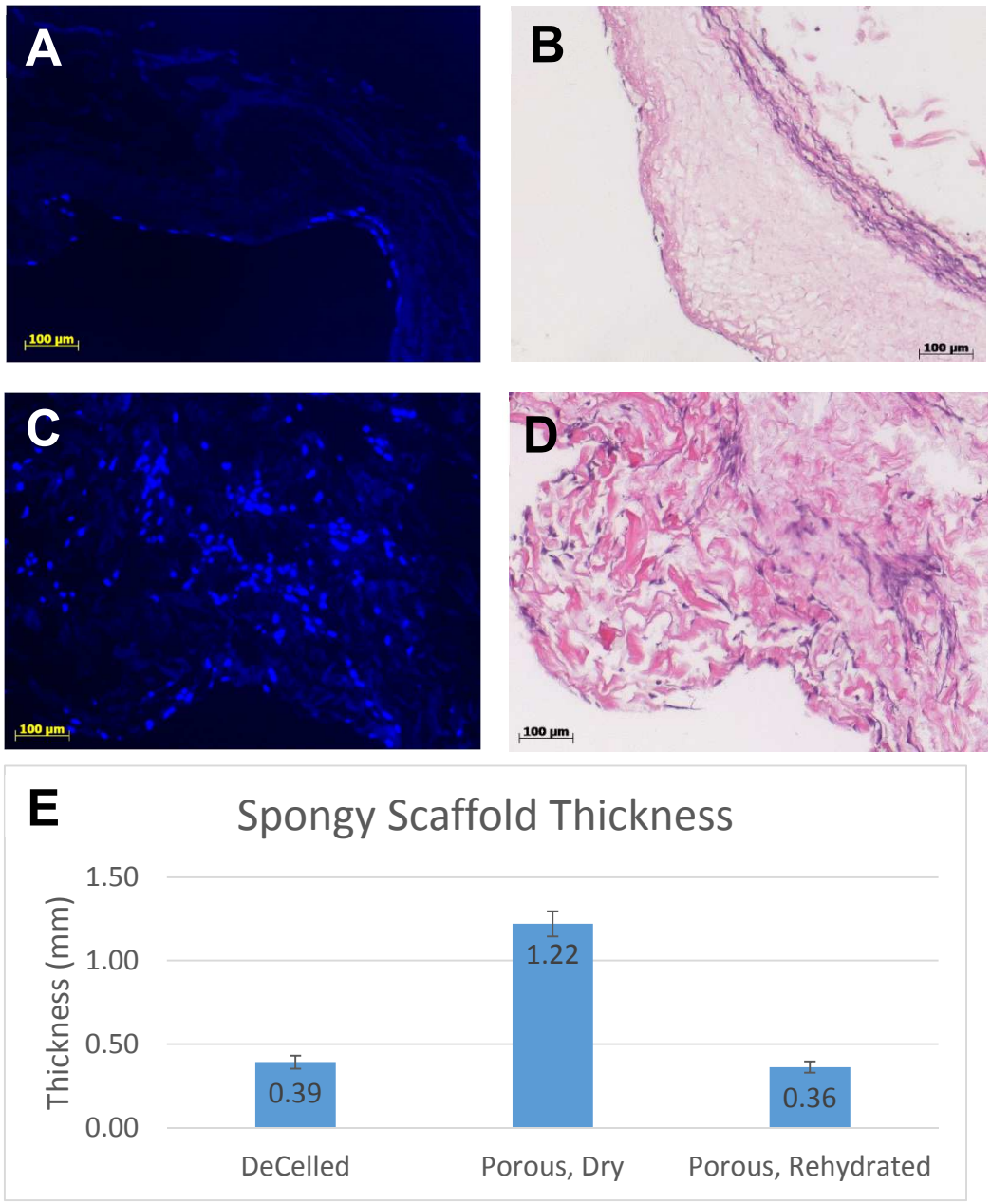

Figure 4.1. Non-porous spongy scaffolds seeded wet (A,B) and porous spongy scaffolds seeded dry (C,D). DAPI (A,C) (nuclei = blue). Hematoxylin and Eosin (B,D) (H&E, dark purple = nuclei, pink = background substance). Scaffold thickness is measured throughout the process of drying and rehydrating (E).

4.3.2 Microneedle Rolling and Seeding of Fibrous Scaffolds

Fibrous scaffolds are largely composed of thick sheets of collagen, which remain intact after scaffold porosity is increased. Microneedle rolling treatment (**Fig 4.2A-B**) provided access to the porous scaffold interior. When cut obliquely and imaged with a scanning electron microscope, the topmost collagen sheet of the fibrous scaffold is shown as a barrier preventing access to the porous scaffold below (**Fig 4.2C**). A schematic diagram of the results of cell seeding on nonporous, porous, and microneedle porous scaffolds (**Fig 4.2D-F**) is shown. Mason's Trichrome stain of the fibrous scaffold showing collagen in blue (**Fig 4.2G**) illustrates the unbroken collagen sheet on top of the fibrous scaffold that prevents cellular infiltration (indicated by black arrow). The resultant cellular access points (indicated by black arrow) created by microneedle rolling are shown in **Fig 4.2H**. Cells are seen moving into the scaffold through the access point crated by microneedle rolling in **Fig 4.2I**. En face and cross sectional SEM imaging of fibrous scaffolds shows the effects of microneedle rolling (**Fig 4.3**).

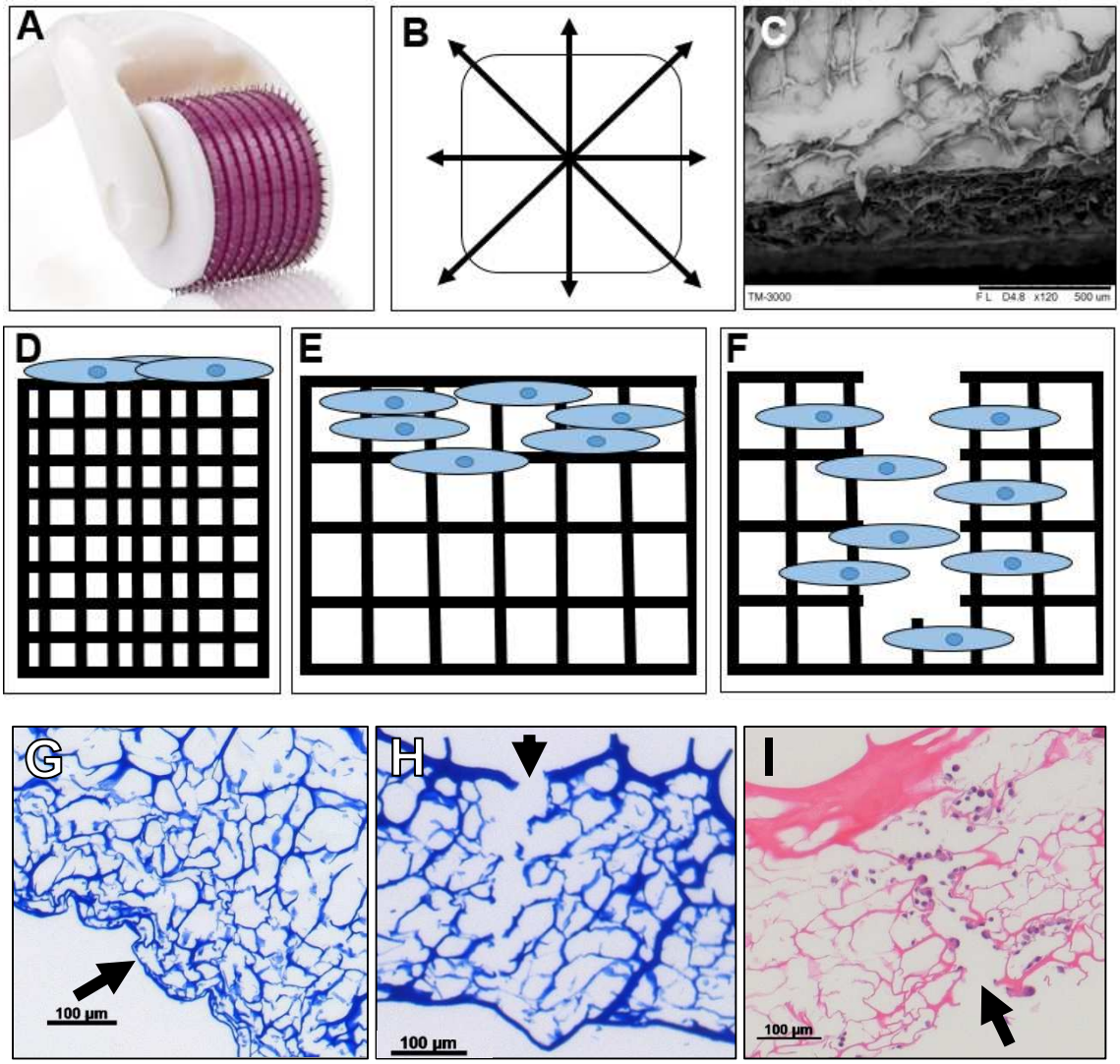

Figure 4.2. Microneedles (A) rolled across the scaffold in the pattern shown in (B). SEM of trilayer scaffold cut obliquely showing unbroken surface and porous interior (C). Schematic of fibrous scaffolds showing cell distribution for seeding on nonporous (D), porous (E), and porous, microneedle rolled (F) scaffolds. Mason's trichrome (collagen=blue) of porous fibrous scaffolds showing unbroken collagen surface (G – arrow) and result of microneede treatment (H – arrow). Hematoxylin and Eosin stain showing cell infiltration into scaffold through a microneedle-produced break in the scaffold (I).

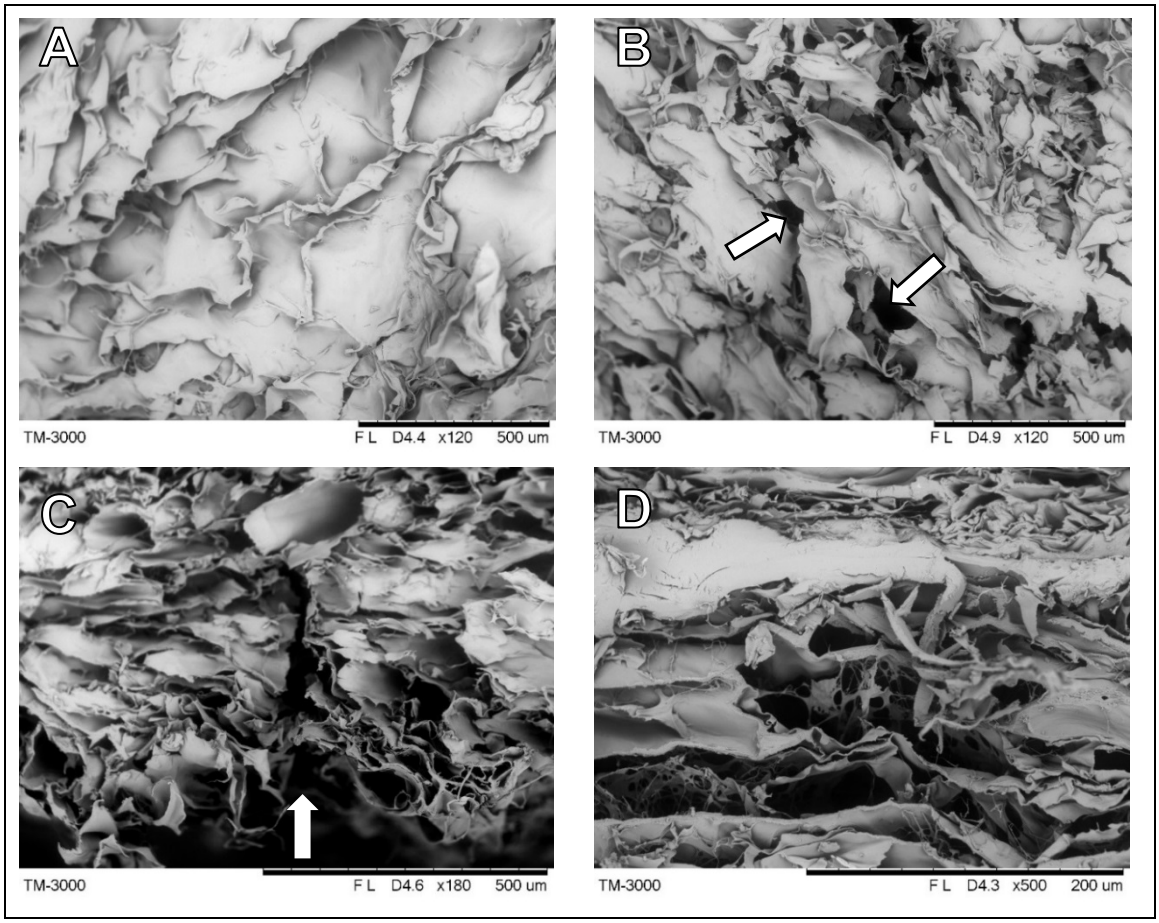

Figure 4.3. En face imaging of fibrous scaffolds showing unbroken collagen surface (A) and microneedle-produced holes (B – arrows). Cross sectional view of microneedle rolled scaffold (C) and porous, non-rolled scaffold (D).

Cell infiltration into the deeper potions of fibrous scaffolds increases with poration and microneedle rolling. The percent of total cells at a given distance away from the scaffold surface is shown. 97% of total seeded cells were located in the first 50µm of nonporous fibrous scaffolds. Porated scaffolds showed a shift of cells inwards with 56% of cells in the first 50µm, 21% located in the 50-100µm region, and 10% in 50-100µm. Microneedle rolled scaffolds contain an even greater percentage of cells located in the

inner portion of the scaffold. Approximately 35% of cells infiltrated over 200μm into the porous scaffold treated with 14 microneedle rolling applications. DAPI images converted to grayscale (Nuclei = white) and stitched together show 3cm long representative sections of seeded fibrous scaffolds. Cell distribution shifts to the interior of the scaffold in porous and microneedle rolled scaffolds (**Fig 4.5**). Hematoxylin and Eosin staining shows similar cell infiltration results. Cells can be seen in close proximity to collagen fibers, not unattached in the central region of pores, indicating cell attachment to the scaffold (**Fig 4.6**).

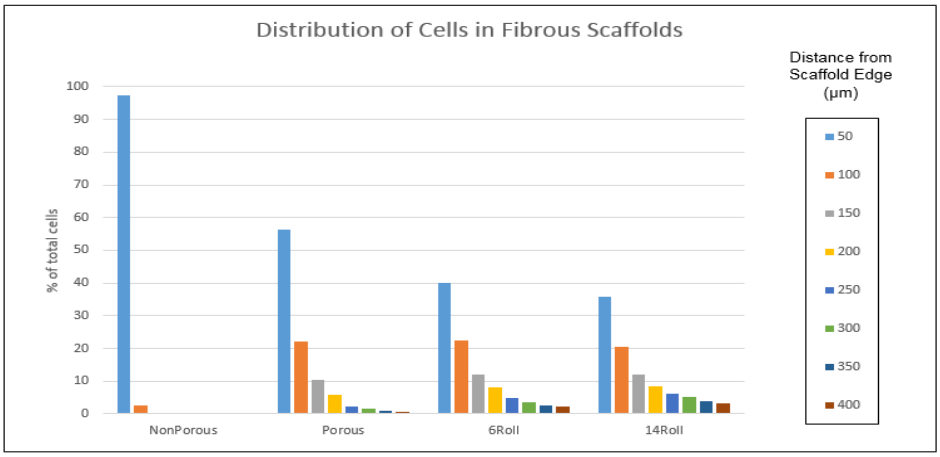

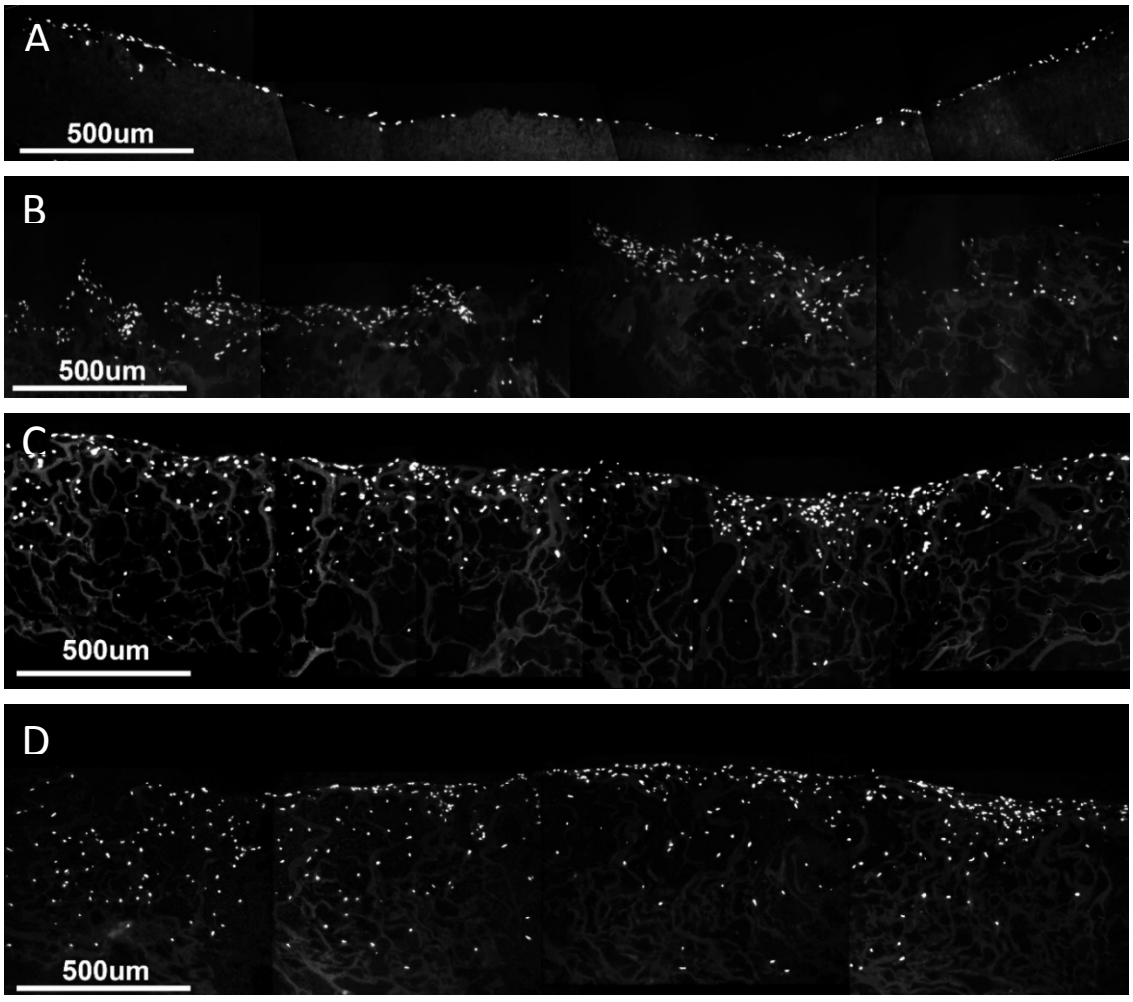

Figure 4.4. Cell distribution throughout scaffolds. DAPI staining (Grayscale, Nuclei = white) of nonporous (A), porous (B), porous 6 rolled (C), and porous 14 rolled (D) scaffolds.

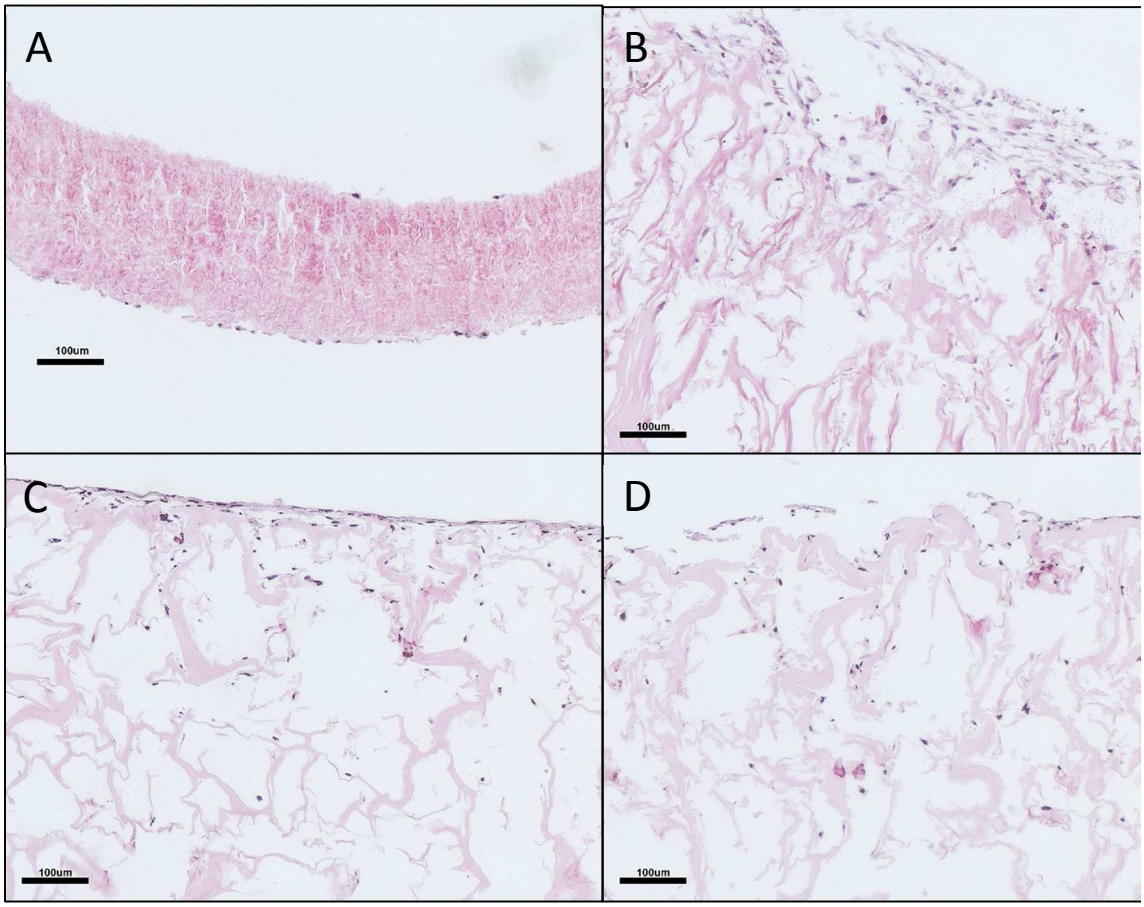

Figure 4.5. Hematoxylin and Eosin stain (dark purple = nuclei, pink = background substance) of nonporous (A), porous (B), porous 6 rolled (C), and porous 14 rolled (D) scaffolds.

4.3.3 Assembly and Function of Trilayer Valves

The crush mounting system was used to reliable create uniformly shaped trilayer heart valves. A trained operator can assemble a heart valve from three cell-seeded cusps in approximately 45 minutes (**Fig 4.8**). The crush mount fit directly into the heart valve bioreactor developed in our lab by Lee Sierad[2] (**Fig 4.9**). Trilayer valves possess excellent

hemodynamics and toughness. The trilayer valve withstood sustained pressures of 900/800 mmHg and flows over 150mL/stroke without failure (data not shown).

High speed video of mechanical, trilayer, and bioprosthetic heart valves loaded under pulmonic pressures and flows were recorded. Still images representing 0, 25, 50, 75, and 100% of maximum GOA in both opening and closing movements were extracted from the videos (**Fig 4.10**). Bioprosthetic valves open uniformly with each cusp opening at the same rate. In contrast, trilayer valves open one cusp after another until maximum GOA is reached. Mechanical valve cusps open and close with near perfect symmetry.

GOA data was split into three phases; opening, open, and closing. The opening phase lasted from the first observed increase in GOA until maximum GOA was reached. The open phase lasted until GOA began to rapidly decline. The closing phase started immediately where the open phase ended and continued until GOA reached $0cm^2$. Bioprosthetic valves had the largest maximum GOA of all valves tested. Trilayer valves have a significantly larger maximum GOA than mechanical valves. However, this GOA peak occurs at the beginning of the open phase as the ends of the cusps flare outwards. Immediately after this flare, the belly of the cusps protrude inward, lowering the trilayer valve's GOA. The same behavior is observed in the bioprosthetic valve. When the open phase GOAs are averaged, the mechanical and trilayer valves show no significant difference (**Fig 4-10C**). The trilayer valve took the longest time to reach maximum GOA,

likely due to the cusps opening one at a time (**Fig 4-10D**). Mechanical valves closed rapidly while trilayer and bioprosthetic valves closed in same amount of time (**Fig 4-10E**).

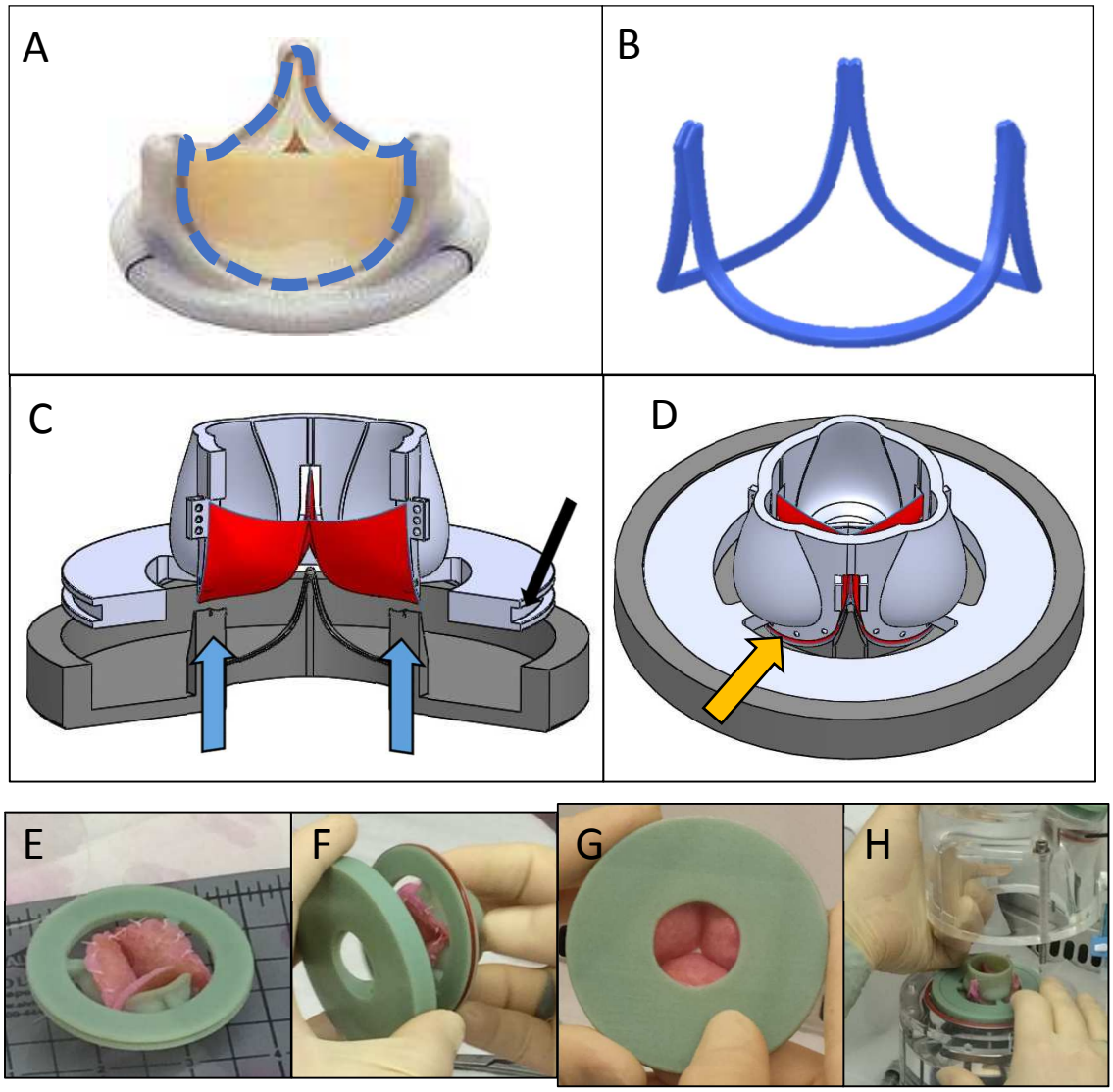

Figure 4.8. A 29mm Edwards Perimount valve was measured to attain the geometry of the annulus, shown as a dashed blue line in (A). The annulus geometry was then modeled in Solidworks (B) and used as the basis for shaping valves for in-vitro testing. The crush mount pieces are pressed together and an O-ring set in the groove (C - indicated by black arrow) holds the system together. Leaflets (D - yellow arrow) are held tightly between the two pieces of the crush mount. Cusps are sutured to the top

(E), the o-ring is places and the two pieces are pressed together (F). Inflow side of the valve (G) before being placed in the heart valve bioreactor (H).

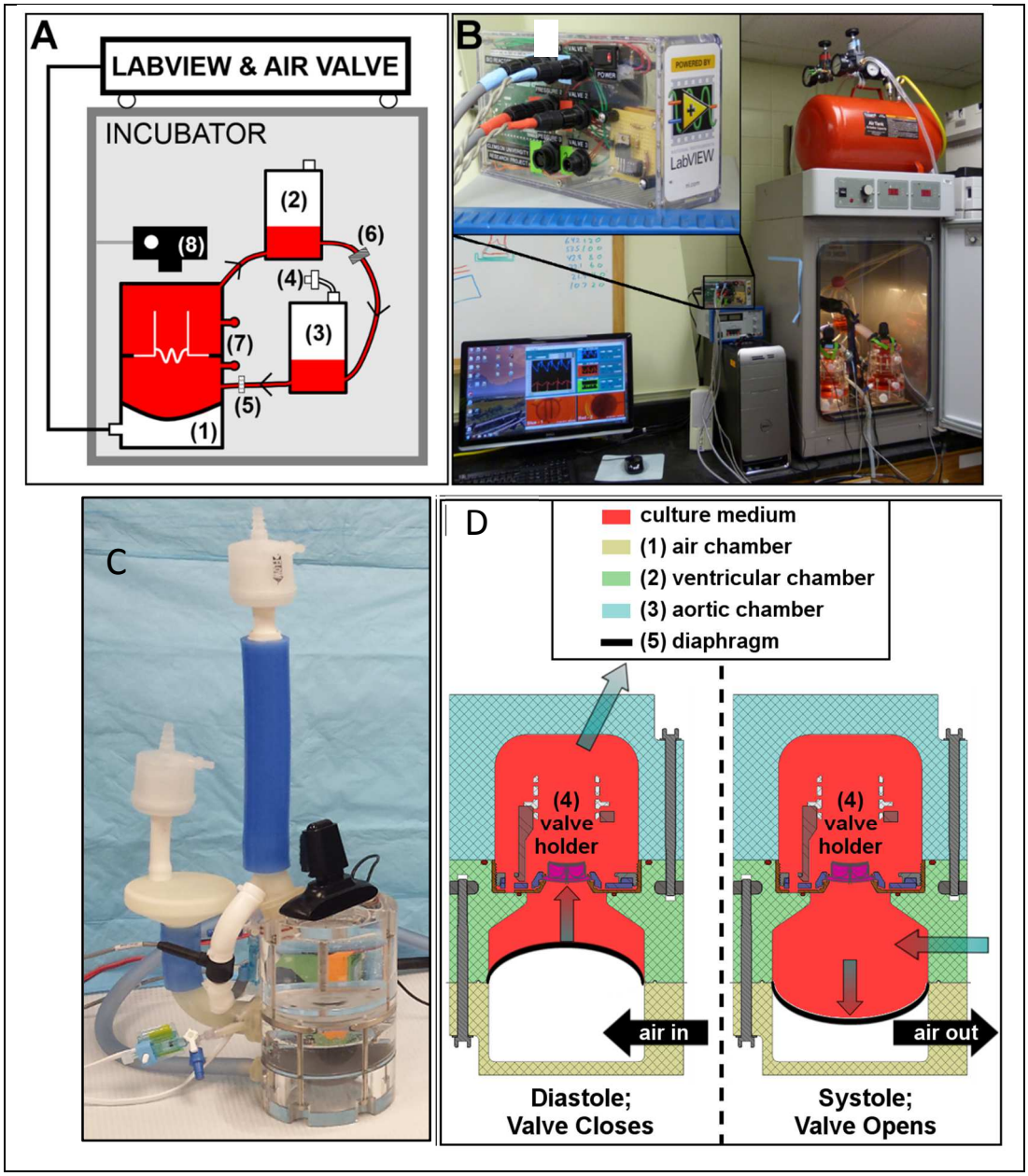

Figure 4.9. The conditioning system (A) consists of a three-chambered heart valve bioreactor (1), an optional pressurized compliance tank (2), a reservoir tank (3) with sterile filter (4) for gas exchange, one-way valves (5), resistance valves (6), pressure transducers (7), a flow meter, a webcam (8), and an air supply. External LabView software and custom hardware (B) monitor and control the system. Control of pressure

and flow coupled with the webcam video data allow for the valve to be tested and observed under a wide range of conditions (C). Cross sectional view of bioreactor showing function (D). Curtesy Lee Sierad.

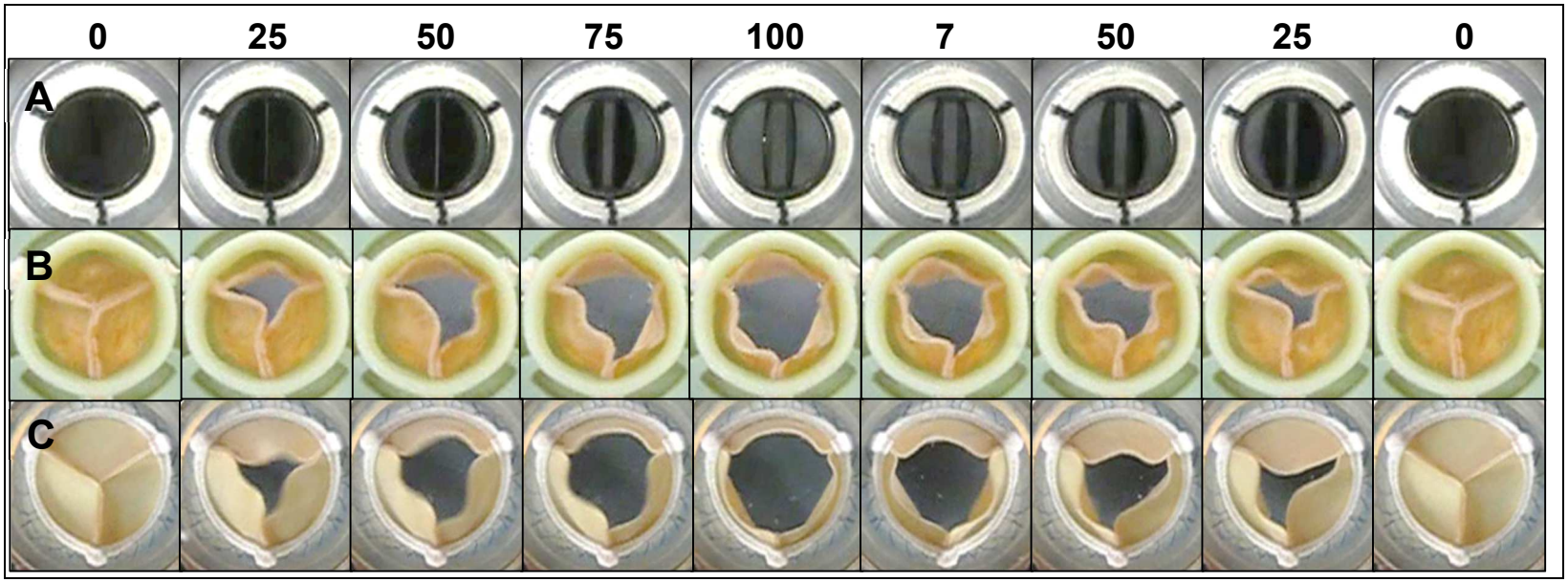

Figure 4.10. Representative images of mechanical (A), trilayer (B), and bioprosthetic (C) valves at 0, 25, 50, 75, and 100% of maximum GOA for both opening and closing movements.

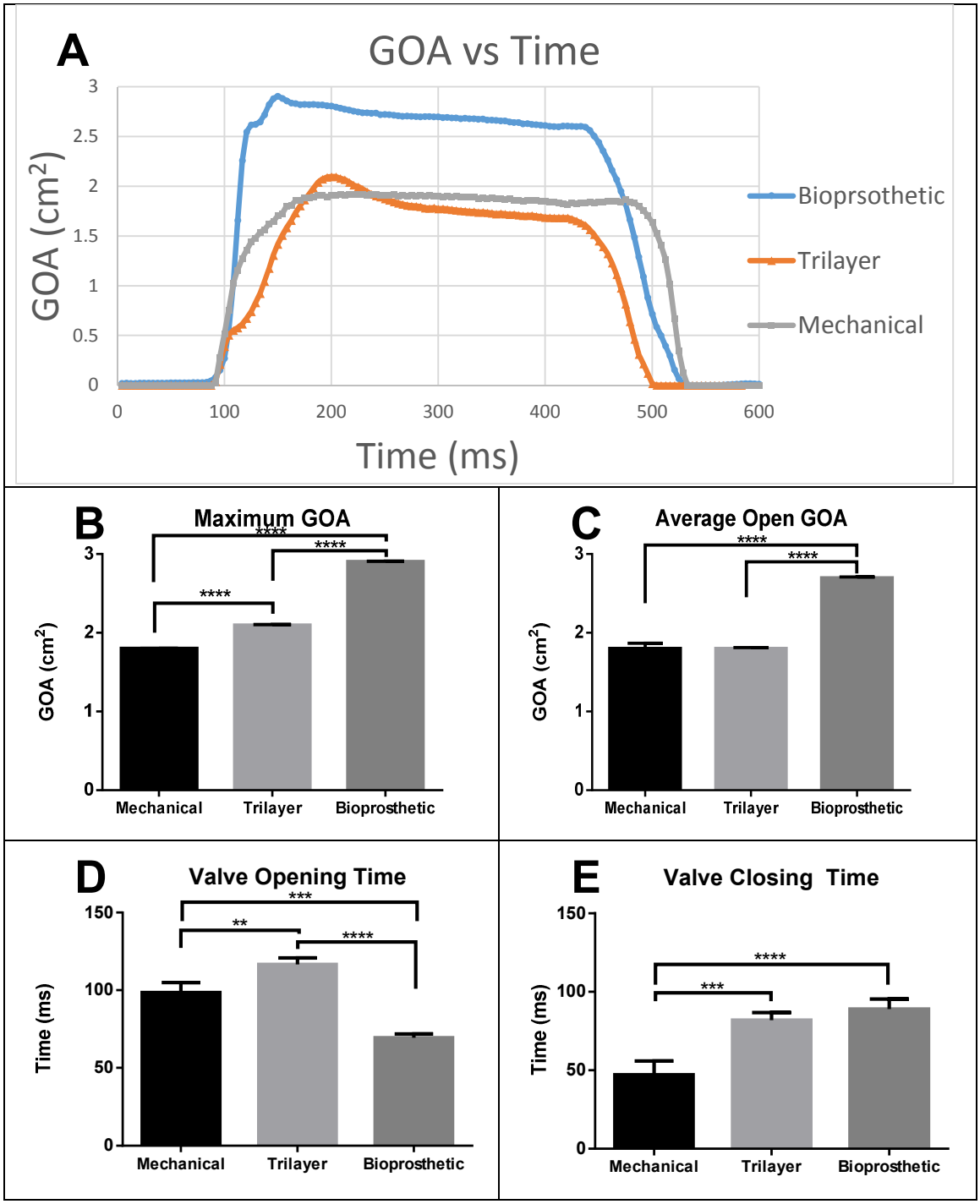

Figure 4.11. Average GOA of bioprosthetic, trilayer, and mechanical valves through one open and closing cycle (A). Maximum GOA reached (B) and average GOA of valves while open (C). Time for valves to transition from closed to open (D) and open to closed (E).

4.3.4 Bioreactor Maturation of Trilayer Heart Valves

Trilayer valves maintained excellent hemodynamics throughout the three week conditioning period. Gross analysis of valves showed no tearing or damage after conditioning. Cusps remained in excellent condition without any signs of "ballooning" as seen in valves made with hydrogels (**Fig 5-11**).

Bioreactor conditioning produced significant changes in scaffold mechanical properties (**Fig 4.12**). Mechanical properties are compared to fresh porcine aortic valve samples taken in the circumferential direction. Unconditioned trilayer valves had significantly lower UTS and strain at break values than PAV tissues, which changed to no statistical difference after bioreactor conditioning (**Fig 4.12B-C**). Bioreactor conditioning decreased the stiffness of trilayer valves, lowering both peak and secant modulus values (**Fig 4.12D-E**).

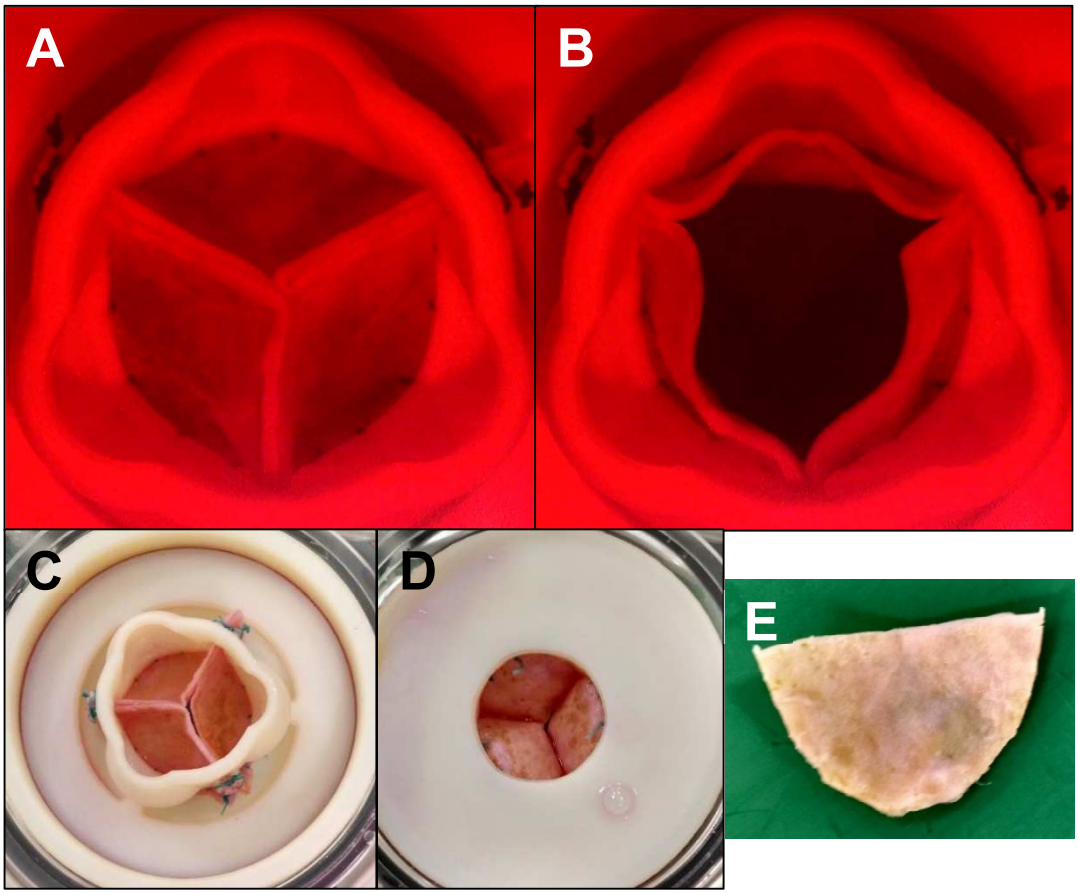

Figure 4.12. Cell seeded trilayer heart valve after 3 weeks of bioreactor conditioning in diastole (A) and systole (B). Outflow (C) and inflow (D) sides of the valve after being removed from the bioreactor. A trilayer cusp removed from the crush mount after bioreactor conditioning (E).

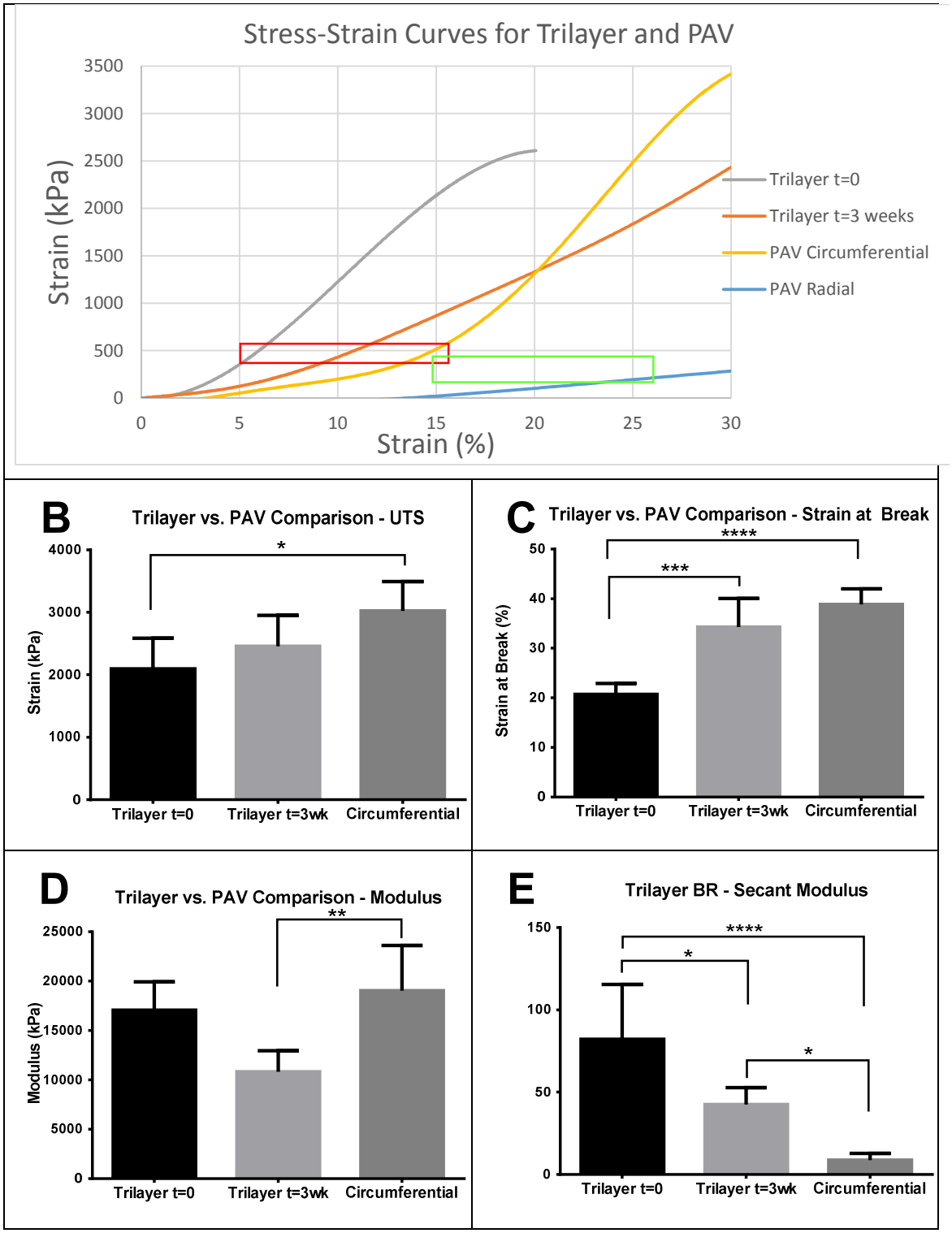

Figure 4.13. Comparison between mechanical properties of trilayer scaffolds before (t=0), after (t=3 wk) three weeks of bioreactor conditioning, and circumferential

samples of PAV cusps. Representative stress-strain curves; boxes represent normal physiological maximum stress-strains in circumferential (red) and radial (green) directions (A), UTS (B), Strain at break (C), Peak Modulus (D), and Secant modulus at a strain of 10% (E).

4.3.5 A Nitinol Stent-Mounted Trilayer Valve

The crush mounting system was created to allow for easily repeatable *in-vitro* testing of valves. However, this system would not be useful for *in-vivo* studies. The trilayer cusp is produced from flat sheets of scaffold, and can therefore be shaped to fit a wide variety of applications. A proof of concept valve was produced to fit into the same 22mm nitinol scaffold used by other groups in large animal testing (**Fig 4.13**).

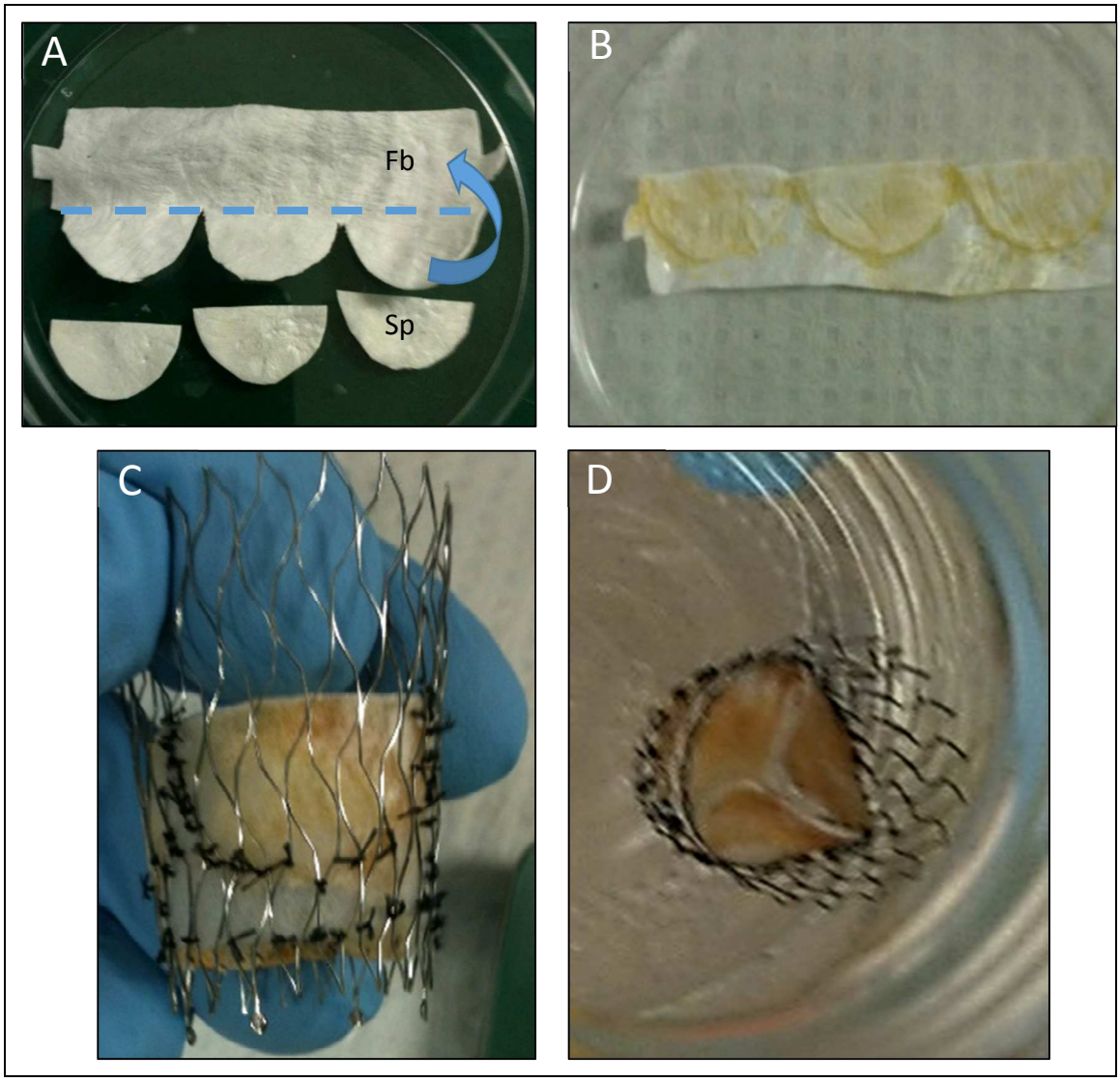

Figure 4.14. Assembly of stented trilayer valve. Dry, porous scaffolds (A) are cut to shape following a template (Fb= fibrous scaffold, Sp=Spongy scaffold). BSA glue and glutaraldehyde are applied and the scaffolds are folded to form three trilayer cusps and a single layer cuff region (B). The folded trilayer scaffold is sutured inside a collapsible nitinol stent (C-D).

4.4 Discussion

The results presented here introduce a novel cell seeding technique for rapid full-thickness seeding of biological scaffolds. Early cell seeding efforts produced a mono-layer of cells on the fibrous scaffold surface. The thick, non-porous collagen scaffold produced by decellularizing pericardium down not promote cellular infiltration[3]. Two treatments were employed to allow for rapid cellular infiltration. First, scaffolds were rendered porous and dry by acetic acid treatment and lyophilizaiton. This technique has been used to create myocardial scaffolds that performed well in a rat model of ischemic heart disease[456]. A cell suspension is placed on these scaffolds and allowed to soak into the tissue. This process takes approximately 45minutes. The dry scaffold draws the cell suspension in, allowing cells to repopulate the outermost portion of the scaffold. Cell seeding on these scaffold showed that cells will infiltrate readily into the first 150μm of the scaffold. Much recent research has been done on the use of microneedles to deliver drugs and vaccines into the dermal layer of skin[7–11]. However, these systems are designed for the delivery of very small molecules, not cells. In this study microneedle rolling was used to provide access through the dense, outer sheets of collagen, into the porous interior of the scaffolds. These access sites allowed cell suspensions to soak into the dry scaffolds, yielding increased population of the interior portions of the scaffold. This is the first example of an *in-vitro* cell seeding technique that can rapidly populate a biological matrix with cells.

Fibrous and spongy scaffolds were assembled into valves and functionally tested in a bioreactor. The mechanical testing data presented in chapter three showed that trilayer scaffolds possessed more than sufficient mechanical strength to function in a physiologically relevant system of forces. However, the mechanical properties of a scaffold are not the sole determinant of proper valve function. Many scaffolds, including hydrogels[12–15], have been proposed for use in heart valve tissue engineering. The effectiveness of these scaffolds as functional valves cannot be proven until a valve is constructed form them and a rigorous analysis of valve function is produced. To this end, trilayer valves were tested and compared with bioprosthetic and mechanical valves. The primary testing criteria was geometric orifice area (GOA). This measurement provides a cross sectional area of the valve available for blood to move through. Clinically, cardiac magnetic resonance (CMR) planimetry can be used to obtain a GOA value[16]. However, the most common metric of valve function is effective orifice area (EOA)[17]. EOA is measured by determining the location where the cross-section area of the jet produced by blood moving through the valve is at a minimum, measured by Doppler echocardiography. The bioreactor used in the study allows for precise, high-speed videos to be captured allowing GOA to be analyzed throughout opening and closing cycles.

GOA data showed that the no significant difference between trilayer and mechanical average open GOA values. While the trilayer valve was slower to open then both prosthetic valves, there was no difference between closing times when comparing

bioprosthetic and trilayer valves. Trilayer valves showed excellent hemodynamics, proving their readiness for longer term testing in the bioreactor.

Pre-conditioning valves prior to implantation is a common strategy in heart valve tissue engineering[218–23]. Determining the effect of mechanical forces on the valve prior to using an animal model is advantageous. A three week study of cell-seeded trilayer valves was performed. Valves functioned well throughout the test, with no tearing or failures observed. Mechanical testing showed that trilayer cusps significantly changed in mechanical properties, behaving more like native tissue tested in the circumferential direction. Unfortunately, no cells were able to be located in the valve, therefore for cell phenotype was not investigated.

The trilayer valves tested in the bioreactor were formed in the crush mounting system. This system was developed and used to provide rapid, reproducible assembly of heart valves from scaffolds. The crush mount system would not translate to the clinical environment as it is not able to be implanted. Therefore, the same trilayer scaffold production technique used in the bioreactor valve was applied to create a nitinol stent-mounted valve. Collapsable stent valves are currently being used as a delivery system for TAVI procedures and for several tissue engineered valves[24–29]. This proof-of concept shows the trilayer method of valve creation can be formed into a system that is ready for *in-vivo* testing.

4.5 Conclusion

A novel cell seeding technique on porous and microneedle treated fibrous scaffolds shows rapid, full-thickness cell seeding of scaffolds. Functional heart valves were made using a crush-mounting system. This system allowed for rapid and reproducible production of valves for *in vitro* testing. A comparison between mechanical, bioprosthetic, and trilayer valves revealed excellent hemodynamic performance of trilayer valves. These valves functioned well for three weeks in a bioreactor. A collapsible stent-mounted trilayer valve was produced as a proof of concept for further *in-vivo* testing.

4.6 Chapter 4 References

1. Tedder ME, Liao J, Weed B, et al. Stabilized collagen scaffolds for heart valve tissue engineering. *Tissue Eng Part A*. 2009;15(6):1257-1268. doi:10.1089/ten.tea.2008.0263.

2. Sierad LN, Simionescu A, Albers C, et al. Design and Testing of a Pulsatile Conditioning System for Dynamic Endothelialization of Polyphenol-Stabilized Tissue Engineered Heart Valves. *Cardiovasc Eng Technol*. 2010;1(2):138-153. doi:10.1007/s13239-010-0014-6.

3. Santoro R, Consolo F, Spiccia M, et al. Feasibility of pig and human-derived aortic valve interstitial cells seeding on fixative-free decellularized animal pericardium. *J Biomed Mater Res B Appl Biomater*. 2015. doi:10.1002/jbm.b.33404.

4. Chang Y, Chen S-C, Wei H-J, et al. Tissue regeneration observed in a porous acellular bovine pericardium used to repair a myocardial defect in the right ventricle of a rat model. *J Thorac Cardiovasc Surg*. 2005;130(3):705-711. doi:10.1016/j.jtcvs.2005.04.007.

5. Chang Y, Lai P-H, Wei H-J, et al. Tissue regeneration observed in a basic fibroblast growth factor–loaded porous acellular bovine pericardium populated with mesenchymal stem cells. *J Thorac Cardiovasc Surg*. 2007;134(1):65-73.e4. doi:10.1016/j.jtcvs.2007.02.019.6. Chen C-H, Wei H-J, Lin W-W, et al. Porous tissue grafts sandwiched with multilayered mesenchymal stromal cell sheets induce tissue regeneration for cardiac repair. *Cardiovasc Res*. 2008;80(1):88-95. doi:10.1093/cvr/cvn149.

7. Sivamani RK, Stoeber B, Liepmann D, Maibach HI. Microneedle penetration and injection past the stratum corneum in humans. *J Dermatolog Treat*. 2009;20(3):156-159. doi:10.1080/09546630802512679.

8. Mikolajewska P, Donnelly RF, Garland MJ, et al. Microneedle pre-treatment of human skin improves 5-aminolevulininc acid (ALA)- and 5-aminolevulinic acid methyl ester (MAL)-induced PpIX production for topical photodynamic therapy without increase in pain or erythema. *Pharm Res*. 2010;27(10):2213-2220. doi:10.1007/s11095-010-0227-2.

9. Enfield J, O'Connell M-L, Lawlor K, Jonathan E, O'Mahony C, Leahy M. In-vivo dynamic characterization of microneedle skin penetration using optical coherence tomography. *J Biomed Opt*. 2010;15(4):046001. doi:10.1117/1.3463002.

10. Gardeniers HJGE, Luttge R, Berenschot EJW, et al. Silicon micromachined hollow microneedles for transdermal liquid transport. *J Microelectromechanical Syst*. 2003;12(6):855-862. doi:10.1109/JMEMS.2003.820293.

11. Fernando GJP, Chen X, Primiero CA, et al. Nanopatch targeted delivery of both antigen and adjuvant to skin synergistically drives enhanced antibody responses. *J Control Release*. 2012;159(2):215-221. doi:10.1016/j.jconrel.2012.01.030.

12. Tseng H, Cuchiara ML, Durst CA, et al. Fabrication and Mechanical Evaluation of Anatomically-Inspired Quasilaminate Hydrogel Structures with Layer-Specific Formulations. *Ann Biomed Eng*. 2012;41(2):398-407. doi:10.1007/s10439-012-0666-5.

13. Duan B, Hockaday LA, Kapetanovic E, Kang KH, Butcher JT. Stiffness and adhesivity control aortic valve interstitial cell behavior within hyaluronic acid based hydrogels. *Acta Biomater*. 2013;9(8):7640-7650. doi:10.1016/j.actbio.2013.04.050.

14. Eslami M, Vrana NE, Zorlutuna P, et al. Fiber-reinforced hydrogel scaffolds for heart valve tissue engineering. *J Biomater Appl*. 2014;29(3):399-410. doi:10.1177/0885328214530589.

15. Zhang X, Xu B, Puperi DS, et al. Integrating valve-inspired design features into poly(ethylene glycol) hydrogel scaffolds for heart valve tissue engineering. *Acta Biomater*. 2015;14:11-21. doi:10.1016/j.actbio.2014.11.042.

16. Pouleur A-C, le Polain de Waroux J-B, Pasquet A, Vancraeynest D, Vanoverschelde J-LJ, Gerber BL. Planimetric and continuity equation assessment of aortic valve area: Head to head comparison between cardiac magnetic resonance and echocardiography. *J Magn Reson Imaging*. 2007;26(6):1436-1443. doi:10.1002/jmri.21182.

17. Garcia D, Pibarot P, Landry C, et al. Estimation of aortic valve effective orifice area by Doppler echocardiography: effects of valve inflow shape and flow rate. *J Am Soc Echocardiogr*. 2004;17(7):756-765. doi:10.1016/j.echo.2004.03.030.

18. Aleksieva G, Hollweck T, Thierfelder N, et al. Use of a special bioreactor for the cultivation of a new flexible polyurethane scaffold for aortic valve tissue engineering. *Biomed Eng Online*. 2012;11:92. doi:10.1186/1475-925X-11-92.

19. Thierfelder N, Koenig F, Bombien R, et al. In vitro comparison of novel polyurethane aortic valves and homografts after seeding and conditioning. *ASAIO J*. 59(3):309-316. doi:10.1097/MAT.0b013e318289b95e.

20. Syedain ZH, Meier LA, Reimer JM, Tranquillo RT. Tubular heart valves from decellularized engineered tissue. *Ann Biomed Eng*. 2013;41(12):2645-2654. doi:10.1007/s10439-013-0872-9.

21. Iop L, Bonetti A, Naso F, et al. Decellularized allogeneic heart valves demonstrate self-regeneration potential after a long-term preclinical evaluation. *PLoS One*. 2014;9(6):e99593. doi:10.1371/journal.pone.0099593.

22. Ramaswamy S, Boronyak SM, Le T, Holmes A, Sotiropoulos F, Sacks MS. A novel bioreactor for mechanobiological studies of engineered heart valve tissue formation under pulmonary arterial physiological flow conditions. *J Biomech Eng*. 2014;136(12):121009. doi:10.1115/1.4028815.

23. Moreira R, Velz T, Alves N, et al. Tissue-Engineered Heart Valve with a Tubular Leaflet Design for Minimally Invasive Transcatheter Implantation. *Tissue Eng Part C Methods*. 2014. doi:10.1089/ten.TEC.2014.0214.

24. Emmert MY, Weber B, Behr L, et al. Transcatheter aortic valve implantation using anatomically oriented, marrow stromal cell-based, stented, tissue-engineered heart valves: technical considerations and implications for translational cell-based

heart valve concepts. *Eur J Cardiothorac Surg*. 2014;45(1):61-68. doi:10.1093/ejcts/ezt243.

25. Wenaweser P, Stortecky S, Heg D, et al. Short-term clinical outcomes among patients undergoing transcatheter aortic valve implantation in Switzerland: the Swiss TAVI registry. *EuroIntervention*. 2014;10(8):982-989. doi:10.4244/EIJV10I8A166.

26. Chakravarty T, Van Belle E, Jilaihawi H, et al. Meta-analysis of the impact of mitral regurgitation on outcomes after transcatheter aortic valve implantation. *Am J Cardiol*. 2015;115(7):942-949. doi:10.1016/j.amjcard.2015.01.022.

27. Phan K, Wong S, Phan S, Ha H, Qian P, Yan TD. Transcatheter Aortic Valve Implantation (TAVI) in Patients With Bicuspid Aortic Valve Stenosis – Systematic Review and Meta-Analysis. *Hear Lung Circ*. 2015. doi:10.1016/j.hlc.2014.12.163.

28. Virk SA, Tian DH, Liou K, et al. Systematic review of percutaneous coronary intervention and transcatheter aortic valve implantation for concomitant aortic stenosis and coronary artery disease. *Int J Cardiol*. 2015;187:453-455. doi:10.1016/j.ijcard.2015.03.391.

29. Stokłosa P, Szymański P, Dąbrowski M, et al. The impact of transcatheter aortic valve implantation on left ventricular performance and wall thickness - single-centre experience. *Postępy w Kardiol interwencyjnej = Adv Interv Cardiol*. 2015;11(1):37-43. doi:10.5114/pwki.2015.49183.

CHAPTER 5: CONCLUSIONS AND RECOMMENDATIONS FOR FUTURE WORK

5.1 Conclusions

Aortic valve disease (AVD) is the cause of 370,000 yearly valve replacements worldwide[1]. Due to both increasing and aging populations, this is projected to increase to 850,000 annual replacements by 2050[2]. Currently, there are good valve replacements available, but they still come with serious drawbacks. Young patients are faced with the choice of repeat operations or lifelong anticoagulant therapy. Tissue engineering has the potential to produce the ideal valve replacement; with long term durability, excellent hemodynamics, and the potential for growth in young patients. The three primary goals of this research were to create a valve with patient-specific shape, to create a robust trilayer scaffold with mechainical properties tuned to perform under physiological conditions, and to use these scaffolds to create a cell-seeded valve with excellent hemodynamic properties.

We showed that valves can be modeled from medical imaging data, 3D printed, and used as molds to create patient-specific heart valves. The valve scaffolds supported cell attachment, growth, and proliferation. However, functional testing revealed shearing of the spongiosa, likely due to insufficiently-robust spongiosa scaffolds. Further studies

into robust, moldable scaffolds shaped using the modeling process described could produce a mechanically-viable patient-specific heart valve.

In chapter 3 porous, dry scaffolds were effectively glued together to form one cohesive trilayer scaffold. These scaffolds resemble the human valve's unique histoarchitecture. A meta-analysis of literature defined maximum normal stresses and strains experienced by the native valve; providing a target set of mechanical properties to be replicated by the tissue-engineered valve. Increasing porosity and microneedle rolling treatments produced scaffolds with excellent mechanical strength that were more than strong enough to function in physiological conditions.

A novel cell seeding technique was developed to rapidly seed porous and microneedle treated fibrous scaffolds; resulting in full-thickness cell seeding. Functional heart valves were made using a crush-mounting system. This system allowed for rapid and reproducible production of valves for *in vitro* testing. A comparison between mechanical, bioprosthetic, and trilayer valves revealed excellent hemodynamic performance of trilayer valves. These valves functioned well for three weeks in a bioreactor. A collapsible stent-mounted trilayer valve was produced as a proof of concept for further *in-vivo* testing.

5.2 Recommendations for Future Work

5.2.1 Assessment of Stem Cell Phenotype in Bioreactor Conditioned Valves at Pulmonic and Aortic Conditons.

Trilayer valves will be constructed and cell seeded as described in chapter 4. A bioreactor study as described in section 4.2.13 will be performed. Trilayer valves have been tested well beyond physiological forces; being subjected to 900mmHg of pressure without any adverse consequences. Therefore, it is reasonable to assume they will withstand 3 weeks of conditioning at aortic pressures of 120/80 mmHg and 70mL stroke volume. Concurrently, a valve will be tested under pulmonary conditons of 20/10mmHg and 70mL stroke volume.

To assess mechanical properties, 10x20 mm sections will be cut in both circumferential and radial directions. Samples will be clamped into a MTS load frame (MTS system Corp. Eden Prarie, MN) and wetted with PBS throughout testing. Uniaxial tensile tests will be performed by preloading the scaffolds to 0.01N and extending to failure at a rate of 5mm/min using a 100N load cell.

To assess scaffold morphology, histological techniques of mason's trichrome and H&E will be used. Von Kossa staining will reveal the extent of any calcification formed. IHC for vimentin, αSMA, and vWF will provide information on the phenotype of the interstitial cells.

5.3 Further Mechanical Analysis of Trilayer Scaffolds

5.3.1 Flexural Testing of Trilayer scaffolds

During normal movement, heart valves experience rapid flexural deformations[3]. Flexural testing and comparison of both the porcine aortic valve and the trilayer scaffold will produce a useful comparison. Thin strips of tissue will be mounted between two bars. One bar is fixed while the other bar (bending bar) applies a load directed towards the other bar, causing the tissue to bend. Markers will be placed on the tissue and tracked with a camera. Analyzing the position of these markers as force is applied provides a value for curvature change ($\Delta\kappa$) vs. applied load. The axial force being applied is then used to calculate a value for moment (M). A graph of $\Delta\kappa$ vs M will be prepared for both trlayer scaffolds and PAVs.

5.3.2 Viscoelastic Analysis through Incremental Loading

Native aortic valves show a hysteresis effect under incremental loading[4]. Therefore, it is sensible to also investigate the response of trilayer scaffolds to incremental loading. Thin strips of trilayer scaffolds will be produced and mounted in the load frame (MTS system Corp. Eden Prarie, MN) as described in section 3.2.11. Ultimate tensile tests have provided a maximum load for trilayer scaffolds. Scaffolds will be loaded to 8 different maximums, starting at 10% of UTS and increasing an additional 10% until 80% UTS is reached. Test will be cyclic, loading to the prescribed maximum, then returning

to 0% load. Recoverability – the area beneath the loading curve divided by the area beneath the unloading curve - will then be calculated for each maximum.

5.3.3 Testing Trilayer Valves in a Large Animal Model

Trilayer valves to will be produced and cell seeded as described. These valves will be mounted in collapsible nitinol stents donated by our collaborators at the University of Kiel, Germany as described in figure 4.16. Our collaborators in Kiel implantat valves using the following technique. Sheep receive Ketanest (2%) and Propofol (2%) for sedation, then Cefuroxime (100 mL), Heparin (5000 IU), and Protamin (5000 IU) during implantation and Rimadyl (1 mL) at the ending of the study. The antibiotic Baytril (10%) was given on the following five days for prevention of infection.The size of the native valve was measured before implantation using angiography. The transventricular implantation procedure was done through 4th and 5th intercostal space. For implantation, the valved stent was crimped carefully and inserted into a special delivery system. The 20-French delivery system was inserted to the chest and the autologous tissue-engineered valved stent was successfully positioned in the pulmonary annulus under fluoroscopic control. Three months after implantation, animals underwent re-angiography with subsequent euthanasia and heart explantation followed by postmortem investigation. Surgical description curtesy Jessica Boldt[5–7].

In vivo valve performance will be assessed by measuring arterial, right ventricular, and pulmonary artery pressure at time points throughout the study (t=0, and 1,2, and 3 weeks).

After retrieval of the valve, histological techniques of mason's trichrome and H&E will reveal scaffold structure and cell infiltration. Von Kossa staining will reveal the extent of any calcification formed. IHC for vimentin, αSMA, vWF, and CD68 will provide information on what phenotype the interstitial cells are expressing, and if there is an inflammatory infiltrate.

5.4 Chapter 5 References

1. Butany J, Collins MJ. Analysis of prosthetic cardiac devices: a guide for the practising pathologist. *J Clin Pathol*. 2005;58(2):113-124. doi:10.1136/jcp.2004.020271.

2. Yacoub MH, Takkenberg JJM. Will heart valve tissue engineering change the world? *Nat Clin Pract Cardiovasc Med*. 2005;2(2):60-61. doi:10.1038/ncpcardio0112.

3. Buchanan RM, Sacks MS. Interlayer micromechanics of the aortic heart valve leaflet. *Biomech Model Mechanobiol*. 2014;13(4):813-826. doi:10.1007/s10237-013-0536-6.

4. Anssari-Benam A, Bader DL, Screen HRC. A combined experimental and modelling approach to aortic valve viscoelasticity in tensile deformation. *J Mater Sci Mater Med*. 2011;22(2):253-262. doi:10.1007/s10856-010-4210-6.

5. Metzner A, Stock UA, Iino K, et al. Percutaneous pulmonary valve replacement: autologous tissue-engineered valved stents. *Cardiovasc Res*. 2010;88(3):453-461. doi:10.1093/cvr/cvq212.

6. Iino K, Boldt J, Lozonschi L, et al. Off-pump transapical mitral valve replacement: evaluation after one month. *Eur J Cardiothorac Surg*. 2012;41(3):512-517. doi:10.1093/ejcts/ezr106.

7. Emmert MY, Weber B, Behr L, et al. Transcatheter aortic valve implantation using anatomically oriented, marrow stromal cell-based, stented, tissue-engineered heart valves: technical considerations and implications for translational cell-based heart valve concepts. *Eur J Cardiothorac Surg*. 2014;45(1):61-68. doi:10.1093/ejcts/ezt243.